C.P. No. 880

C.P. No. 880

MINISTRY OF AVIATION

AERONAUTICAL RESEARCH COUNCIL

CURRENT PAPERS

The Interaction of the Reflected Shock with the Boundary Layer in a Shock Tube and its Influence on the Duration of Hot Flow in the Reflected-Shock Tunnel. Part I

By

L. Davies, Ph.D., A.Inst.P.

LONDON: HER MAJESTY'S STATIONERY OFFICE

1966

Price 5s. 6d. net

C.P. No.880

July, 1965

The Interaction of the Reflected Shock with the Boundary Layer in a Shock Tube and its Influence on the Duration of Hot Flow in the Reflected-Shock Tunnel. Part 1

- By -
L. Davies, Ph.D., A.Inst.P.

SUMMARY

An extension is made of the simple model proposed by Mark for the interaction of the reflected shock with the boundary layer in a shock tube. It leads to the prediction of a flow of gas along the walls of the tube, originating at the bifurcated foot and directed towards the end wall. When this analysis is applied to the transmitted shock, the prediction is that cold driver gas will quickly arrive at the end of the tube, cooling the gas in the reservoir of the shock tunnel. This occurs for $M_4 > 3{\cdot}5$ for helium driving nitrogen. It is a faster movement of cold gas towards the end plate than that caused by the general movement of the contact surface.

Experimental evidence in support of the theoretical model is given in the form of schlieren photographs, pressure measurements and heat transfer measurements.

The bifurcated foot mechanism is compared with the instability of the contact surface mechanism for cooling the reservoir gas. Both mechanisms predict cooling to occur for $M_4 > 3{\cdot}5$. An experiment is suggested whereby the two mechanisms may be separated.

Test section hot flow duration measurements in conjunction with the theoretical model suggest that where helium is driver and nitrogen is test gas for $M_4 < 3{\cdot}5$ the hot flow and high pressure durations will be similar.

Replaces N.P.L. Aero Report 1158 - A.R.C.27 110

List of Contents

Nomenclature

A	cross sectional area
a	sound speed
a_{ij}	a_i/a_j
h	enthalpy
L	length
M	Mach number
M_1	primary shock Mach number

m/

m	molecular weight
m^*	mass flow through nozzle
p	pressure
P_{ij}	p_i/p_j
t	time
T	temperature
T_{ij}	T_i/T_j
U	velocity
u	velocity
U_{ij}	u_i/a_j
x	distance
Δx	distance
ρ	density
γ	specific heat ratio = c_p/c_v
α_i	$\frac{\gamma_i + 1}{\gamma_i - 1}$
β_i	$\frac{\gamma_i - 1}{2\gamma_i}$
δ_i	$\sqrt{\frac{2}{\gamma_i(\gamma_i-1)}}$

Subscripts

1,2,3,4, ...	refer to regions shown in Fig. 1
$b\ell$	boundary-layer conditions
st.$b\ell$	stagnation conditions in boundary-layer fluid

Abbreviation

He:N_2	refers to helium as high pressure driver gas and nitrogen as low pressure channel gas.

1./

1. Introduction

The simple shock tube, which is a long, constant cross-sectional area duct divided internally into two compartments by means of a diaphragm (see Fig. 1), can be used to provide a reservoir of high enthalpy gas suitable for the production of hypersonic flow. The shock wave, which is produced when the diaphragm between the high pressure and low pressure compartment is burst, reflects from the end of the low pressure compartment producing a region of very hot, high pressure gas adjacent to the end wall. (Throughout this paper "reflected shock" will refer to this primary shock reflection at the end wall.) When a small hole in this end wall connects the shock tube to an expansion nozzle the gas on expansion produces hypersonic flow, the character of which depends on the initial conditions in the reservoir. In order to use this flow for hypersonic research the conditions prevailing in the reservoir must be known. It is also most important that the duration of these conditions be known.

In Fig. 1 the idealised wave diagram for a simple shock tube is shown. When the reflected shock interacts with the contact surface the shock passing through the contact surface gives rise to either an expansion wave or a shock wave as the reflected disturbance, which travels from the point of interaction towards the end wall (Figs. 2a, 2b). Under certain conditions the shock wave will pass through the contact surface without giving rise to additional disturbances (Fig. 2c) other than a Mach wave. This is known as "tailoring" and when this is used as the condition for the production of the high enthalpy reservoir gas, it is known as the "tailored interface" technique. The condition shown in Fig. 2a is known as "under tailored" as this occurs at a primary shock Mach number lower than the "tailoring" Mach number, and the condition shown in Fig. 2b is known as "over tailored" as this condition obtains at a primary shock Mach number above the tailoring Mach number. In the under tailored condition, the situation at the end plate remains steady until the arrival of the expansion wave reflected from the contact surface, whereas in the over tailored case the limiting factor is the shock reflected from the contact surface. At the tailoring Mach number only a Mach wave is reflected from the contact surface, and thus the flow parameters should remain unaltered until the arrival of the head, or the tail, of the expansion wave produced when the diaphragm burst. (At $M_1 = 6{\cdot}02$ for hydrogen as driver and nitrogen as driven gas for example.) (see Fig. 1).

The tailored interface technique is used widely in shock-tunnel research, due to its promise of longer testing times as a result of the extended duration of constant conditions at the end plate. Over the last few years, however, it has been discovered that, whereas the duration of high pressure at the end plate behaves more or less as predicted by this simple theory, the duration of high temperature does not. Lapworth[1] has shown for example, that for hydrogen as high pressure gas and nitrogen as low pressure gas, the duration of high temperature at the end plate at tailoring is much less than the duration of high pressure. Similar effects are reported by Lapworth and Townsend[2] when helium is used as the high pressure gas. This phenomenon is not explained by means of the simple shock tube theory. When the stability of the contact surface after interaction with the reflected shock is examined, Bird et al[4] have shown that this phenomenon limits the range of enthalpies for shock tunnel operation. Lapworth and Townsend have shown, using Markstein's[3] small perturbation approach, that the instability of the shocked contact surface (i.e., after passing through the reflected shock) could cause cooling of the hot gas at roughly the same Mach number as that at which the duration of high temperature begins to become less than the duration of high pressure. The result of instability of the contact

surface/

surface would be a breaking up of the surface promoting mixing with the hot reservoir gas, causing cooling at the end plate for $M_4 > 3{\cdot}56$ in ($He:N_2$) (see Nomenclature). Copper[5] has examined the effect, on the hot gas produced by the reflected shock, of the combustion at the interface when hydrogen and air are used as high and low pressure gases respectively. He explains the dip in pressure immediately after reflection of the primary shock, which is characteristic of these conditions, in terms of interface combustion. Penetration of the hot reservoir gas by these burned interface gases is considered by Copper[5] to be a limiting factor on shock tunnel usage when hydrogen and air are employed. If we restrict our attention to helium and nitrogen, then interface combustion may be eliminated as a limitation on testing time.

Holder[6] has observed a penetration of the hot reflected region gas by a flow of gas from the shocked contact surface along the walls of the tube, meeting the end plate and finally surrounding a core of hot gas. This is a means by which cold gas could reach the end plate far sooner than any general movement of the contact surface as described by the simple wave diagram.

The aim of this paper is to examine this last mentioned phenomenon, suggest a mechanism by which it occurs, and consider its relevance to the cooling of the reservoir gas. An attempt will be made to determine the relative importance of this phenomenon, and contact-surface instability, with regard to the duration of hot flow in the shock tunnel.

The examination of a series of pictures of the reflected shock wave before and after passing through the contact surface (Fig. 3) shows the growth of a region of disturbance in the corners of the end plate. These suggest that this flow of gas occurs from the instant of reflection, that it grows in extent and continues after the shock has passed through the contact surface. This flow appears to be closely linked with the bifurcation of the reflected shock wave and it will be shown that a simple model based on a Mark-Hess[7,8] approach will predict this wall flow and when the cold gas from behind the contact surface arrives at the end plate.

2. Simple Bifurcation Model for Reflected Shock Waves

The simple bifurcation model developed in this section is based upon that of Mark[7]. The essential point is that the boundary layer in the path of the reflected shock is taken to be a layer of gas of unspecified thickness 't' at wall temperature and having wall velocity with pressure equal to the free-stream value. All parameters are uniform throughout the boundary layer (see Fig. 4a). In the analysis it is assumed that the shock wave is stationary and the wall is moving. It is then assumed that the bifurcation of the shock is brought about by the boundary layer being brought to rest at the foot of the shock under the forward limb OA. It has been shown by Mark that the stagnation pressure of the boundary layer within the range $M_4 = 1{\cdot}8 \rightarrow 16$ for air for example is less than the pressure behind the normal shock, and hence the boundary-layer fluid is barred from entering the region behind the normal shock. The boundary-layer fluid therefore gathers at the foot of the shock and the size of the bifurcated foot grows with time. That part of the main flow, outside the boundary layer, which is turned on passing through the forward limb (OA) of the bifurcated foot is further compressed and turned parallel to the mainstream by the rear limb AB. This flow, having passed through two oblique shocks, is moving faster relative to the shock than the flow which has passed through the normal shock. (This point will be demonstrated mathematically below.) If we now consider this analysis applied to the reflected shock in

laboratory co-ordinates, then the flow which has passed through the normal shock is brought to rest, whereas the flow which has passed through the two oblique shocks moves along near the tube wall towards the end wall. This phenomenon was not discussed by Mark in his analysis. Mark calculated the angles COA and COB (see Fig. 4a). In the present analysis Mark's model is extended to calculate the remaining angles in the bifurcated foot and to estimate the initial velocity of the flow towards the end wall which starts at AB. The model will then be applied to the shock transmitted through the contact surface where it will be shown that the flow towards the end wall caused by the bifurcation of the transmitted shock will be of cold driver gas and hence this mechanism provides a means for cold gas to arrive at the end of the shock tube in times which may in some cases be far shorter than the arrival time of the contact surface as a whole. These times will also be estimated.

Returning to the bifurcation model, the sketch in Fig. 4a is rather unrealistic. This sketch will be used to define the various regions in the flow but omits some important features. In Fig. 4b a more realistic diagram is presented along with some suggested velocity profiles through the flow. (These velocity profiles are different from those postulated by the theory used in this paper.) Where the rear limb AB meets the stagnation bubble there must be an expansion: this is necessary because as Mark points out the pressure at B is very near the stagnation pressure of the accumulated gas, so that when the shock AB meets the free boundary of this accumulated gas an expansion is reflected from the surface. Since the flow behind the rear limb AB is subsonic, this expansion cannot entirely be a Prandtl-Meyer expansion, but must be preceded on its upstream side by some rapid subsonic expansion. Leading downstream from the intersection at A of the three shocks there is a vortex sheet between the two flows which emerge through the shock systems. The region immediately behind the rear limb of the bifurcated foot is most difficult to analyse and in the analysis below the pressure behind the rear limb is assumed to be the pressure behind the normal shock. Matching both pressure and flow angles leads to unrealistic results and the justification for choosing pressure is mainly empirical.

In calculating the time of arrival of the flow at the end wall due to this bifurcation model the velocity of the emergent flow (from the rear limb of the bifurcated foot) has been used. This is again controversial but may be justified by the fact that even if after emerging through the rearward limb of the bifurcated foot various pressure and velocity changes occur, the flow pressure has been experimentally observed eventually to reach the pressure behind the normal shock. The flow velocity far downstream then is felt to be near that computed as if the flow had normal shock pressure immediately on emerging through the rearward limb. Curvature of the normal shock near the interaction point could cause a difference in pressure in this region. However, through an oblique shock inclined at an angle β to the original flow direction the pressure change from region (i) in front of the shock (say) to a region (j) behind it is given by

$$\frac{p_j}{p_i} = \frac{2\gamma}{(\gamma+1)} M_i^2 \sin^2\beta - \frac{(\gamma-1)}{(\gamma+1)}$$

and since β is very nearly 90° in most of the observed shocks the pressure may be taken to be that behind the normal shock.

In/

In Fig.4(b), AF is the normal shock, OA and AB are the fore and rear limbs of the bifurcated foot. The line (1) (3) (5) (8) is the outer edge of the boundary layer, the line from (A) to (7) is the vortex sheet, the expansion (E) is shown where the flow accelerates over the rear of the stagnation bubble, and the compression waves (C) are shown where the flow turns parallel to the wall.

The velocity profiles shown below the sketch are related to the corresponding labelling in the sketch. Note that the wall is moving relative to the shock.

(1) to (2)

Here the velocity varies from free-stream value at the outer edge of the boundary layer (1) to the wall velocity at (2).

(3) to (4)

Within the fluid accumulating under the bifurcated foot the velocity falls to zero in the middle of the region but must again reach wall velocity at (4). The zero velocity region arises from the assumption that the flow is brought to rest, relative to the normal shock, under the forward limb of the bifurcated foot.

(5) to (6)

At the rear of the stagnation region there must be some means of matching the conditions within the bubble to those downstream of the normal shock and a region of turbulent mixing and matching is envisaged with a velocity profile perhaps as shown.

(7) to (8)

Across (7) to (8) the flow towards the end plate exists.

(8) to (9)

Finally, below this faster flow is the residual boundary-layer profile.

The mathematical model described below is undeniably crude but its application may be justified in that it provides a useful picture of the phenomena associated with the reflected and transmitted shock waves. A more detailed derivation of the formulae presented below is given in Appendix I.

Referring to Fig. 4a, in order to calculate the angles in the bifurcated foot and the emergent gas velocity the following formulae may be used:

Knowing the boundary-layer Mach number ($M_{b\ell}$) then for $M_{b\ell} > 1$ the boundary-layer stagnation pressure is given by the Rayleigh supersonic pitot formula (i.e., for a compression preceded by a normal shock[7])

$$\frac{p_{st.b\ell}}{p_i}$$

$$\frac{p_{st.b\ell}}{p_i} = \frac{\left[\frac{(\gamma_1+1)}{2} M_{b\ell}^2\right]^{\frac{\gamma_1}{\gamma_1-1}}}{\left[\frac{2\gamma_1}{(\gamma_1+1)} M_{b\ell}^2 - \left(\frac{\gamma_1-1}{\gamma_1+1}\right)\right]^{\frac{1}{\gamma_1-1}}}$$

(over the range of primary shock Mach numbers discussed in this paper the boundary-layer Mach number ($M_{b\ell}$) > 1). For nomenclature see Fig. 4a. γ_1 is the specific heat ratio in the boundary-layer gas which is always a driven gas boundary layer (see Appendix I).

In order to apply this formula to either the reflected or over- or under-tailored transmitted shock cases one merely chooses $M_{b\ell}$ from:

$$M_{b\ell} = \frac{2M_1^2(\gamma_1-1) - (\gamma_1-3)}{(\gamma_1+1) M_1} \quad \ldots\ldots \text{ for the reflected shock}$$

$$M_{b\ell} = a_{31}\left[\frac{P_{73} + \alpha_3}{\delta_3 \gamma_3 (\alpha_3 P_{73}+1)^{\frac{1}{2}}} + \frac{2a_{53}}{(\gamma_1-1)}(1 - P_{65}{}^{\beta_1})\right] \quad \ldots\ldots$$

$\ldots\ldots$ for the under-tailored transmitted shock

$$M_{b\ell} = a_{31}\left[\frac{P_{73} + \alpha_3}{\delta_3 \gamma_3 (\alpha_3 P_{73}+1)^{\frac{1}{2}}} - \frac{a_{53}\ \delta_1\ (P_{65}-1)}{(\alpha_1\ P_{65} + 1)^{\frac{1}{2}}}\right] \quad \ldots\ldots$$

$\ldots\ldots$ for the over-tailored transmitted shock.

Then the angles COA and COB may be obtained from

$$M_i^2 \sin^2(COA) = \frac{(\gamma_i+1)\frac{p_{st.b\ell}}{p_i} + (\gamma_i-1)}{2\gamma_i}$$

and

$$\frac{\tan(COA-COB)}{\tan COA} = \frac{(\gamma_i-1) M_i^2 \sin^2 COA + 2}{(\gamma_i+1) M_i^2 \sin^2 COA}$$

where $M_i = \left[\frac{2\gamma_1 M_1^2 - (\gamma_1-1)}{(\gamma_1-1)M_1^2 + 2}\right]^{\frac{1}{2}}$ $\ldots\ldots$ for the reflected shock

and $M_i = \left[\frac{\gamma_3-1}{2\gamma_3}(\alpha_3 P_{73} + 1)\right]^{\frac{1}{2}}$ $\ldots\ldots$ for the transmitted shock.

The flow Mach number within the triangle OAB is obtained from

M_x^2/

$$M_x^2 \sin^2 (COA-COB) = \frac{(\gamma_i-1)\frac{p_{st.b\ell}}{p_i} + (\gamma_i+1)}{2\gamma_i \frac{p_{st.b\ell}}{p_i}}.$$

Angles DAB and DAC and the emergent flow Mach number may be obtained using $(p_j/p_{st.b\ell})$ values in similar equations as shown in Appendix I.

Using these formulae it can be shown that the flow which emerges through the two oblique shocks is moving faster relative to the shock than the flow which has passed through the normal shock (see Table 1, Appendix I). The velocity of this flow can be used to compute the time after primary-shock reflection at which cold gas should be expected at the end plate. If the flow which emerges through AB (Fig. 4b) has velocity U_7^* then the time after shock reflection at which cold gas should arrive at the end plate is given by

$$t = \frac{LU_3}{(U_3+u_3)}\left(1 - \frac{u_3}{U_1}\right)\left(\frac{1}{U_3} + \frac{1}{(U_7^*-U_1)}\right)$$

(see Figs. 10(a) and (b)).

In order to differentiate between the shock reflected from the end plate and the shock transmitted through the boundary-layer flow parameters and bifurcated foot angles the transmitted-shock variables have been marked with a 'prime' symbol. For example, the transmitted shock boundary-layer Mach number is $M'_{b\ell}$ and the angles in the transmitted-shock bifurcated foot are

COA', COB', etc.

3. Discussion on the Simple Flow Model

The simplified approach to the interaction of a shock wave with a boundary layer in a shock tube proposed by Mark[7], and a similar earlier model where a shock interacts with a hot layer proposed by Hess[8], in both of which the boundary layer is assumed to have no velocity or thermal gradients, have been shown by Mark to give a good general description of the phenomenon. Indeed in the shock tube they predict within the experimental scatter the angles in the bifurcated foot for M_1 up to 4, (see, for example, Fig. 11). Expanding this analysis it is found that the flow which emerges through the bifurcated foot is not at rest and constitutes a flow of gas along the wall of the tube. This flow is arrested at the end plate where it accumulates.

The model chosen is undeniably a very crude one. The boundary layer is not considered to have thermal or velocity gradients, the manner in which the stagnant gas under the bifurcated foot adjusts to the higher pressure which exists downstream is not examined, the motion of the flow which emerges through the rear limb of the bifurcated foot is not carefully followed, no attempt is made to consider the effects of turbulence in the boundary layer. A more refined analysis which includes these effects would be a most useful addition to the present knowledge of the problem. However crude the model may be, experiments which have been performed by Mark, and further experiments conducted at the

N.P.L. have shown that the model provides a most useful and in some cases surprisingly accurate description of the bifurcation phenomenon. The flow of gas along the wall as a result of reflected-shock bifurcation accumulates at and moves across the end plate. The motion of this gas across the end plate can readily be seen in Fig. 3 and is easily detected by heat transfer gauges. For the reflected-shock case this gas is not cold and it is bifurcation of the transmitted shock which results in the arrival of cold gas at the end plate.

When the reflected shock interacts with the contact surface and the interaction of the transmitted wave with the boundary layer is examined, it is found that the flow picture for increasing M_4 differs from the reflected-shock case (Figs. 12(a) to (d)). For $M_4 > 3$ the angle COA in the reflected-shock bifurcated foot increases with increasing M_4 (Fig. 8a) whereas the angle COA' (Fig. 12a) in the transmitted shock case decreases with increasing M_4. Experimental values of COA and COA' confirm this situation. The boundary-layer stagnation pressure increases with increasing M_4 (Fig. 13b), for the reflected-shock case but decreases with increasing M_4 for the transmitted shock case (see Fig. 13c), becoming equal to unity when the transmitted shock has zero velocity relative to the tube wall. This situation is discussed in Appendix II. Experimental values (see Fig. 13a) confirm this trend for the transmitted shock interaction but for reasons given below in Section 8 no accurate measurement of $p'_{st.b\ell}$ was obtained. An important consequence of the decreasing value of $p'_{st.b\ell}$ (with increasing M_4) is the prediction that the interaction of the transmitted shock with the boundary layer should become more violent at the higher Mach numbers. Therefore, the amount of cold driver gas (which must constitute the wall flow in this latter case) which arrives at the end plate as a result of bifurcation of the transmitted shock will increase with M_4. Here, then, is a mechanism by which cold gas can arrive at the end plate far sooner than by any movement of the contact surface as a whole and in increasing amounts as M_4 increases. As this is also linked with a decrease in the time between primary shock reflection and the arrival of this cold gas (Fig. 10b) at the end plate, this model predicts that the duration of hot flow at the end plate of a shock tube will decrease as the primary shock Mach number increases. Mark proposes that when $(p_{st.b\ell}/p_1) < 0{\cdot}8$ in the analogous situation for the reflected shock, bifurcation will be negligible. This value occurs at about $M_4 = 3{\cdot}5$ in the transmitted shock case and it is for $M_4 > 3{\cdot}5$ that any significant cooling effects should be expected. Comparing this with the stability of the contact surface[2,3] after interaction with the reflected shock wave it is found that instability leading to cooling of the hot gas should occur for $M_4 > 3{\cdot}56$. (Helium as driver gas and nitrogen as driven gas.) This is unfortunate since it means that the two mechanisms in this case cannot be separately observed. [In Part ii a situation which could possibly allow these two mechanisms to be observed separately by using helium as driver gas and argon as driven gas, is discussed.] The success of the simple model in predicting the cooling time can be judged from Fig. 10c where the arrival of cold gas at the end plate is compared with Lapworth's experimental results. The curve should only be expected to predict a trend; even so the close agreement is encouraging.

Some experiments designed to detect the effects, due to bifurcation, at the end of the shock tube, to examine the motion of the reflected shock photographically and to determine the actual duration of hot flow in a hypersonic shock tunnel, are described in the next section.

4./

4. Experimental Evidence

4.1 Schlieren photographs

Experimental evidence for the formation of this flow and its accumulation in a vortex at the end plate is obtained from a paper by Holder, Stuart and North[9], presented at Liege in 1962. Further photographic evidence has been obtained by North[20] in the N.P.L. 6 × 3½ in. shock tube and is shown in Figs. 3a and b. In the photographs reproduced here three Mach numbers are shown at about 3·35, 4·0 and 6. Helium was used in each case as the driver gas and nitrogen was used as the driven gas. Bifurcation of the reflected shock wave is clearly seen and the contact surface is only observed after interaction with the reflected shock wave. The end plate is on the right hand side of the photographs and the appearance of disturbances in the corners is clearly seen. The deformation of the contact surface becomes apparent after interaction with the reflected shock wave, and agrees with the concept of a faster moving flow near the walls of the tube.

The disturbances in the corners of the end plate, it is suggested, are due to the accumulation of the fluid flowing along the walls of the tube as a result of the bifurcation of the reflected shock. This accumulation continues after the reflected shock wave has interacted with the contact surface and suggests that the colder driver gas very soon constitutes a large part of this end plate vortex. That the accumulated gas quickly covers the end plate is important, and the effect on shock tunnel operation would be the early arrival of driver (originally the high pressure) gas in the working section. These photographs were obtained in the N.P.L. 6 in. × 3½ in. shock tube at a low driver pressure (~ 60 lb/in.^{2} abs) and further experiments were needed in a typical shock tunnel using the pressures associated with hypersonic shock-tunnel research. These are described below.

One further piece of information obtained from these photographs is the degree of bifurcation of the shock after passing through the contact surface. For low Mach numbers ($M_1 \sim 3{\cdot}0$) the stagnation pressure of the boundary-layer gas (in this simplified approach) is greater than P_{73}. However, as M_1 increases, a rapid divergence of these pressures occurs so that at $M_1 = 5{\cdot}9$ P_{73} is several times larger than $P'_{st.b\ell}$. This would mean that violent interaction between the shock transmitted through the contact surface and the boundary layer may be expected as M_1 increases, and this is indeed observed (see Fig. 3b).

In Fig. 11 the agreement of the angles in the bifurcated foot predicted by this simple theory and an experimental bifurcated foot (enlarged photograph from the 6 in. × 3½ in. shock tube photographs) is shown, and in Fig. 14 the experimental and theoretical values of COA' are plotted versus M_1.

4.2 Pressure measurements

One of the predictions of the simple theory is, as mentioned above, that the stagnation pressure in the boundary layer and the pressure across the normal transmitted shock diverge for $M > 3{\cdot}5$. It should be possible then to observe this by measuring the initial rise in pressure across the shock transmitted through the contact surface as seen by a pressure gauge in the side wall of the tube. Unfortunately the rise time of the pressure gauge available, in the 2 in. shock tube a distance of 6 in. from the end plate, is 20 microseconds

which/

which means that probably only an indication of this divergence should be possible, especially as the schlieren photographs suggest that the time taken for the bifurcated foot to cross a pressure point would only be ~ 50 microseconds. The pressure measurements obtained using this gauge are shown in Fig. 13a and are plotted in Fig. 13b. The initial pressure is much less than p_7. The pressure then rises through the region beneath the bifurcated foot until it reaches p_7 downstream. It is suggested that with a faster rise time gauge and better spatial resolution (the gauge head in this case was $\frac{1}{4}$ in. diameter) a more accurate picture of this phenomenon may be obtained. The pressure measured under the bifurcated foot should be near the predicted stagnation pressure, and should then follow the pressure variation as the stagnation conditions under the foot approach those existing far downstream. The gauges employed in this investigation show much of this process.

4.3 Heat transfer experiments

In order to investigate the occurrence of this phenomenon in the various diameter shock tubes in use in the N.P.L. a means of detecting and following the progress of this gas accumulation and movement across the end plate was required. So as not to disturb too greatly the existing experimental conditions it was considered that a set of thin film thermometers inserted into the end plate of the various tubes should be able to pick up the change in heat transfer rate as the gas moved across the end plate. In order to evaluate this technique and compare the results with existing data, the 6 in. × $3\frac{1}{2}$ in. shock tube end plate was modified as shown in Fig. 15. A diagram of the end plate explaining the essential features is shown in Fig. 16.

With the end plate thus prepared, the thin film nearest the edge of the plate should first be covered with the end plate vortex. Since the moving gas will be compressed and turned on meeting the end plate and since it has a pressure and temperature similar to the gas in region (5) before being arrested, a higher pressure and temperature may be expected in this region. This will result in an increase in heat transfer rate. At the top of Fig. 16 a sketch of a representative heat transfer record obtained in the 6 in. × $3\frac{1}{2}$ in. shock tube is labelled indicating the important features. The movement of gas across the end plate should therefore be detectable. Records at various primary shock Mach numbers are shown in Fig. 17. As can be seen the motion of gas across the end plate agrees with the general description of the phenomenon arriving at gauges (1) and (5) first and (3) last. A comparison between gas movement rates obtained from photographs and heat transfer gauges is shown in Fig. 18. The good agreement - as far as order of magnitude and trend is concerned - suggested that this technique would be adequate to detect the presence of this phenomenon in tubes not equipped with a schlieren optical system. Further rate data obtained from the 6 in. × $3\frac{1}{2}$ in. shock tube is shown in Fig. 19.

It must be noted that the heat transfer gauges were used in conjunction with an analogue network as described by Meyer[15].

The experiment was repeated in the 3 in. shock tube using the end plate shown in Fig. 20. The gauges in this case were as shown in Fig. 21. Owing to the fact that these were shorter than in the case of the 6 in. × $3\frac{1}{2}$ in. shock tube and were in a circular section a certain degree of ambiguity arose. This was due to the fact that gas accumulating and moving across the end plate could sometimes reach the second film in from the edge before that gas which passed across the first film owing to the circular cross-section of the tube.

The/

The results were not as satisfactory as in the 6 in. × $3\frac{1}{2}$ in. tube case and some records with the derived data are shown in Figs. 22 and 23. In this case the experiment was first carried out at an initial driver pressure of 60 lb/in.^{2} abs for comparison with the 6 in. × $3\frac{1}{2}$ in. results, and then at 400 lb/in.^{2} abs to provide data under the same conditions as the temperature measurements of Ref. 2.

Finally the technique was used in the 2 in. shock tunnel, but in this case the gauges were contoured as shown in Fig. 24a. The results obtained (Fig.24b,c,d) were much better than the 3 in. shock tube records and compared favourably with the 6 in. × $3\frac{1}{2}$ in. shock tube records. Experimental details of the rate of movement of gas across the end plate are to be found in Fig. 25. An important feature of the tests carried out in the 2 in. shock tunnel is that movement of gas across the end plate is detected even when driver pressures of the order 2×10^3 lb/in.^{2} are used. This suggests that the phenomenon is a potential limit to flow duration even at these higher pressure levels since the means of transporting cold gas to the end plate appears to be present.

Using the records obtained in the 2 in. shock tunnel an attempt was made to determine the arrival time of cold driver gas at the end plate. Gauges (1) or (5) were used and a sharp decrease in heat transfer rate, as long as no other wave explanation was relevant, was considered to be an indication of the arrival of cold gas. The results are plotted in Fig. 10b and are in rough agreement with the ideal theoretical prediction of the arrival of cold gas at the end plate. The experimental results show a lower value than the theoretical, but this would be consistent with the hot flow duration (between the primary shock and the contact surface) being less than ideal theory predicts as has been discussed by Roshko[13] and by Hooker[14] for example.

It would appear possible, then, to detect and follow the movement of gas across the end plate in a shock tube caused by the accumulation of wall flow gas initiated by bifurcation of the reflected shock wave.

In Fig. 2b a record obtained in argon at $M = 3{\cdot}18$ is compared with one obtained in nitrogen at $M = 3{\cdot}2$. In the nitrogen case the change in heat transfer rate due to the arrival of the wall flow is clearly seen, but there is no similar effect in the argon case. This is consistent with the bifurcation explanation of this wall flow. No bifurcation should occur in argon at this primary shock Mach number[7]. A more detailed discussion on the use of argon as test gas is given in Part ii of this paper.

4.4 Test section experiments

A series of tests were carried out in the working section of the N.P.L. 2 in. shock tunnel to determine the available hot flow duration under operational conditions and thus to assess the effect of the cooling of the reservoir gas. This took the form of flat plate heat transfer measurements.

The flat plate shown in Fig. 27 was used, and a constant heat transfer rate was considered to be an indication of constant flow conditions in the working section. Some records obtained are shown in Fig. 28 and the estimated duration of constant flow conditions plotted as a function of primary shock Mach number in Fig. 29a. The driver pressure in all cases was 1000 lb/in.^{2} abs and the driver gas was room temperature helium. The driven gas was nitrogen.

As can be seen in Fig. 29a, a constant flow duration of about 5 milliseconds at $M_4 = 3{\cdot}6$ falling to 2·9 milliseconds at $4{\cdot}63$ is obtained.

This/

This fall is probably associated with cooling of the reservoir gas and is not associated with the arrival at the end plate of disturbances from the high pressure section. In Fig. 29b the arrival of the first disturbance from the high pressure section (using a driver-reservoir) is plotted as a function of M_1. This time is seen to increase with M_1 as compared with the hot flow duration measurements. The significance of this last fact is that there is no relationship between the hot flow duration and the arrival of the first disturbance from the high pressure section (remembering that the driver-reservoir technique[16] was used in these tests).

A similar series of tests were carried out in the N.P.L. 6 in. shock tunnel and the results are plotted in Fig. 29c. Here, however, constant hot flow conditions are obtained for and up to $M_1 = 4$. This is in agreement with the prediction discussed in the next section with regard to the effect of non-ideal driving conditions on tailoring Mach number. These conditions suggest that for $He:N_2$ the 6 in. shock tunnel should tailor at $M_1 = 4$ and also that the neutral stability Mach number and/or bifurcation effects should become significant for a higher M_1 than ideal.

5. The Instability of the Shocked Contact Surface

The theoretical model for bifurcation of the reflected and transmitted shock waves has been given and the experimental evidence discussed. Before the final discussion on the duration of hot flow in the shock tunnel, a brief description of the contact surface instability model in the shock tube will be given and the relevance of this phenomenon will be discussed in the next section along with the above bifurcation model.

The stability of an interface between two fluids, of different densities, when the two fluids are accelerated in a direction perpendicular to their interface has been discussed by Taylor.[17] When both fluids are deep compared with the wavelength of the disturbance of the interface, and considering axes moving with the interface, Taylor[17] uses the velocity potentials of motion

$$\phi_1 = Ae^{-Ky+nt}\cos Kx \qquad \text{fluid 1}$$

and

$$\phi_2 = -Ae^{Ky+nt}\cos Kx \qquad \text{fluid 2}$$

where A = amplitude, to examine the stability of the interface and shows that the rate of development of the instability is proportional to $\sqrt{\dfrac{\rho_2 - \rho_1}{\rho_2 + \rho_1}}$.

Markstein[3], following Taylor's analysis, examines the stability of the contact surface in a shock tube after interaction with the reflected shock wave. Markstein simplifies the analysis by calculating the effect of a constant acceleration 'a' of very short duration 'τ' (where $a\tau = U$, the difference in velocity $U = (u_3 - u_7)$ in shock tube terminology (Fig. 1)) on a slightly distorted interface. The result is an expression for the disturbance flow field which exists immediately after the acceleration has occurred. This has the form

$$u(x,y) = UkA\frac{(\rho_2 - \rho_1)}{(\rho_2 + \rho_1)}e^{k(\pm x+iy)}$$

where $k = 2\pi/\lambda$, A = amplitude.

The/

The sign of this perturbation velocity depends on $(\rho_2 - \rho_1)$. If this analysis is now applied to the shock tube flow defined in Fig. 1 then the sign will depend on $(\rho_2 - \rho_3)$; for helium as driver gas and nitrogen as driven gas the critical term is $T_2 - 7T_3$. Neutral stability in this case occurs then when $T_2 = 7T_3$, i.e., at $M_1 = 3{\cdot}56$. Lapworth and Townsend[2] have used this as a comparison with their experimental measurement of hot flow duration and find that this figure agrees within acceptable limits with the actual onset of cooling at the end of the shock tube. The instability of the interface is considered to be the mechanism which promotes the mixing and cooling of the hot gas (ideally between the contact surface and the end plate). It is interesting to note that if real shock tube behaviour is considered, then on examining the effect of P_{41} greater than or less than $(P_{41})_{ideal}$ (the diaphragm pressure ratio obtained from simple theory) the variation shown in Fig. 30 is obtained. Note that where $(P_{41})_{actual}$ (experimental diaphragm pressure ratio) is less than $(P_{41})_{ideal}$ the suggestion is that the Mach number at which neutral stability occurs increases. Thus where $(P_{41})_{actual} = 0{\cdot}75\ (P_{41})_{ideal}$ as is obtained in the N.P.L. 6 in. shock tunnel the decrease in required diaphragm pressure ratio for a given M_1 offsets the occurrence of instability of the shocked contact surface causing cooling.

When the driver and driven gases are the same, the neutral instability Mach number is unity.

Not too much emphasis must be laid on actual values in this section, however, and the results can only be taken as an indication of the broad trend of events.

6. Discussion on the Factors which Limit the Duration of Hot Flow in the Reflected-Shock Tunnel

Using the analysis outlined above it is found that a flow of gas along the wall of the tube, directed towards the end plate, originating at the bifurcated foot, may be predicted. This flow is arrested and turned on meeting the end plate and flows across it. When this analysis is applied to the transmitted shock, after reflected shock and contact surface interaction, it is found that for $M_1 > 3{\cdot}5$ an increasingly strong interaction as M_1 increases should occur. Again, a flow of gas along the wall of the tube directed towards the end plate is predicted. This time, however, it consists of cold driver gas. On meeting the end plate this flow is compressed and turned and causes mixing and cooling of the gases at the end plate. This cold driver gas will reach the end plate at times after reflection (of the primary shock) much shorter than by any general movement of the contact surface after interaction with the reflected shock. This is a possible explanation of the early cooling of the reservoir gas at the end plate observed for example by Lapworth[1,2]. Various predictions of the theory, for example the variation of bifurcated foot shock angles, are borne out by experimental evidence. Although the model is crude, reasonably good agreement with experiment is obtained, and it is felt that non-ideal shock tube behaviour may be at least as great a source of deviation between theory and experiment as the extreme simplification of the theoretical approach (see Appendix IV).

Another explanation for the cooling of the reservoir gas is the instability of the contact surface[3] after passing through the reflected shock. A simplified approach developed by Markstein[3] may be used to predict that for

M_1/

$M_4 > 3{\cdot}56$ the contact surface after interaction with the reflected shock will be unstable resulting in a mixing and cooling of the hot driven gas.

At modest pressures, that is in the 400 lb/in.^{2} abs driver pressure range, the above cooling mechanisms may rival each other in significance, but as the overall pressure level is increased it is felt that the bifurcation mechanism may decrease in importance. (It is found experimentally, however, that indications of the bifurcation mechanism are observed for $p_4 = 1000$ lb/in.^{2} abs.) Unfortunately both models suggest that cooling should occur for $M_4 > 3{\cdot}5 \rightarrow 3{\cdot}56$ (using He:N_2) and hence a temperature measuring experiment will not differentiate between the two effects. There is a suggestion (in Part ii) that these two effects may be separated using He:A since cooling due to instability of the contact surface is expected to occur for $M > 3{\cdot}85$ whereas cooling due to bifurcation of the transmitted shock should be evident only for $M_4 > 4{\cdot}3$.

When the duration of useful flow is investigated using flat plate heat transfer measurement in the working section of the N.P.L. 2 in. and 6 in. shock tunnels, useful running times of 5 milliseconds at $M_4 = 3{\cdot}6$ for the 2 in. and 7 milliseconds at $M_4 = 4$ for the 6 in. are obtained (the operational Mach numbers). Both mechanisms, however, favour longer driven length tunnels. The N.P.L. 6 in. shock tunnel has a driven, or low pressure channel, length of 39 ft. This would treble the time taken for any cold gas to reach the end plate, as a result of bifurcation interaction, compared with the 12 ft long 2 in. tunnel.

In conclusion, it would appear that for $M_4 \leq 3{\cdot}5$ using He:N_2 the hot flow time in a shock tunnel will be near the high pressure duration value. This limiting Mach number may be higher in practice, as for instance in the N.P.L. 6 in. shock tunnel. For higher Mach numbers pollution of the working section flow with driver gas must be expected before the termination of high reservoir pressure duration.

7. Acknowledgements

Discussions with Dr. K. C. Iapworth are gratefully acknowledged. The detailed discussion on velocity profiles in Section 2 arose from talks with Dr. G. E. Gadd. Heat transfer and pressure measurements were carried out by Mr. K. A. Dolman and Mr. K. Wilson. The calculations were carried out by Miss F. Worsley. The heat transfer films were prepared by Mr. W. Smith of the N.P.L. Workshop. Heat transfer data from the N.P.L. 6 in. shock tunnel were obtained by Mr. R. F. Cash.

References/

References

No.	Author(s)	Title, etc.
1	K. C. Lapworth	Temperature measurements in a hypersonic shock tunnel. pp.255-269 of AGARDograph 68 - 'The High Temperature Aspects of Hypersonic Flow', Pergamon Press, 1964.
2	K. C. Lapworth and J. E. G. Townsend	Temperature and pressure studies in the reservoir of a reflected-shock hypersonic tunnel. A.R.C.26 110. December, 1964.
3	G. H. Markstein	Flow disturbances induced near a slightly wavy contact surface or flame front traversed by a shock wave. J. Aeronaut Sci., Vol.24, 1957, pp.238-239.
4	K. D. Bird, J. F. Martin and T. J. Bell	Recent developments in the use of the hypersonic shock tunnel as a research and development facility. Third Hypervelocity Techniques Symposium, Denver, March, 1964.
5	J. A. Copper	Effects of interface combustion and mixing on shock-tunnel conditions. AIAA Journal, Vol.2, No.9, September, 1964, pp.1669-1671.
6		An assessment of our present status and future requirements for high temperature hypersonic facilities. Round Table Discussion. pp.745-778 of AGARDograph 68 - 'The High Temperature Aspects of Hypersonic Flow', Pergamon Press, 1964.
7	H. Mark	The interaction of a reflected shock wave with the boundary layer in a shock tube. NACA TM 1418, March, 1958.
8	R. V. Hess	Interaction of moving shocks and hot layers. NACA TN 4002, May, 1957.
9	D. W. Holder, C. M. Stuart and R. J. North	The interaction of a reflected shock with the contact surface and boundary layer in a shock tube. A.R.C.22 891. September, 1961.

10/

No.	Author(s)	Title, etc.
10	S. Byron and N. Rott	On the interaction of the reflected shock wave with the laminar boundary layer on the shock tube walls. Proc. 1961 Heat Transfer and Fluid Mechanics Institute. Stanford University Press.
11	D. W. Holder and D. L. Schultz	On the flow in a reflected-shock tunnel. A.R.C. R. & M.3265, August, 1960.
12	R. E. Duff	J. Phys. Fluids 2, 207-216, 1959.
13	A. Roshko	J. Phys. Fluids 3, 835-842, 1960.
14	W. J. Hooker	Testing time and contact-zone phenomena in shock-tube flows. J. Phys. Fluids 4, 1451-1463, 1961.
15	R. F. Meyer	A heat flux meter for use with thin film surface thermometers. National Research Council of Canada, Aeronautical Report LR-279, 1960.
16	B. D. Henshall, R. N. Teng and A. D. Wood	Development of very high enthalpy shock tunnels with extended steady-state test times. Project WS133A, Tech. Report RAD-TR-62-16. Contract AF 04 (694)-36, April, 1962.
17	G. I. Taylor	The instability of liquid surfaces when accelerated in a direction perpendicular to their planes 1. Proc. Roy. Soc. A 201, 1950.
18	L. Davies	High pressure real gas drivers and tailoring in shock tunnels. A.R.C. C.P.770, December, 1963.
19	R. A. Strehlow and A. Cohen	Limitations of the reflected-shock technique for studying fast chemical reactions and its application to the observation of relaxation in nitrogen and oxygen. J. Chem. Phys. 30, 257, 1959.
20	R. J. North	Unpublished work.

APPENDIX I/

APPENDIX I

Derivation of Formulae used to Calculate Bifurcated Foot Angles, Emergent Flow Velocity and Hot Flow Time

1. The fundamental equations of shock tube flow are those of conservation of mass, momentum and energy, and the equation of state. In terms of shock-fixed co-ordinates (see Fig. 4b) these equations are

$$\rho_1 U_1 = \rho_2 (U_1 - u_2) \quad \ldots(1)$$

$$p_1 + \rho_1 U_1^2 = p_2 + \rho_2 (U_1 - u_2)^2 \quad \ldots(2)$$

$$h_1 + \tfrac{1}{2} U_1^2 = h_2 + \tfrac{1}{2}(U_1 - u_2)^2 \quad \ldots(3)$$

$$h = \frac{\gamma}{(\gamma-1)} \frac{p}{\rho}. \quad \ldots(4)$$

If $M_1 = U_1/a_1$, the primary shock Mach number, the well-known shock relations may be derived:

$$\frac{\rho_1}{\rho_2} = \frac{(\gamma_1-1) M_1^2 + 2}{(\gamma_1+1) M_1^2} \quad \ldots(5)$$

$$\frac{p_2}{p_1} = P_{21} = \frac{2\gamma_1 M_1^2 - (\gamma_1-1)}{(\gamma_1+1)} \quad \ldots(6)$$

$$\frac{u_2}{a_1} = U_{21} = \frac{2(M_1^2-1)}{M_1 (\gamma_1+1)} \quad \ldots(7)$$

$$M_2^2 = \frac{(\gamma_1-1)M_1^2 + 2}{2\gamma_1 M_1^2 - (\gamma_1-1)} \quad \ldots(8)$$

$$\frac{T_2}{T_1} = \frac{[2\gamma_1 M_1^2 - (\gamma_1-1)][(\gamma_1-1)M_1^2 + 2]}{(\gamma_1+1)^2 M_1^2}. \quad \ldots(9)$$

If we consider the reflected shock wave (see Fig. 5a) then the boundary condition we have to apply is that $u_5 = 0$ at the end wall. If we change the co-ordinate system so that the shock moves into a stationary gas then we have the situation shown in Fig. 5b. Here $u_5 = u_2$.

By analogy with equation (7)

$$\frac{u_5}{a_2} = \frac{2(M_3^2-1)}{(\gamma_1+1) M_3}$$

where $M_3 = (U_3+u_2)/a_2$.

Putting/

Putting $u_5 = u_2$ we obtain

$$\frac{(M_3^2-1)}{M_3} = \frac{a_1}{a_2} \cdot \frac{(M_1^2-1)}{M_1}.$$

Solving for M_3 we have that

$$M_3 = \left[\frac{2\gamma_1 M_1^2 - (\gamma_1-1)}{(\gamma_1-1)M_1^2 + 2}\right]^{\frac{1}{2}}. \qquad \ldots(10)$$

Using these results and the above assumptions it may easily be shown that:

$$\frac{U_3}{a_1} = M_{b\ell} = \frac{2M_1^2(\gamma_1-1) - (\gamma_1-3)}{(\gamma_1+1)M_1}. \qquad \ldots(11)$$

Assuming, as Mark does, that in the triangle OAB (Fig. 6) the pressure is the stagnation pressure of the boundary layer, then when $M_{b\ell} > 1$ this pressure divided by the static pressure behind the primary shock wave (which is the static pressure in the boundary layer) is given by the Rayleigh supersonic pitot formula, i.e.,

$$\frac{p_{st.b\ell}}{p_2} = \frac{\left[\frac{(\gamma_1+1)}{2} M_{b\ell}^2\right]^{\frac{\gamma_1}{\gamma_1-1}}}{\left[\frac{2\gamma_1}{(\gamma_1+1)} M_{b\ell}^2 - \left(\frac{\gamma_1-1}{\gamma_1+1}\right)\right]^{\frac{1}{\gamma_1-1}}}. \qquad \ldots(12)$$

Referring to Fig. 7, using oblique shock relations, we obtain

$$M_3^2 \sin^2(COA) = \frac{(\gamma_1+1)\frac{p_{st.b\ell}}{p_2} + (\gamma_1-1)}{2\gamma_1} \qquad \ldots(13)$$

and

$$\frac{\tan(COA-COB)}{\tan COA} = \frac{(\gamma_1-1)M_3^2 \sin^2 COA + 2}{(\gamma_1+1)M_3^2 \sin^2 COA} \qquad \ldots(14)$$

from which values for angles COA and COB may be obtained. M_x which is the flow Mach number within the triangle OAB (which is over the accumulated boundary layer gas) is obtained using the equation

$$M_x^2 \sin^2(COA-COB) = \frac{(\gamma_1-1)\frac{p_{st.b\ell}}{p_2} + (\gamma_1+1)}{2\gamma_1 \frac{p_{st.b\ell}}{p_2}}. \qquad \ldots(15)$$

DAB/

DAB and DAC' may be obtained, using M_x and $(p_s/p_{st.b\ell})$ values in similar equations. M_5^* which is the emergent flow Mach number is obtained using the equation

$$(M_5^*)^2 \sin^2 (DAB-DAC') = \frac{(\gamma_1-1)\dfrac{p_5}{p_{st.b\ell}} + (\gamma_1-1)}{2\gamma_1 \dfrac{p_5}{p_{st.b\ell}}}. \qquad \ldots(16)$$

The velocity at which the flow approaches the end wall is $(U_5^* - U_3)$, in laboratory co-ordinates, where U_5^* denotes the velocity of the flow which emerges through AB.

Now
$$\frac{U_5^*}{a_5^*} = M_5^*$$

$$\frac{a_5^*}{a_1} = \left(\frac{T_5^*}{T_1}\right)^{\frac{1}{2}}$$

and T_5^* may be obtained using oblique shock relations. If T_x is the temperature in OAB then

$$\frac{T_x}{T_2} = 1 + \left[\frac{2(\gamma_1-1)\, M_3^2 \sin^2 COA - 1}{(\gamma_1+1)\, M_3^2 \sin^2 COA}\right] [\gamma_1 M_3^2 \sin^2 COA + 1] \qquad \ldots(17)$$

and
$$\frac{T_5^*}{T_x} = 1 + \left[\frac{2(\gamma_1-1)\, M_x^2 \sin^2 DAB - 1}{(\gamma_1+1)\, M_x^2 \sin^2 DAB}\right] [\gamma_1 M_x^2 \sin^2 DAB + 1]. \qquad \ldots(18)$$

Values of the various angles in the bifurcated foot are plotted in Figs. 8a-d, and values for M_x, M_5^* are given in Table 1. It is seen that for the primary shock Mach number range examined $M_5^* > M_5$. This implies a flow of gas adjacent to the wall moving towards the end plate, since $T_5^* \simeq T_5$, and $p_5^* = p_5$.

Table 1

M_1	M_x	M_5^*	M_5
2·5	1·413	0·8309	0·5103
3·0	1·457	0·8205	0·5607
3·5	1·437	0·8941	0·5436
4·0	1·371	0·8678	0·5293
4·5	1·269	0·8489	0·5229

The/

The effect of the mass flow through the nozzle on the bifurcation model is discussed in Appendix II. It is suggested that the model should be little affected by this consideration.

The above results suggest that immediately after reflection the bifurcation of the reflected shock should result in a flow of gas along the walls of the tube towards the end wall. Evidence of such a flow is seen in Fig. 3 and is also discussed in Section 6.

Bifurcation of the shock transmitted through the contact surface will result in a flow of cold driver gas along the tube walls towards the end plate. This situation is examined in the next section.

2. Analysis of Tailoring Conditions[11]

In order to obtain a value for the duration of hot flow at the end of the shock tube before the arrival of cold gas from behind the contact surface, it is necessary to examine the interaction of the transmitted shock with the boundary layer behind the contact surface. It is therefore necessary that the flow in front of and behind the transmitted shock be understood.

A detailed analysis of these conditions is given by Holder and Schultz[11]. Referring to Fig. 9a, then for the tailored condition where the only disturbance is a Mach wave, we have that $u_5 = u_6$, and across the contact surface $u_6 = u_7$ (by definition). Also $u_2 = u_3$, $p_5 = p_6 = p_7$ and $p_2 = p_3$. Then it may easily be shown that the condition for tailoring is

$$\frac{m_3}{m_2}\frac{(\gamma_3-1)}{(\gamma_2-1)} \cdot \frac{T_2}{T_3} = \left(\frac{\alpha_2 + P_{25}}{\alpha_3 + P_{25}}\right) \qquad \ldots(19)$$

where $\alpha_i = \dfrac{\gamma_i+1}{\gamma_i-1}$ and m = molecular weight.

When helium is used as driver gas and nitrogen as driven gas this equation is satisfied when $M_1 = 3{\cdot}4$.

2.1 The under-tailored case

This situation is shown in Fig. 9b. The conditions we have are that $u_2 = u_3$, $u_6 = u_7$, $p_2 = p_3$ and $p_6 = p_7$. Taking velocities directed towards the end plate as being positive then the relationship between the various parameters can be shown to be[11]

$$\delta_3 (P_{73}-1)(\alpha_3 P_{73}+1)^{-\frac{1}{2}} = \frac{u_3}{a_3} + \frac{2}{(\gamma_1-1)} a_{53} \left[1 - (P_{65})^{\beta_1}\right] \qquad \ldots(20)$$

where $\delta_i = \left(\dfrac{2}{\gamma_i(\gamma_i-1)}\right)^{\frac{1}{2}}$ and $\beta_i = \left(\dfrac{\gamma_i-1}{2\gamma_i}\right)$.

2.2/

2.2 The over-tailored case

Referring to Fig. 9c, here $u_6 = u_7$, $u_2 = u_3$, $p_6 = p_7$ and $p_2 = p_3$ and in this case we have

$$\delta_3 (P_{73}-1)(\alpha_3 P_{73}+1)^{-\frac{1}{2}} = \frac{u_3}{a_3} - \delta_1 a_{53} (P_{65}-1)(\alpha_1 P_{65}+1)^{-\frac{1}{2}}. \qquad \ldots(21)$$

3. Bifurcation of the Shock Transmitted through the Contact Surface

The shock is now moving in the expanded high-pressure driver gas region (3) with region (7) behind it. Let us first assume the boundary layer is driven gas. We shall again define the boundary layer as a thin layer of gas moving with wall velocity and having wall temperature. The speed of sound in the boundary layer will therefore be (by analogy to the boundary-layer fluid sound velocity in region (2)) a_4. If the velocity of the transmitted shock in laboratory co-ordinates is U_T then,

$$M'_{b\ell} = \frac{U_T}{a_4}$$

where the boundary-layer Mach number is $M'_{b\ell}$ in shock-fixed co-ordinates. If M_T = transmitted shock Mach number then

$$M_T = \frac{U_T + u_3}{a_3} = \frac{U_T}{a_3} + \frac{u_3}{a_3}$$

so that

$$\frac{U_T}{a_3} = M_T - \frac{u_3}{a_3}. \qquad \ldots(22)$$

From shock relations

$$M_T = \left[\frac{\gamma_3 - 1}{2\gamma_3} (\alpha_3 P_{73} + 1) \right]^{\frac{1}{2}}$$

and where

$$\frac{u_3}{a_3} = \delta_3 (P_{73}-1)(\alpha_3 P_{73}+1)^{-\frac{1}{2}} - \frac{2a_{53}}{(\gamma_1 - 1)} [1 - (P_{65})^{\beta_1}]$$

for the under-tailored case. Substituting for M_T and u_3/a_3 in equation (22) we have

$M'_{b\ell}$/

$$M'_{b\ell} = \frac{U_T}{a_4} = a_{34}\left[\frac{(P_{73}+\alpha_3)}{\delta_3\gamma_3(\alpha_3 P_{73}+1)^{\frac{1}{2}}} + \frac{2a_{53}}{(\gamma_1-1)}\left(1-(P_{65})^{\beta_1}\right)\right]$$

where $a_{53} = \left[\frac{\gamma_1 T_5}{\gamma_3 T_3}\right]^{\frac{1}{2}}$

and $a_{34} = \left[1-\left(\frac{\gamma_4-1}{\gamma_1+1}\right)\frac{(M_1^2-1)}{a_{41}\,M_1}\right]$.

For the over-tailored case, substituting for u_3/a_3 given in equation (21) we have

$$M'_{b\ell} = \frac{U_T}{a_4} = a_{34}\left[\frac{(P_{73}+\alpha_3)}{\delta_3\gamma_3(\alpha_3 P_{73}+1)^{\frac{1}{2}}} - \frac{a_{53}\delta_1(P_{65}-1)}{(\alpha_1 P_{65}+1)^{\frac{1}{2}}}\right]. \qquad \ldots(23)$$

We now have an expression for the boundary-layer Mach number as in the reflected shock region. The analysis of the bifurcated foot angles is carried out in the same manner as for the reflected shock.

We will now assume the boundary layer consists of driven gas. This is reasonable because if we assume the boundary layer to be a thin layer of fluid having wall velocity, then at the contact surface, with contact surface fixed co-ordinates, there is a mass flow past the contact surface along the wall. Using Duff's[12] analogy the contact surface acts as a 'leaky piston'. This concept is used, in a far more refined manner than described here, by Roshko[13], Hooker[14], etc., to account for the decrease in running time in the shock tube hot flow. Thus the transmitted shock wave will be interacting immediately upstream (towards the diaphragm station) of the contact surface, with a boundary layer of the gas initially in the low pressure channel. The sound speed will be a_1 and the under-tailored and over-tailored boundary-layer Mach numbers will now be given by:

Under-tailored $$M'_{b\ell} = \frac{U_T}{a_1} = a_{31}\left[\frac{(P_{73}+\alpha_3)}{\delta_3\gamma_3(\alpha_3 P_{73}+1)^{\frac{1}{2}}} + \frac{2a_{53}}{(\gamma_1-1)}\left[1-(P_{65})^{\beta_1}\right]\right]$$

$\ldots(24)$

and

Over-tailored $$M'_{b\ell} = \frac{U_T}{a_1} = a_{31}\left[\frac{(P_{73}+a_3)}{\delta_3\gamma_3(\alpha_3 P_{73}+1)^{\frac{1}{2}}} - \frac{a_{53}\delta_1(P_{65}-1)}{(\alpha_1 P_{65}+1)^{\frac{1}{2}}}\right].$$

$\ldots(25)$

In this case the boundary-layer stagnation pressure will be obtained as for the reflected shock wave, whereas the rest of the calculation of the bifurcated foot parameters must of course be related to region (3).

This approach gives a reasonable agreement with the experimental bifurcated shock angles and was used to describe the phenomenon for the transmitted shock. In Appendix III the effect of 'real shock tube' behaviour

includes/

includes a discussion on these two methods of calculating the bifurcated foot angles, and from a comparison with experiment it would appear that this is further evidence to support the concept of a mass flow past the contact surface by means of the boundary layer.

In laboratory co-ordinates the velocity with which the flow approaches the end plate is $(U_7^* - U_T)$, see Fig. 10, where U_7^* is the velocity of the flow which emerges through EF.

When U_7^* has been determined the arrival time of cold gas at the end plate may be obtained. If the length of the shock tube be L, the velocity of the primary shock U_1, that of the reflected shock U_3, and the velocity of the contact surface u_3, then it may readily be shown that the time after shock reflection at which cold driver gas reaches the end plate is given by

$$t = \frac{LU_3}{(U_3+u_3)}\left(1 - \frac{u_3}{U_1}\right)\left(\frac{1}{U_3} + \frac{1}{(U_7^*-U_T)}\right). \qquad \ldots(26)$$

Values of t vs. M_1 are plotted in Fig. 10b.

APPENDIX II/

APPENDIX II

Zero Transmitted Shock Velocities

It is interesting to note that it is possible to predict conditions under which the transmitted shock has zero velocity with respect to the tube wall. In other words when the reflected shock meets the contact surface a shock is the reflected disturbance and the transmitted shock remains at the co-ordinate of the interaction point.

The required condition is $U_T = 0$

$$\text{or} \quad M_T = \frac{u_3}{a_3}.$$

The above described phenomenon will occur in the over-tailored case.

We have seen that

$$\frac{U_T}{a_3} = \left[\frac{(P_{73}+\alpha_3)}{\delta_3 \gamma_3 (\alpha_3 P_{73}+1)^{\frac{1}{2}}} - \frac{a_{53}\delta_1 (P_{65}-1)}{(\alpha_1 P_{65}+1)} \right].$$

Therefore in order to satisfy $U_T = 0$

$$\frac{(P_{73}+\alpha_3)}{\delta_3 \gamma_3 (\alpha_3 P_{73}+1)^{\frac{1}{2}}} = \frac{a_{53}\delta_1 (P_{65}-1)}{(\alpha_1 P_{65}+1)^{\frac{1}{2}}}$$

which is the required condition. This occurs ideally at $M_1 = 5{\cdot}6$ for helium driver and nitrogen driver gas.

APPENDIX III/

APPENDIX III

The Effect of Flow through the Nozzle on Reflected-Shock Conditions

When the shock tube is used as a means of producing a high enthalpy reservoir gas for a hypersonic wind tunnel the mass flow through the nozzle will disturb conditions behind the reflected shock. There are possible perturbations of reflected shock Mach number which would affect the above analysis.

If we let the flow parameters at the throat of the nozzle be ρ^*, p^*, T^*, a^*, etc., then the mass flow rate through the nozzle may be expressed as

$$m^* = \rho^* A^* a^* \qquad [A^* = \text{cross-sectional area}].$$

It is possible to relate conditions at the throat to the reflected shock region (i.e., the region between the reflected shock and the end wall) by means of the so-called 'critical ratios', viz.,

$$\frac{T^*}{T_5} = \frac{2}{\gamma_1+1}; \quad \frac{p^*}{p_5} = \left(\frac{2}{\gamma_1+1}\right)^{\frac{\gamma_1}{\gamma_1-1}}; \quad \frac{\rho^*}{\rho_5} = \left(\frac{2}{\gamma_1+1}\right)^{\frac{1}{\gamma_1-1}}. \qquad \ldots(i)$$

Using these values then we can, for the purposes of a simple calculation, relate the nozzle mass flow rate to a mass flow rate through an area equal to that of the end wall. If u_i is the velocity induced in the reflected shock region by virtue of the mass flow through the nozzle then we can have

$$\rho_5 \, A \, u_i = \rho^* \, A^* \, a^*$$

where A = tube cross-sectional area.

So
$$u_i = \frac{\rho^* \, A^* \, a^*}{\rho_5 \, A}.$$

Using equation (i) this becomes

$$u_i = \left(\frac{2}{\gamma_1+1}\right)^{\frac{1}{\gamma_1-1}} \left(\frac{A^*}{A}\right) a^*.$$

Now
$$(a^*)^2 = a_5^2 \frac{T^*}{T_5}.$$

So
$$a^* = a_5 \left(\frac{2}{\gamma_1+1}\right)^{\frac{1}{2}}.$$

Therefore/

$$\text{Therefore } u_i = \left(\frac{2}{\gamma_1+1}\right)^{\frac{\gamma_1+1}{2(\gamma_1-1)}} \left(\frac{A^*}{A}\right) a_5. \qquad \ldots(ii)$$

Across the reflected shock wave the velocity change now becomes (u_2-u_i). Using the shock relations the new reflected shock Mach number as a result of this induced velocity is

$$M_3' = \frac{\{(u_2-u_i)/a_2\} + \{[(u_2-u_i)/a_2)^2 + (16/(\gamma_1+1)^2)\}^{\frac{1}{2}}}{4/(\gamma_1+1)}. \qquad \ldots(iii)$$

When the high pressure gas is helium and the low pressure gas is nitrogen then

$$u_i = a_5 \left(\frac{A^*}{A}\right) (0{\cdot}578).$$

For a $\frac{1}{2}$ in. nozzle at the end of a 2 in. internal diameter shock tube at $M_1 = 3{\cdot}4$ (the tailoring condition)

$$\frac{A^*}{A} = \frac{1}{64} \text{ and } a_5 = 1140\left(\frac{T_5}{T_1}\right)^{\frac{1}{2}} = 2640 \text{ ft/sec}$$

giving $u_i = 23{\cdot}9$ ft/sec

and since $u_2 = 2980$ ft/sec the change in the term $(u_2-u_i)/a_2$ is $\approx 0{\cdot}8\%$. The difference in modified M_3', (i.e., $(M_3')_M$) to M_3' is

$$\frac{(M_3')_M}{M_3'} = \frac{2{\cdot}199}{2{\cdot}207}.$$

The effect on the reflected shock zone except in the immediate vicinity of the nozzle would therefore appear to be negligible.

Immediately after reflection, however, the breaking of the nozzle diaphragm will result in the reflected shock being overtaken by a rarefaction wave. This will have the result of weakening the shock, the pressure as measured at the end plate, however, is not noticeably affected.

APPENDIX IV

The Sensitivity of the Calculations to Variation in Estimating $p_{st.b\ell}$ and $M'_{b\ell}$

One reason for the agreement obtained between the very approximate theoretical model of bifurcation of the transmitted shock and the experimental value could be the insensitivity of the angle COA' to variation in the value attributed to the appropriate stagnation pressure in the boundary layer. This in turn will depend on the Mach number attributed to the boundary-layer gas.

In Fig. 31 the calculated values of COA' vs. M_1, i.e., the transmitted shock case, are plotted as calculated using the model described in this paper (after Mark and Hess). Also shown are two curves representing the effect of varying the stagnation pressure in the boundary layer. The hatched region thus represents the spread in value of COA' due to the variation $p'_{st.b\ell} \pm 0{\cdot}15\ p'_{st.b\ell}$ and it may be seen that for a 15% change in the estimated stagnation pressure the value COA' changes by about 9-10%. Associated with this 15% change in stagnation pressure there will also be a change in the boundary-layer Mach number. It is found that a 15-17% change in $p'_{st.b\ell}$ is associated with about a 10% change in $M'_{b\ell}$. Therefore the angle COA' changes by about the same percentage as the variation in estimation of the boundary-layer Mach number.

When comparing theoretical and experimental results in this case however, the effects of non-ideal shock tube behaviour may be at least as large as any error in the theory. The so-called contact surface is in fact a contact region, and non-ideal reflected and transmitted shock velocities will have a significant effect on $M'_{b\ell}$.

One real shock tube effect has been included in the analysis and this is the "leaky piston"-contact surface analogy (after Duff[12]) where it was assumed that the shock transmitted through the contact surface will be interacting initially with a boundary layer associated with the driver gas. When this approach is compared with that which assumes that the transmitted shock interacts with a driver gas boundary layer (see Fig. 32) the effects of non-ideal shock tube behaviour are seen to have much significance in the estimation of COA', $p'_{st.b\ell}/p_3$ and the related bifurcated foot parameters.

FIG. 1

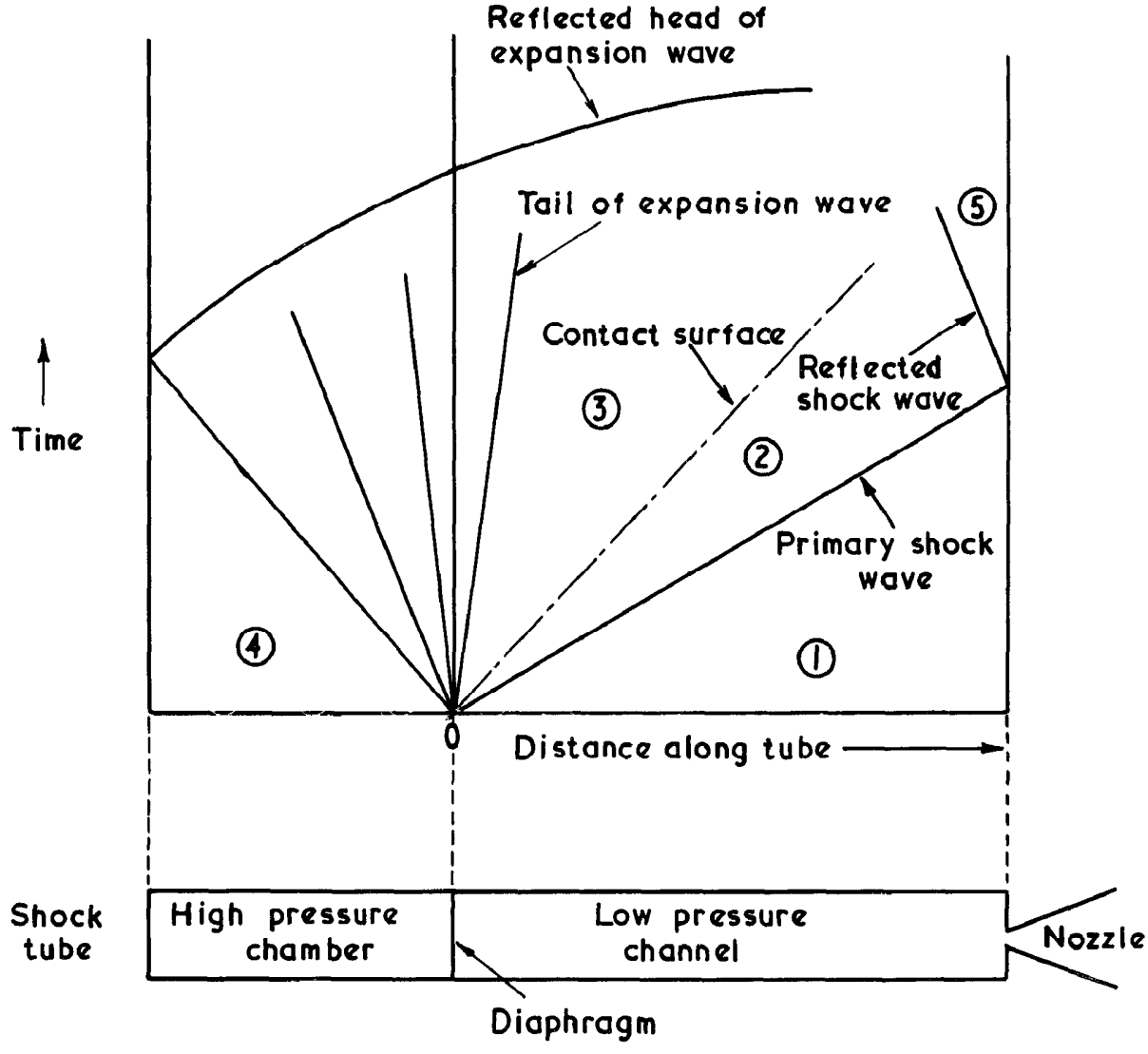

Simple shock tube flow

FIG. 2

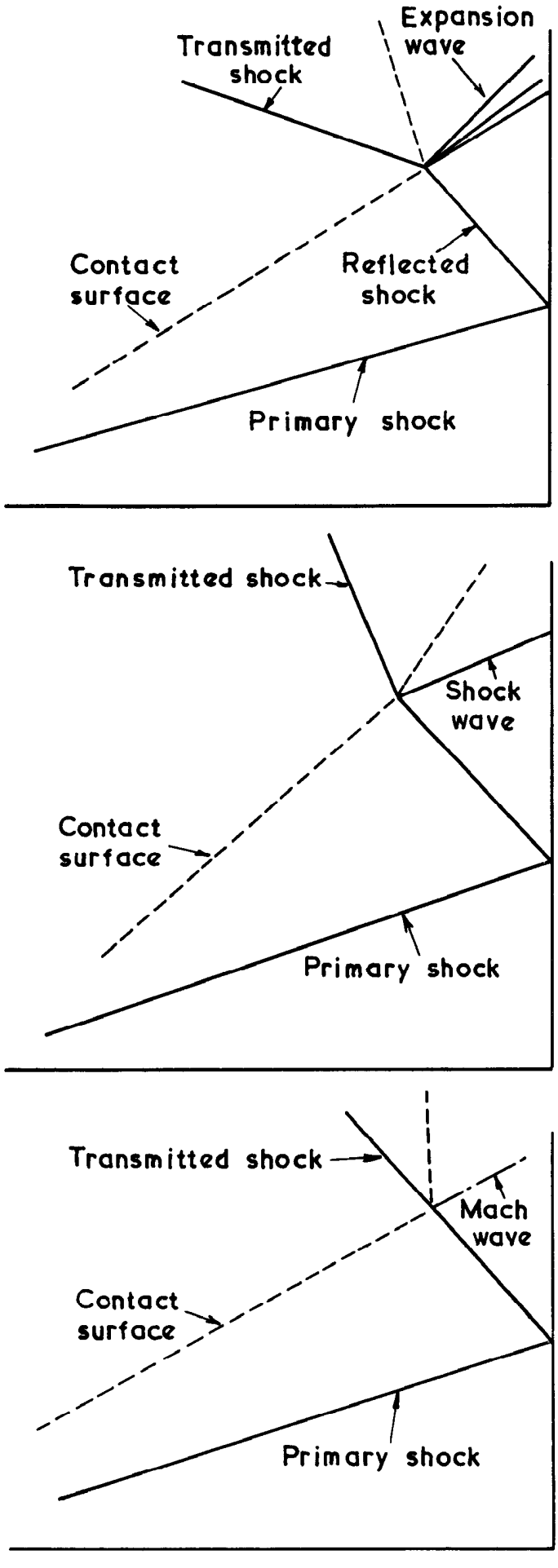

(a) Undertailored case

(b) Overtailored case

(c) Tailored case

Interaction of reflected shock wave with the contact surface

FIG. 3(a)

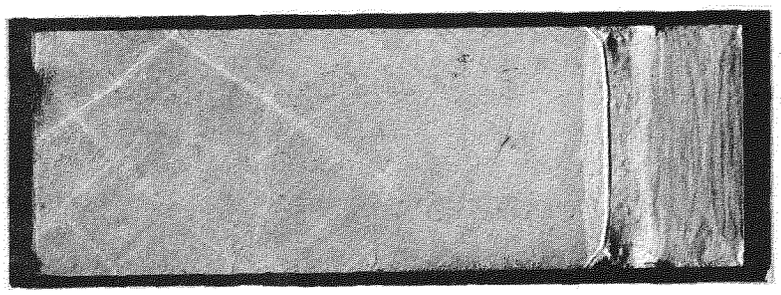

$M_1 = 4{\cdot}04$

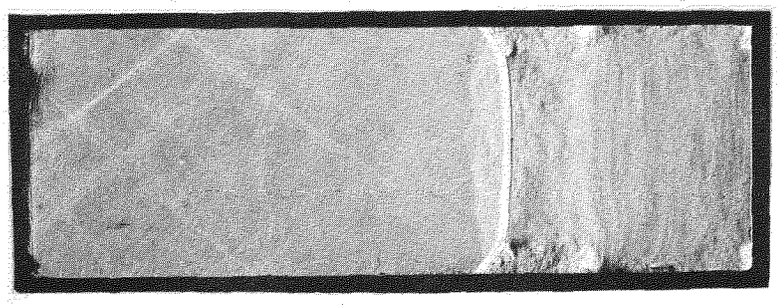

$M_1 = 4{\cdot}34$

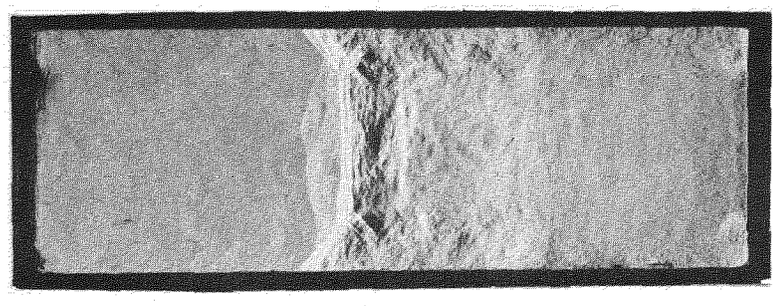

$M_1 = 4{\cdot}07$

$M_1 = 4{\cdot}10$

Reflected shock before and after interaction with the contact surface. He : N_2

Reflected shock
He: N_2 $M_1 = 5{\cdot}93$
before meeting
contact surface

Shock transmitted
through contact
surface He: N_2
$M_1 = 5{\cdot}90$

FIG. 3(b)

FIG. 4 a

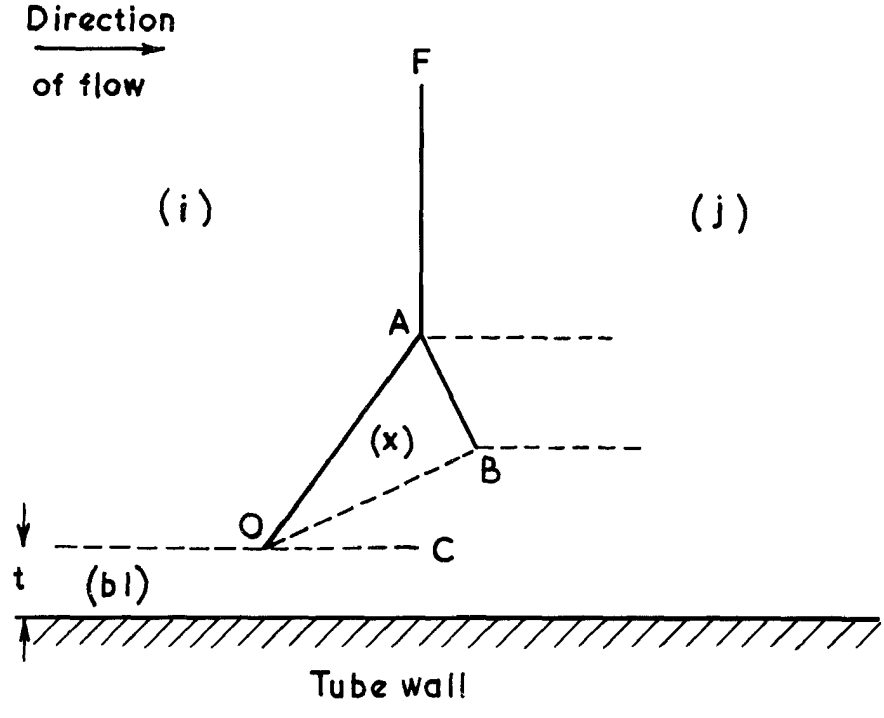

Simple bifurcation model. The solid lines represent shock waves, the dotted lines are merely reference directions

FIG. 4 (b)

Flow diagram

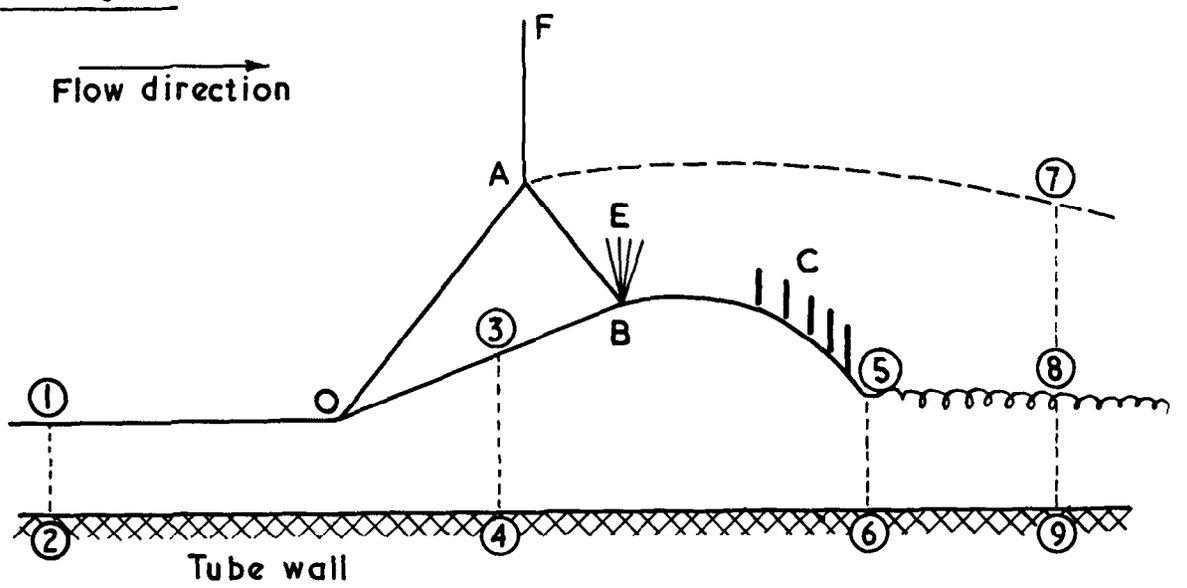

Velocity profiles

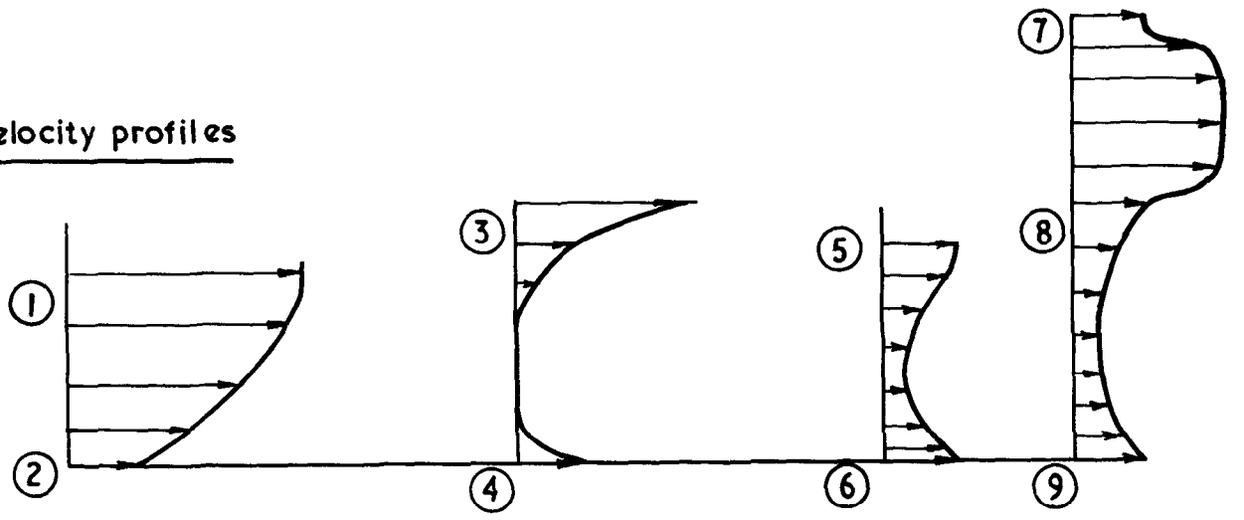

Bifurcated-shock flow diagram

AF, AB, OA	⟶	Shocks
① ③ ⑤ ⑧	⟶	Outer edge of boundary layer
A to ⑦	⟶	Vortex sheet
E	⟶	Expansion wave
C	⟶	Compression waves

FIG. 4(c)

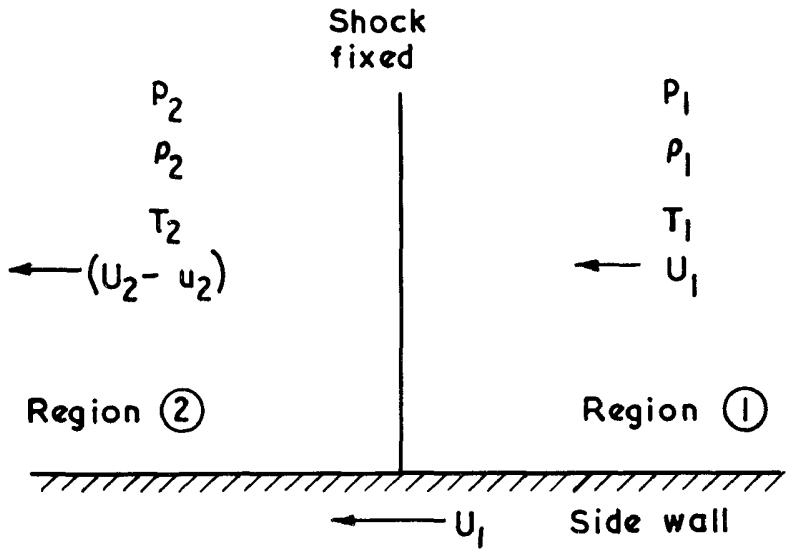

Primary shock fixed coordinate system

FIG. 5 a & b

FIG. 5 (a)

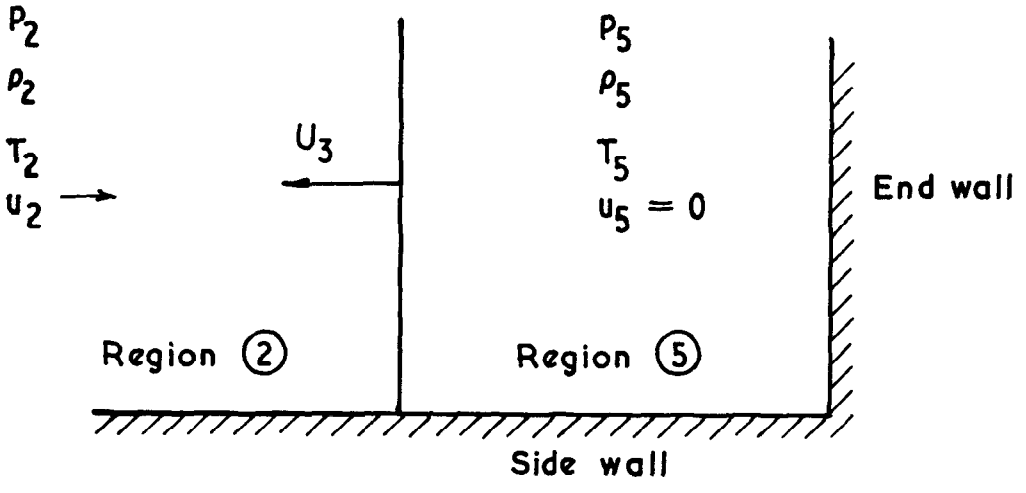

Reflected shock coordinate system

FIG. 5 (b)

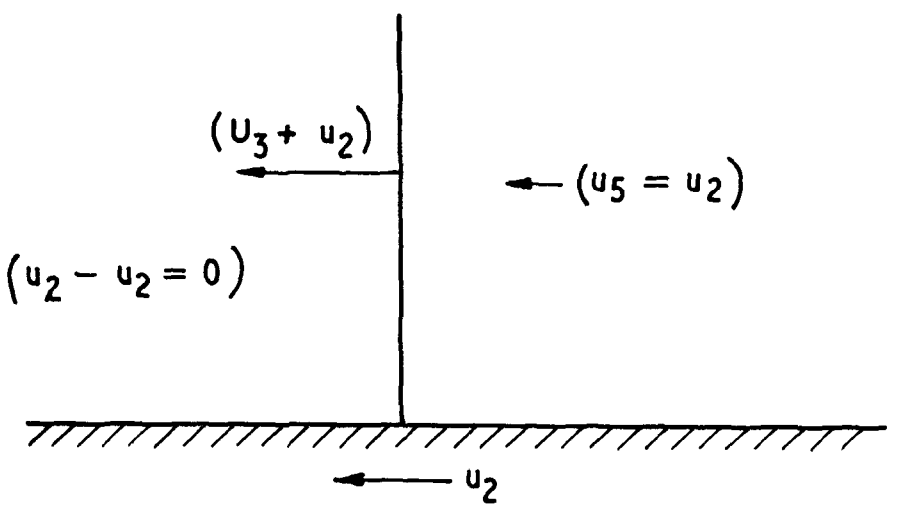

Region 2 fixed coordinate system

FIG. 6

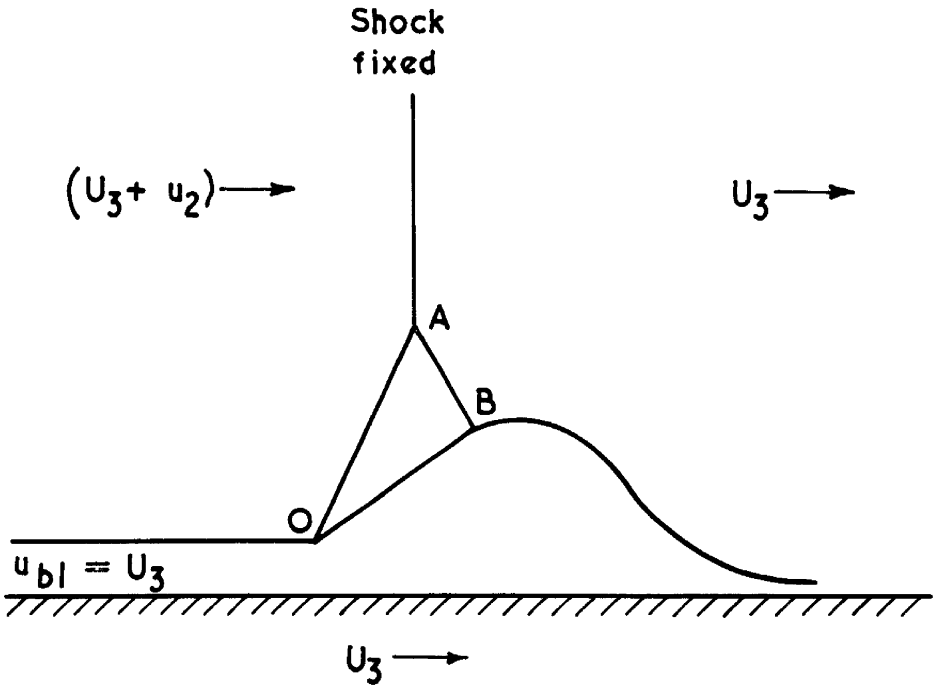

Bifurcated foot of reflected shock

Reflected shock fixed coordinate system

FIG. 7

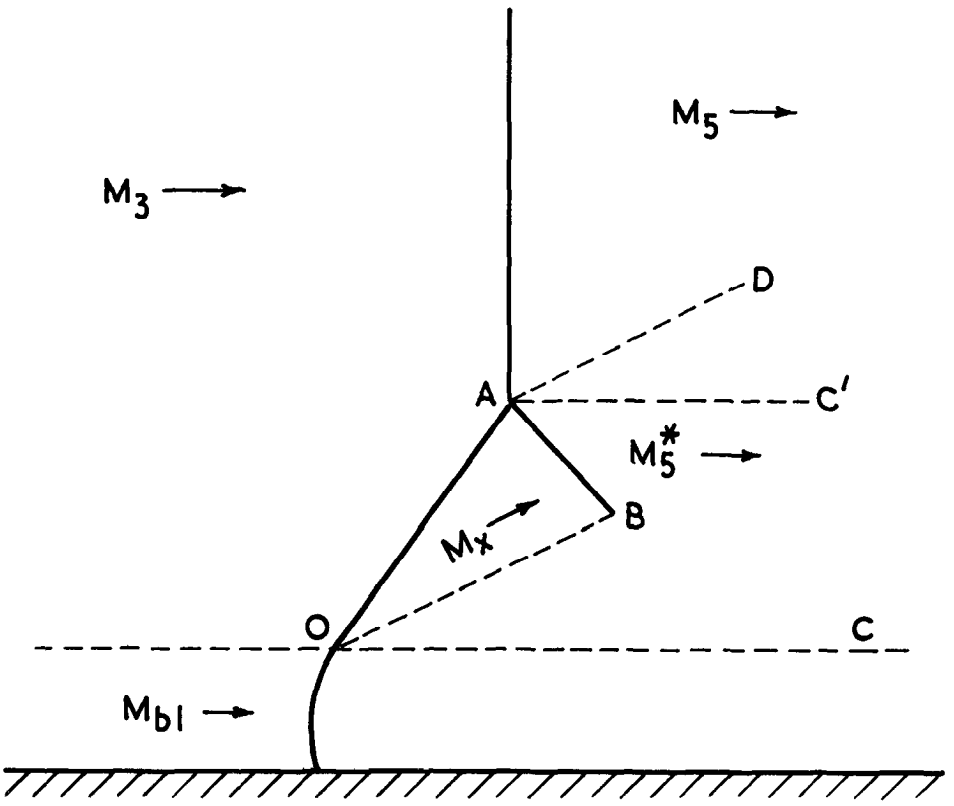

Bifurcated foot of reflected shock wave

FIG. 8 (a & b)

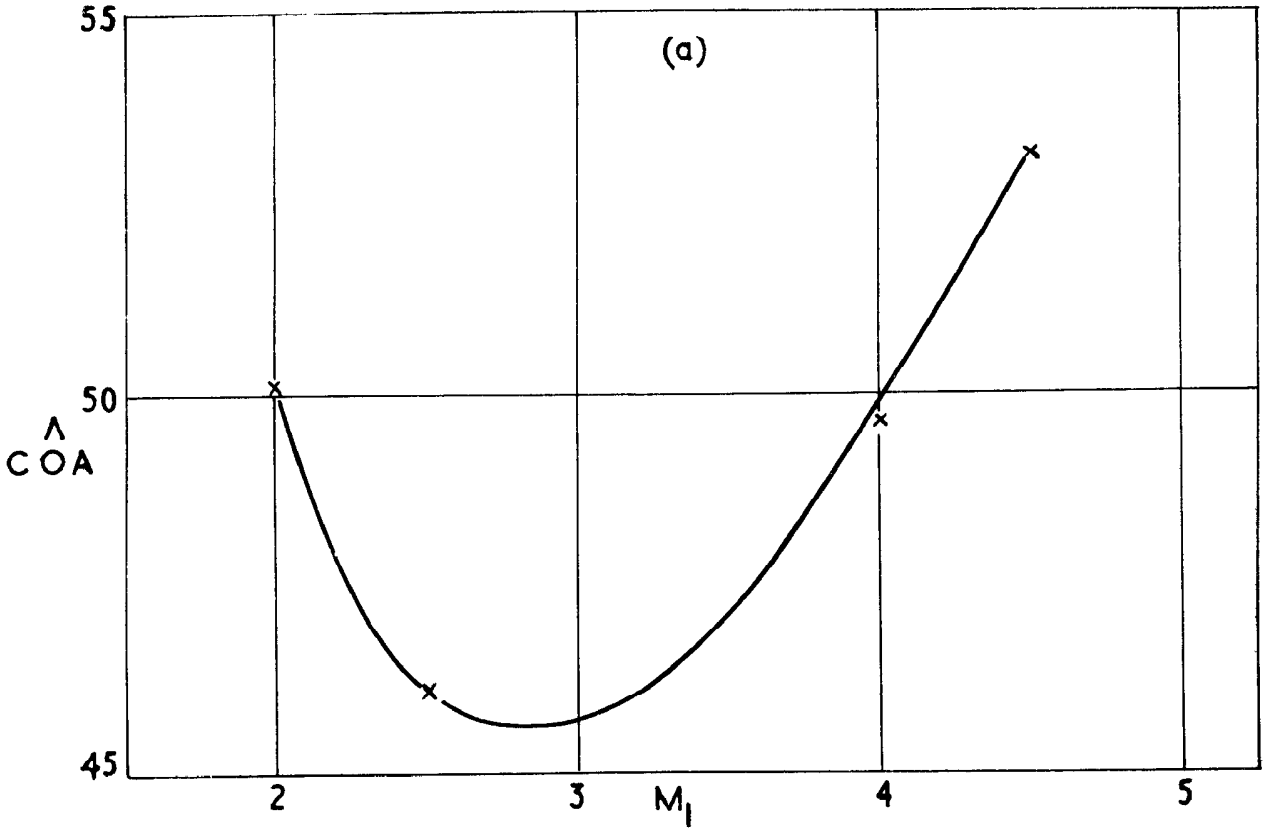

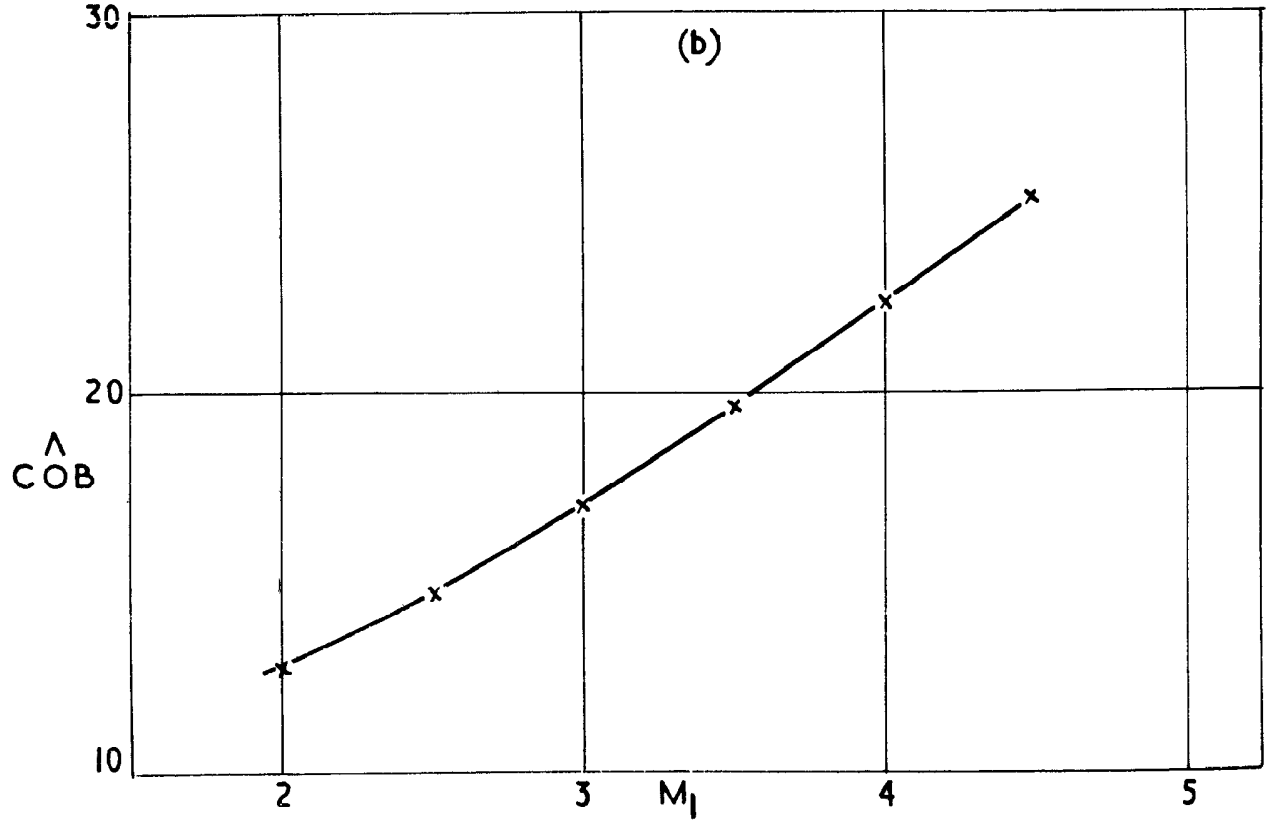

Angles in bifurcated foot of reflected shock wave He / N_2

FIG. 8 (c & d)

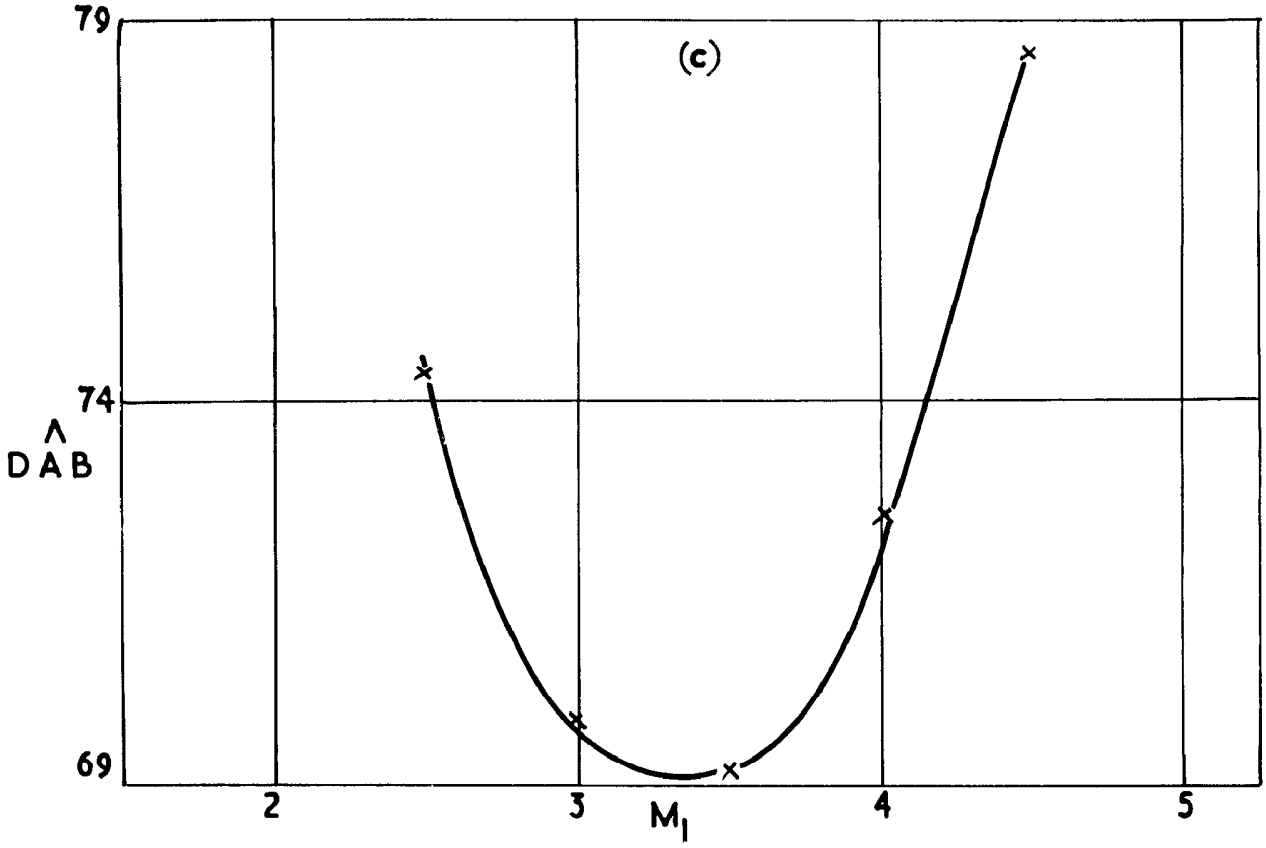

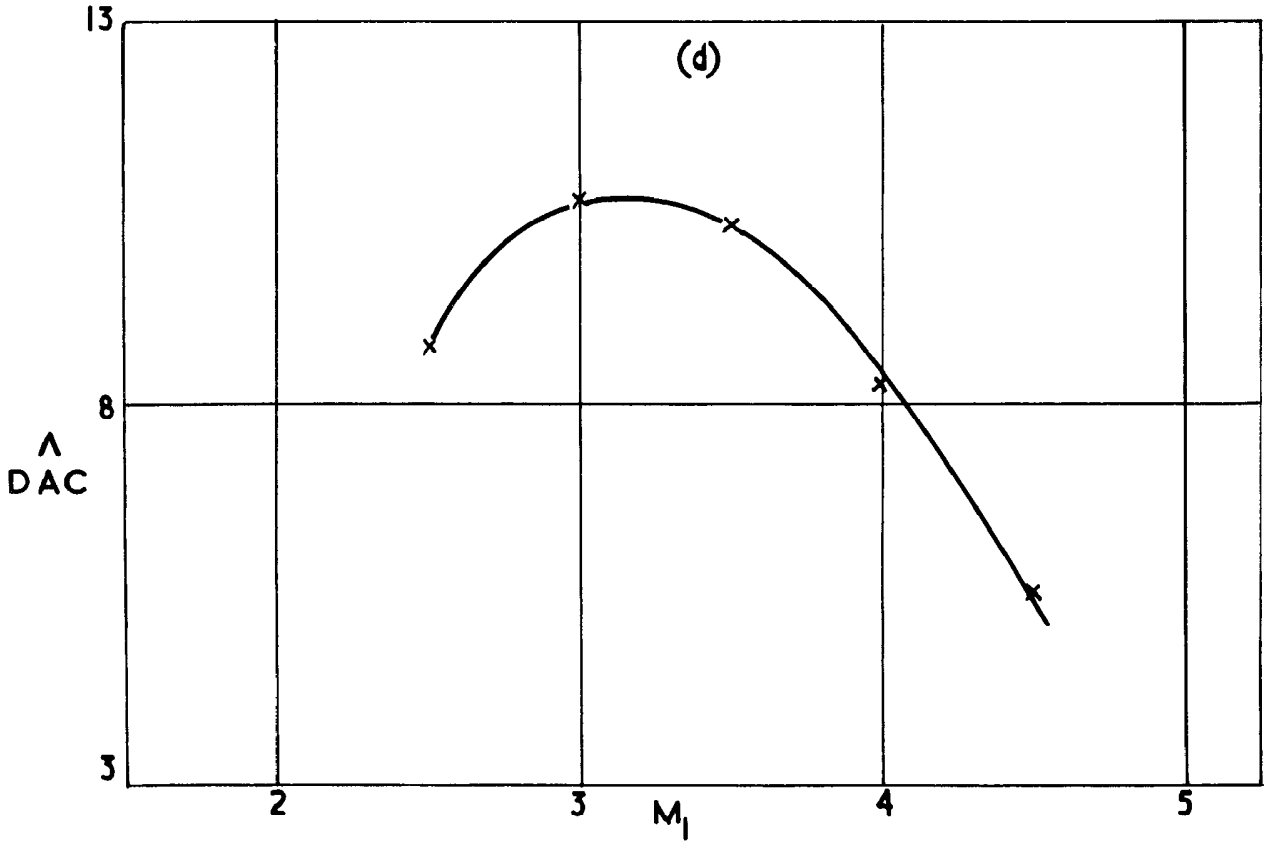

Angles in bifurcated foot of reflected show wave He/ N_2

FIG. 9 (a) & (b)

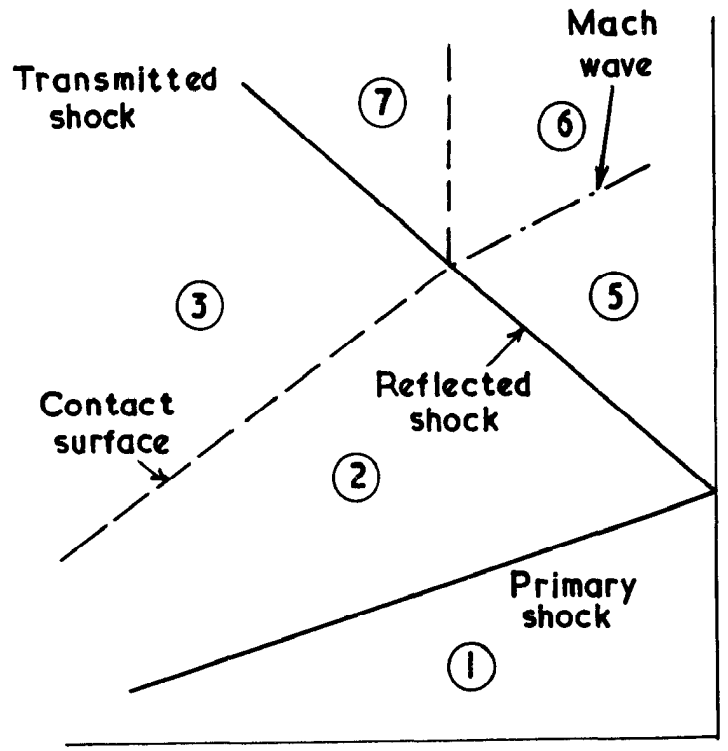

(a)

(a) Tailored interface conditions

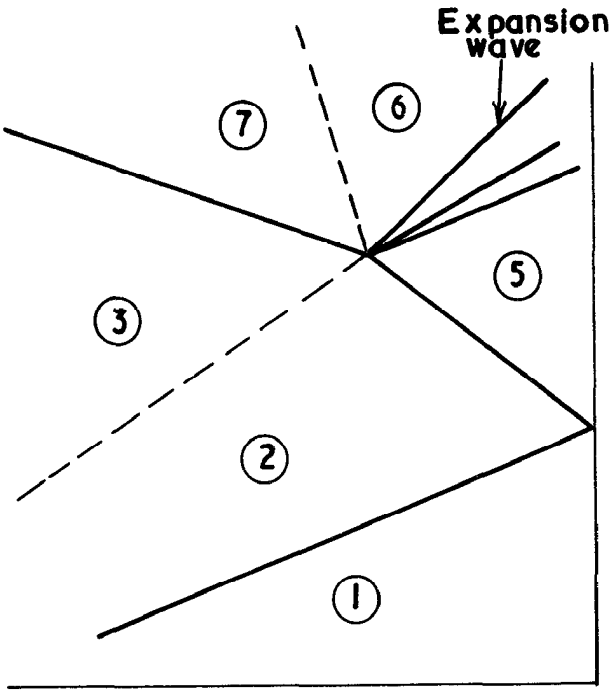

(b)

(b) Under tailored conditions

FIG. 9 (c)

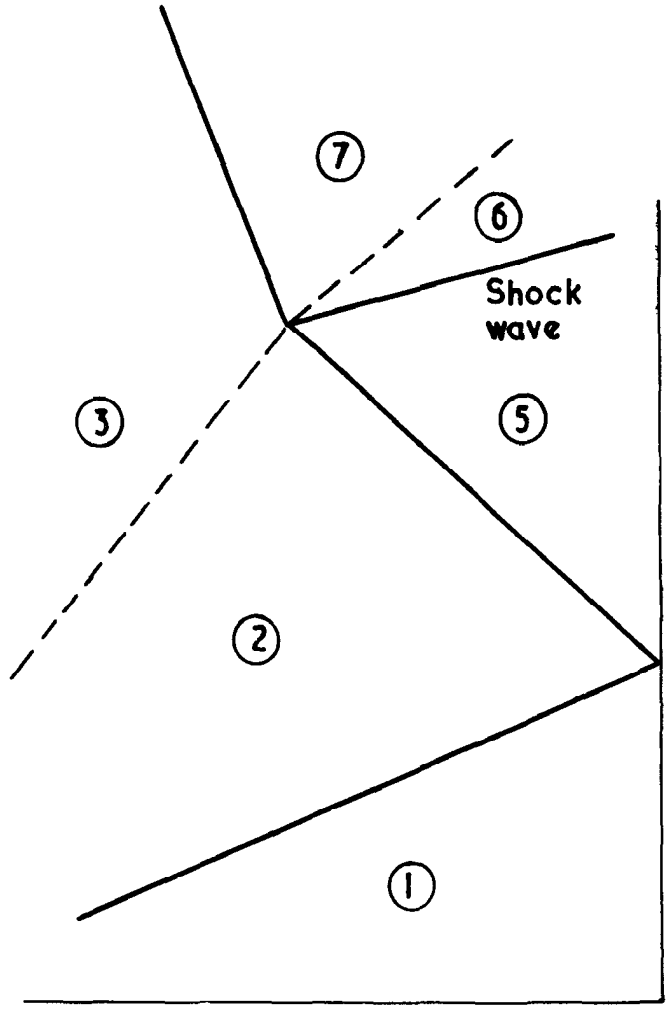

(c)

(c) Overtailored conditions

FIG. 10 (a)

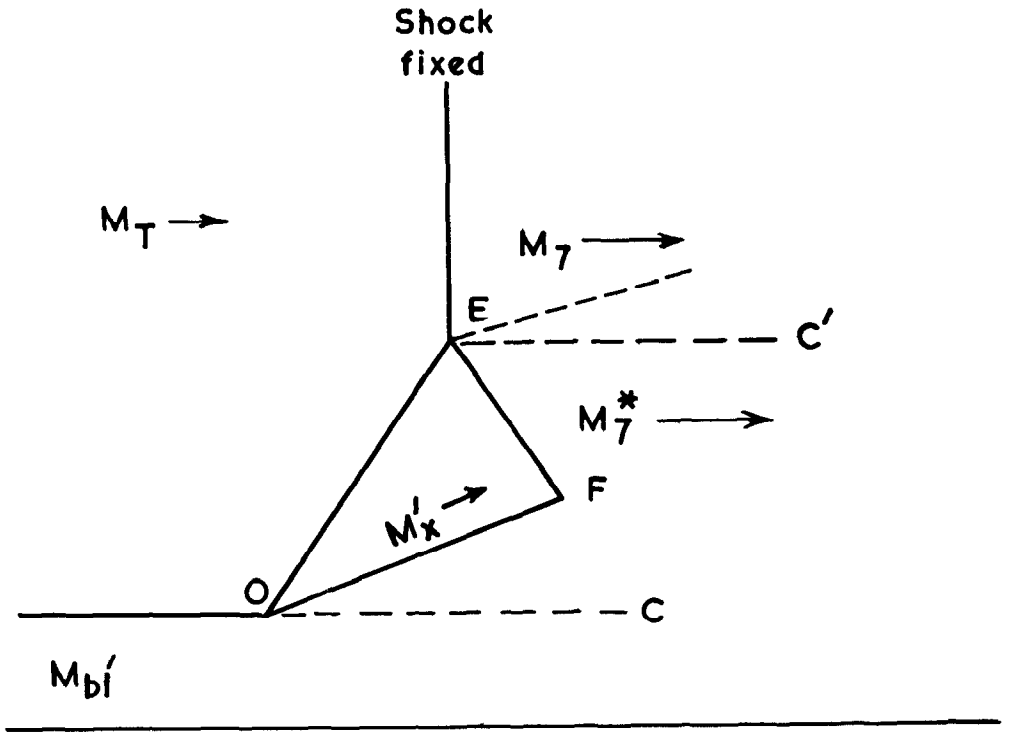

Transmitted shock bifurcated foot

FIG. 10 (b)

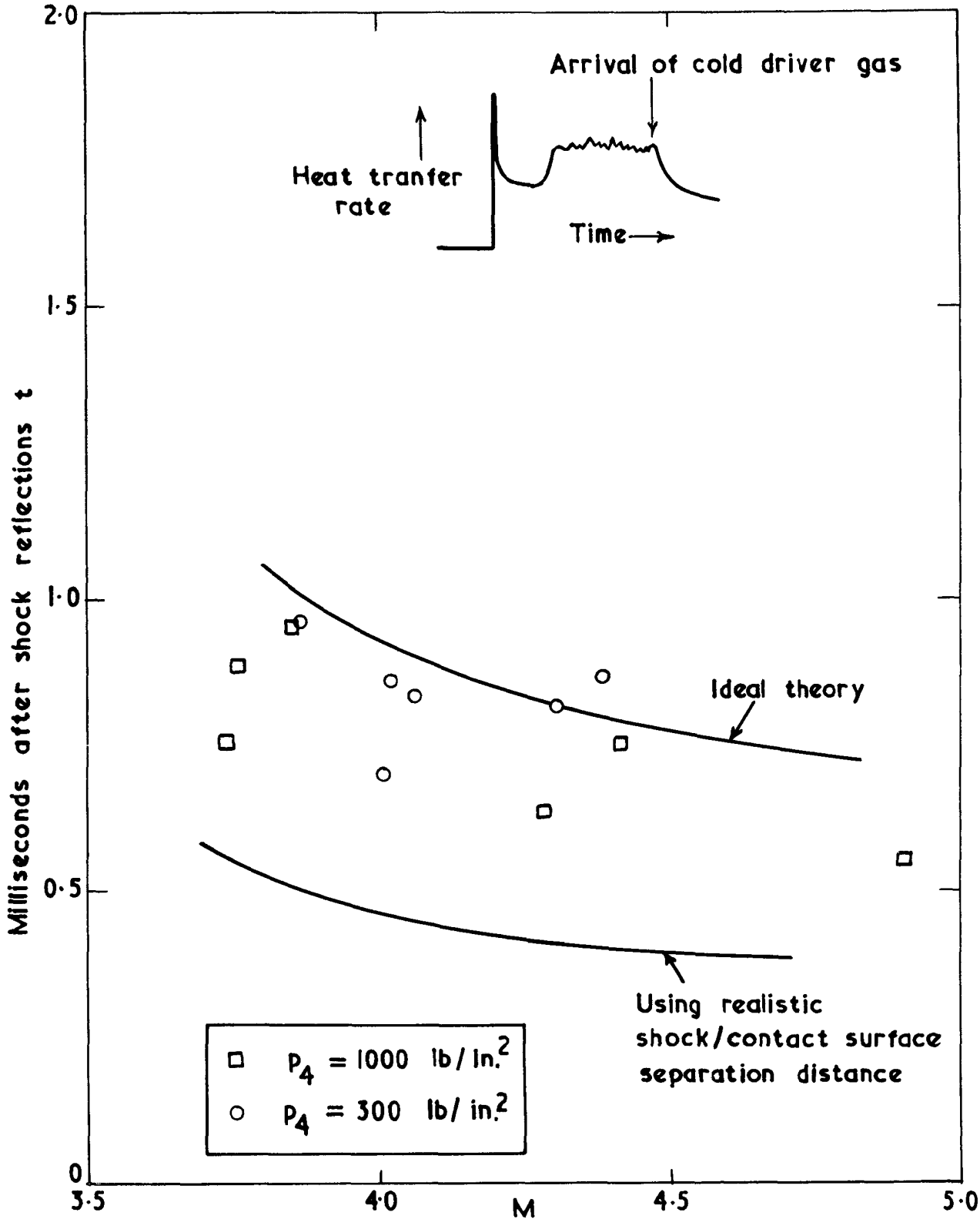

Arrival of cold driver gas at end of 2 in. shock tunnel

$$t = \frac{LU_3}{(U_3+u_3)}\left[\frac{1-u_3}{U_1}\right]\left[\frac{1}{U_3}+\frac{1}{(U^*_7=U_T)}\right]$$

FIG. 10 (c)

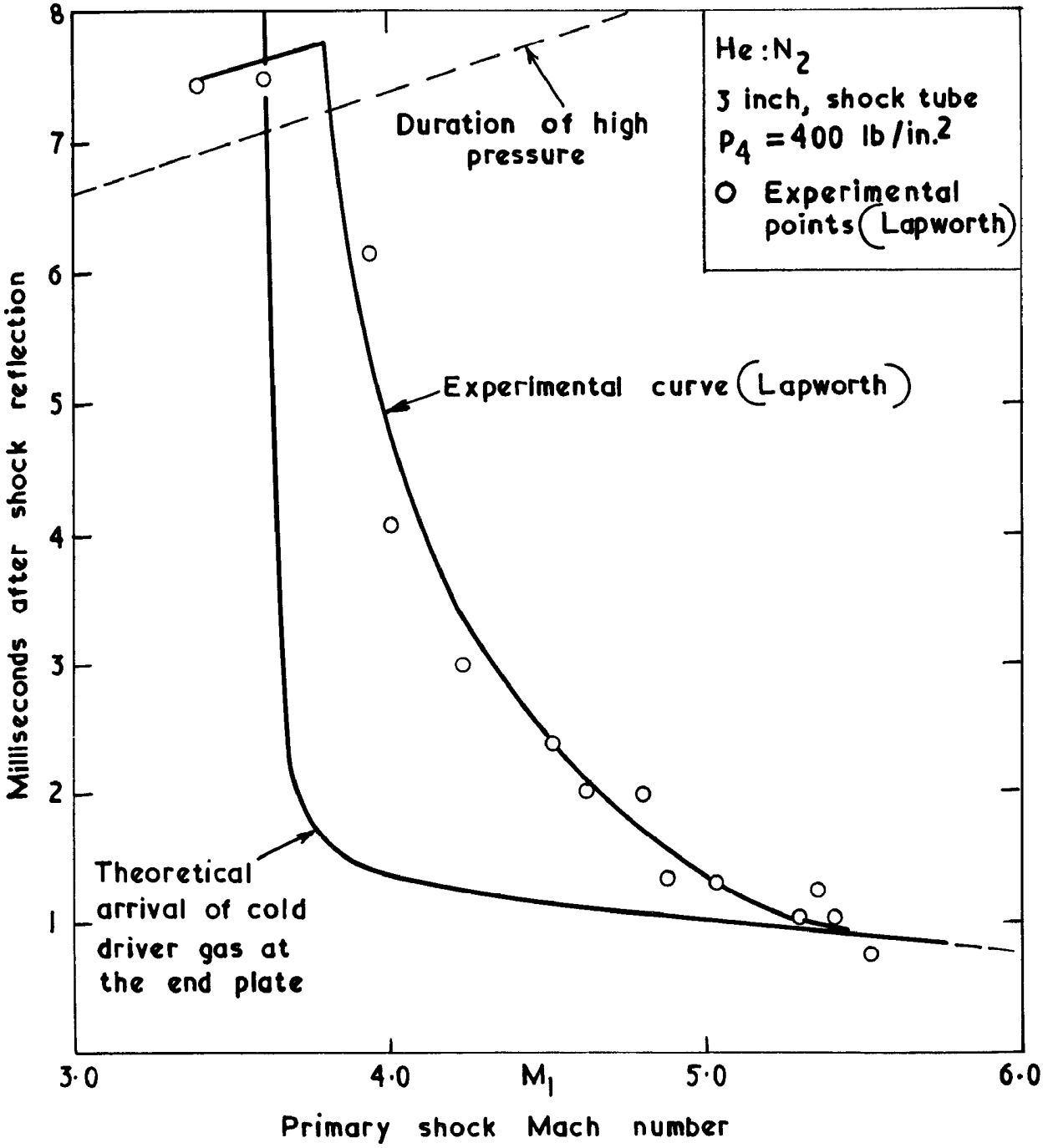

Graph showing theoretical prediction of arrival of cold gas at end plate in N.P.L. 3 inch shock tube compared with experimental high temperature duration measurements.

FIG. 11

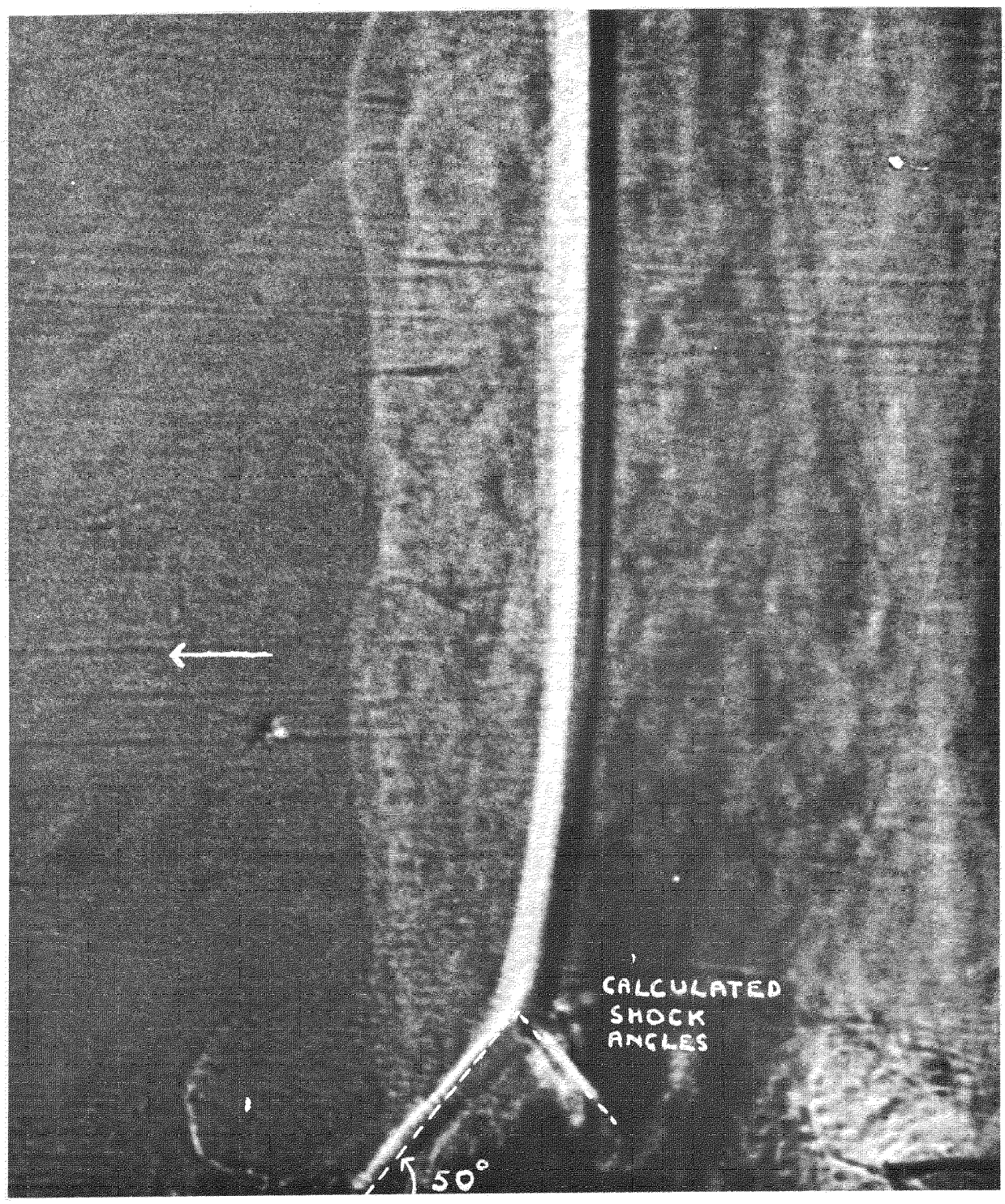

He : N_2 Comparison between experimental and theoretical bifurcated foot angles $m_s = 4.$ $p_1 = 12$ mm. Hg 6 x $3\frac{1}{2}$ inch shock tube.

FIG 12 (a)&(b)

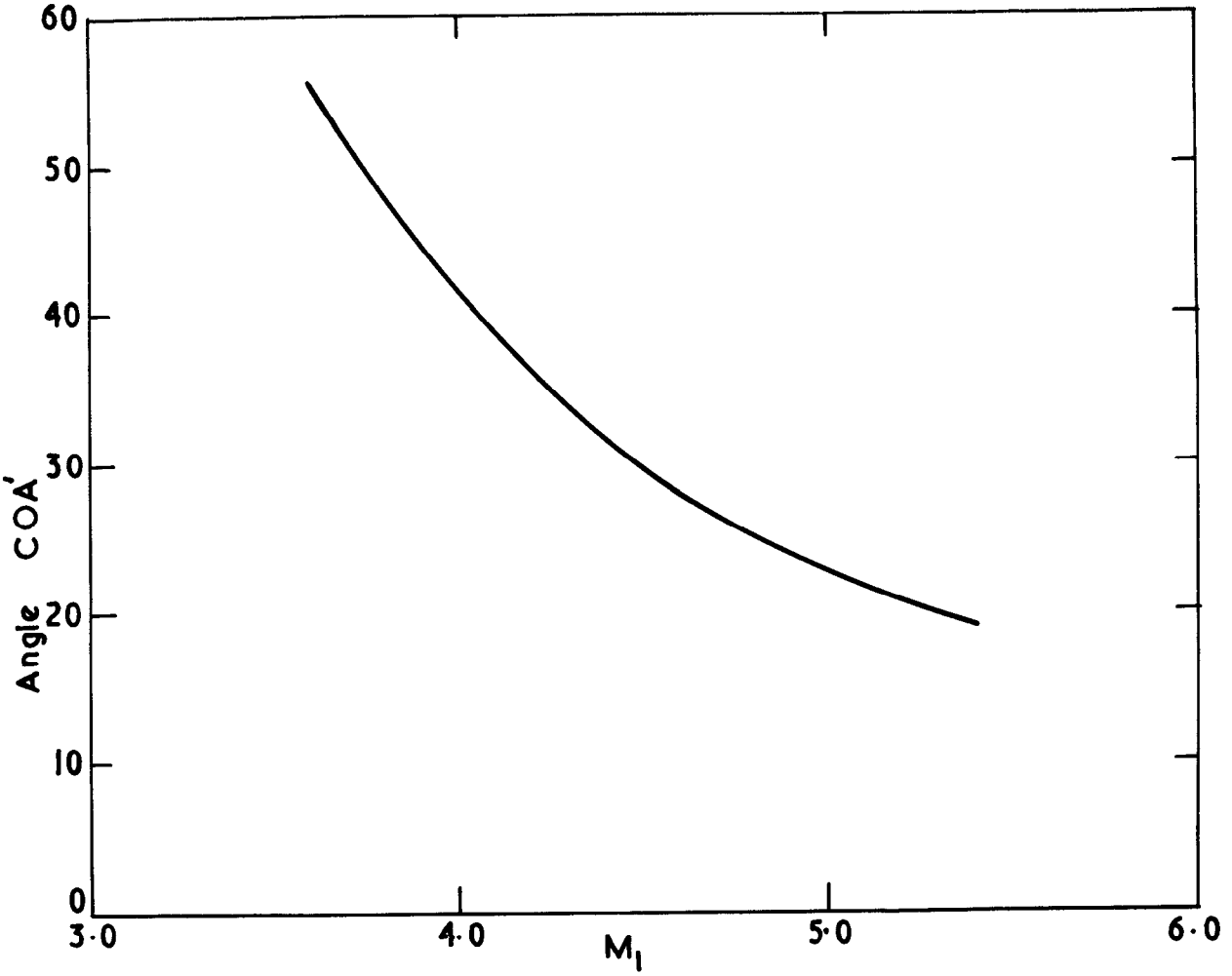

(a) Angle COA' vs M_1 for transmitted shock

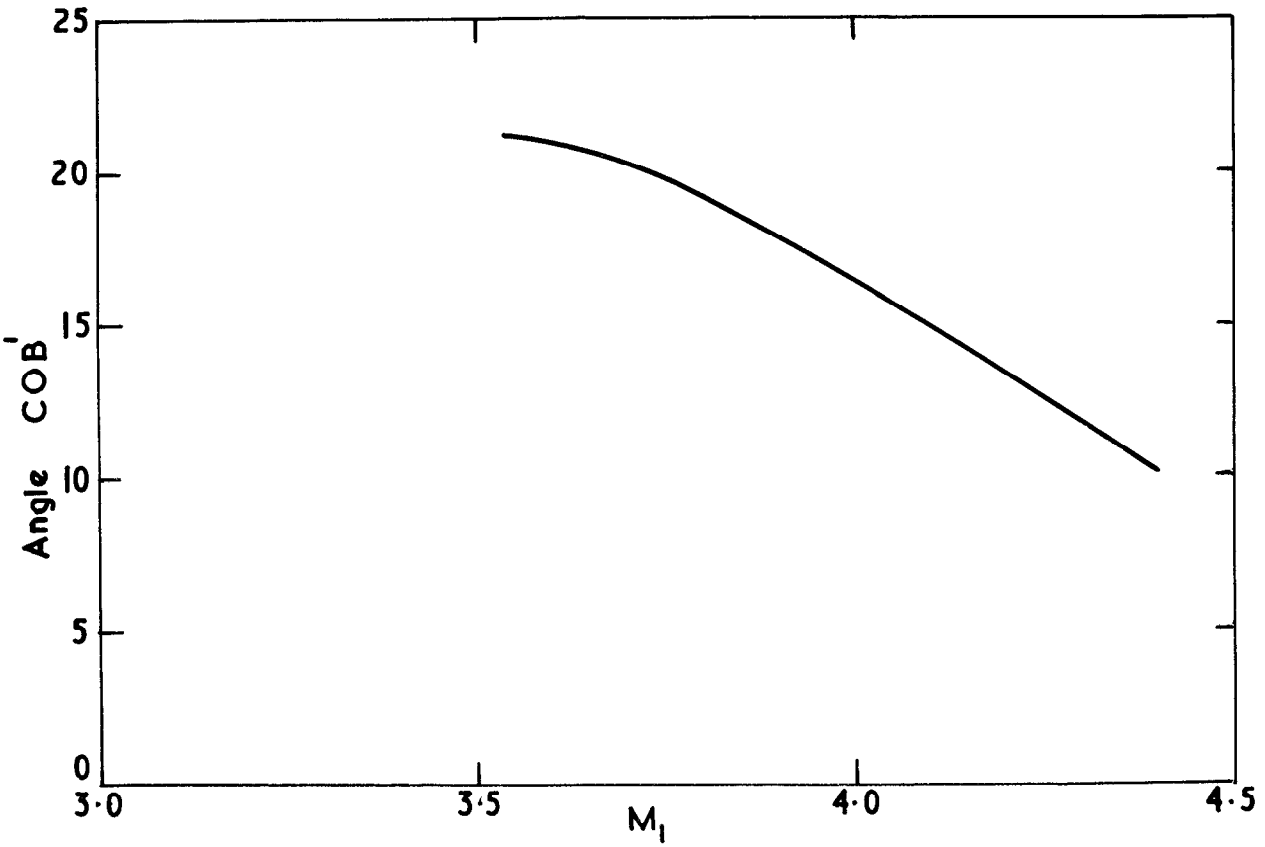

(b) Angle COB' vs M_1 for transmitted shock

FIG.12 (c)&(d)

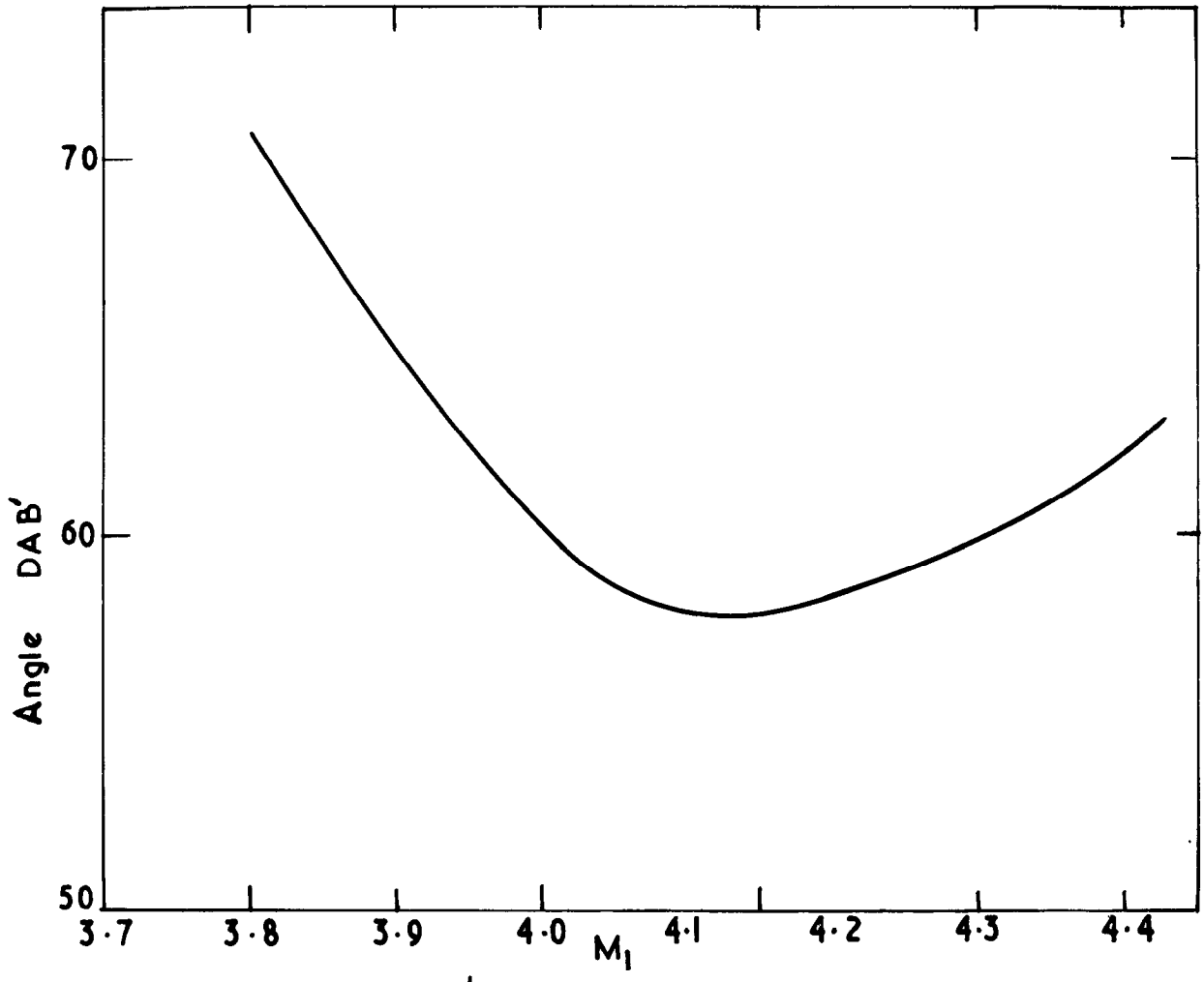

(c) Angle DAB' vs M_1 for transmitted shock

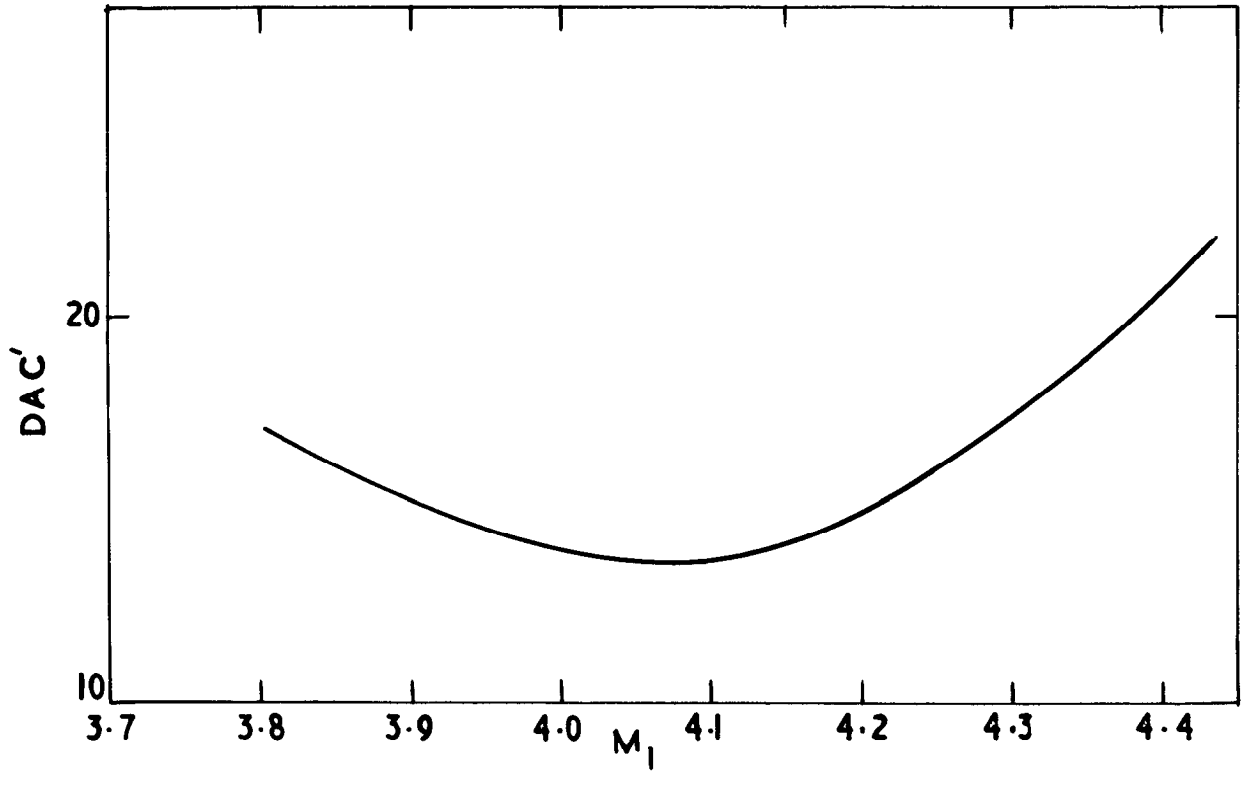

(d) Angle DAC' vs M_1 for transmitted shock

FIG. 13(a)

$P_4 \simeq 300$ p.s.i.

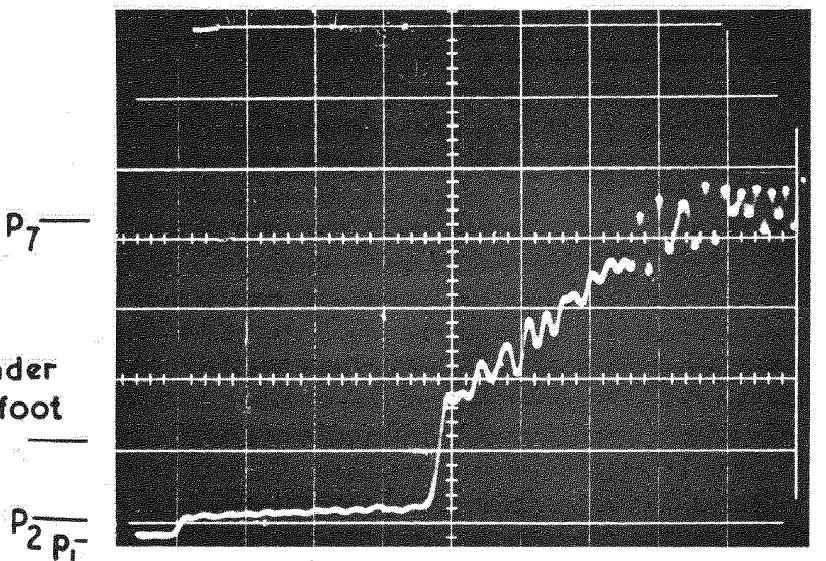

$M_1 = 5{\cdot}24$

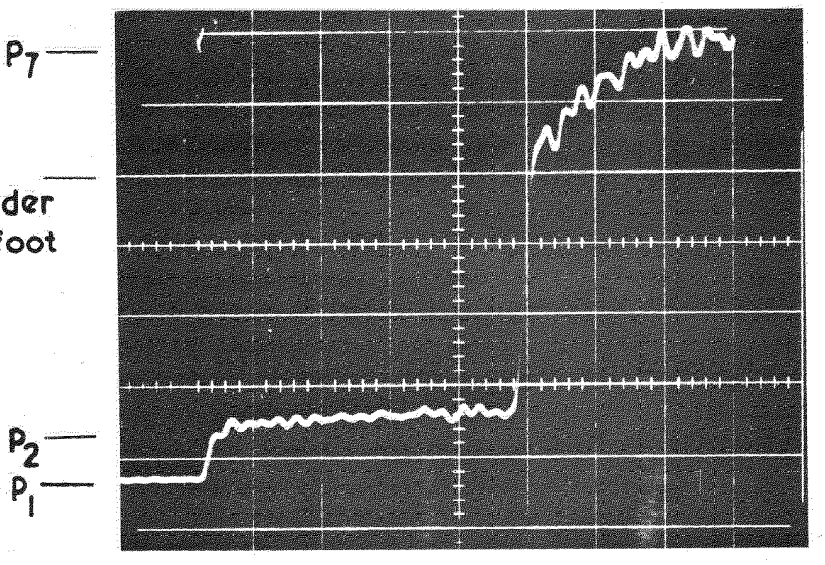

$M_1 = 3{\cdot}87$

Transmitted shock pressure measurements

FIG.13 (b)

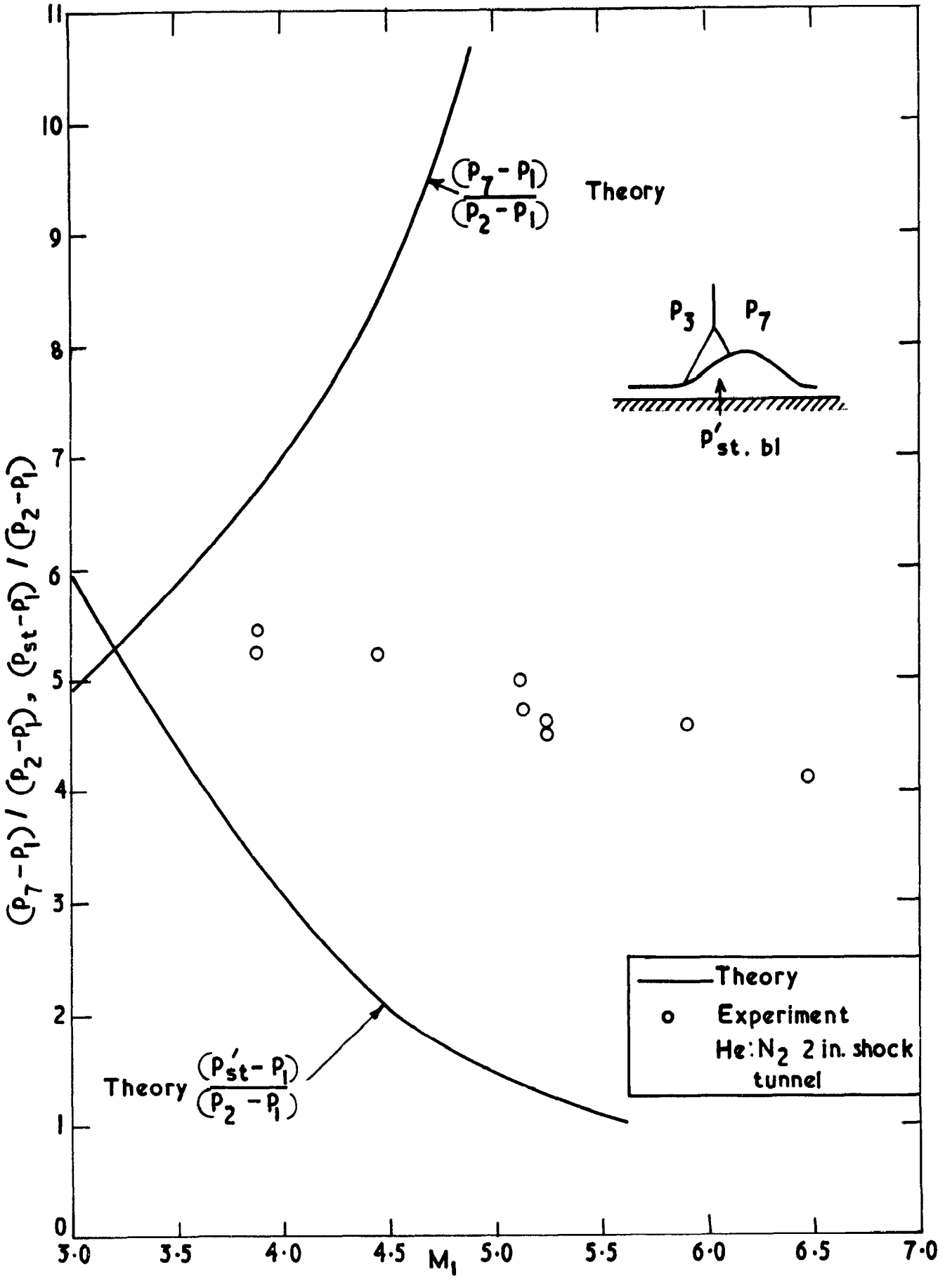

Graph showing divergence of p_7 and p'_{st} values with M_1 increasing for transmitted shock

FIG.13 (c)

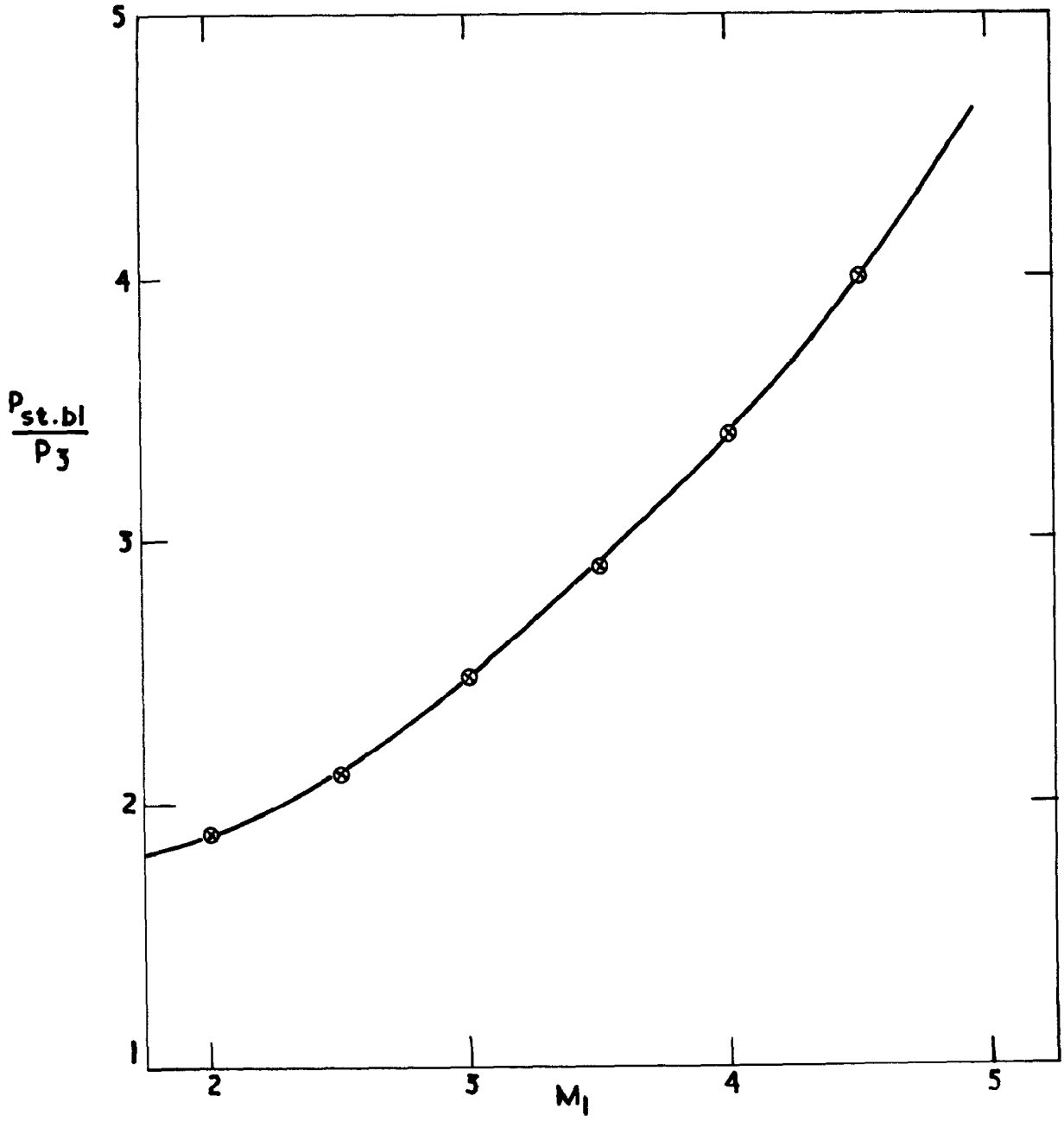

$\frac{P_{st.bl}}{P_3}$ vs M_1 for reflected shock

FIG.14

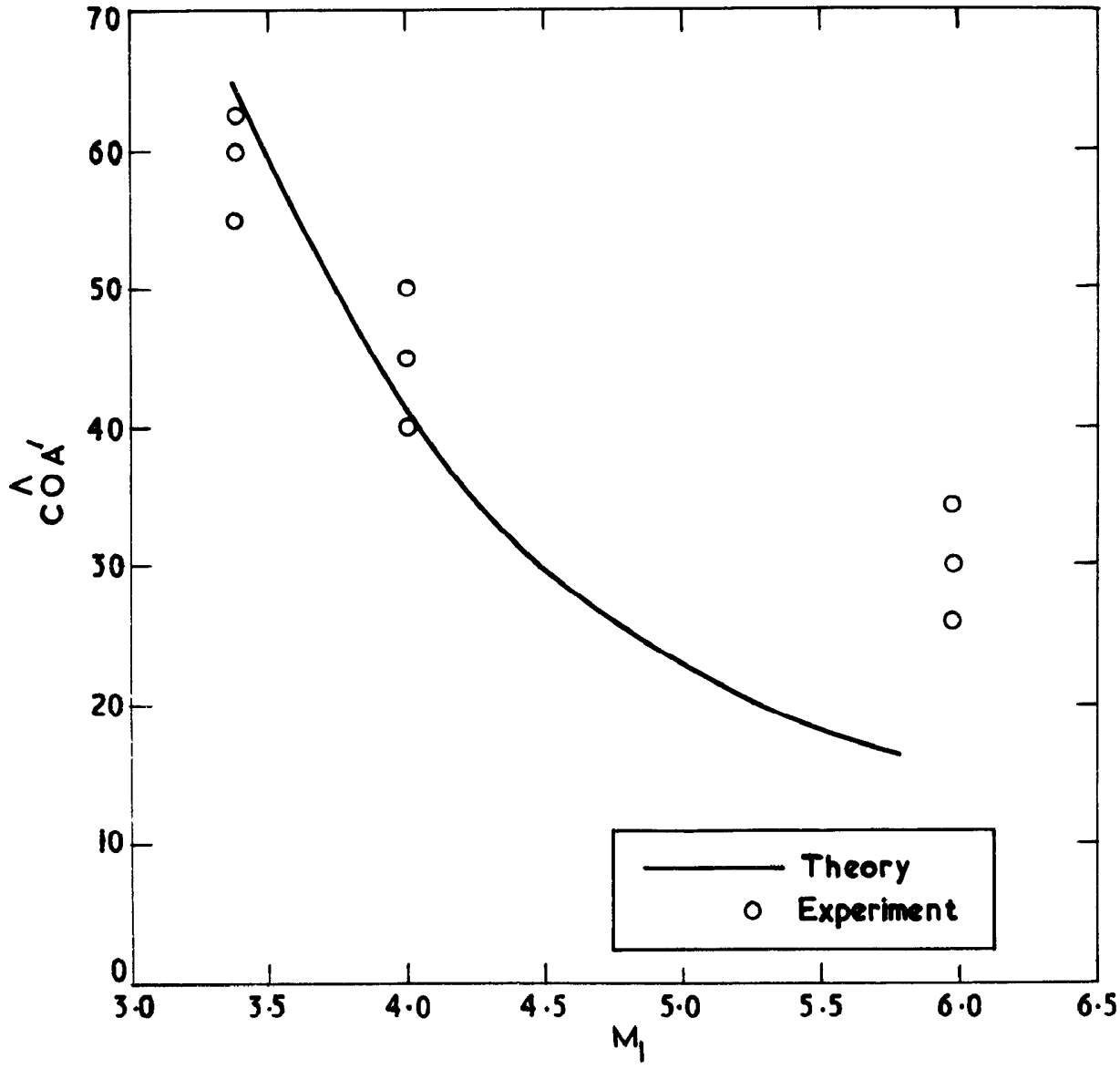

$\angle COA'$ vs M_1 for transmitted shock

FIG.15

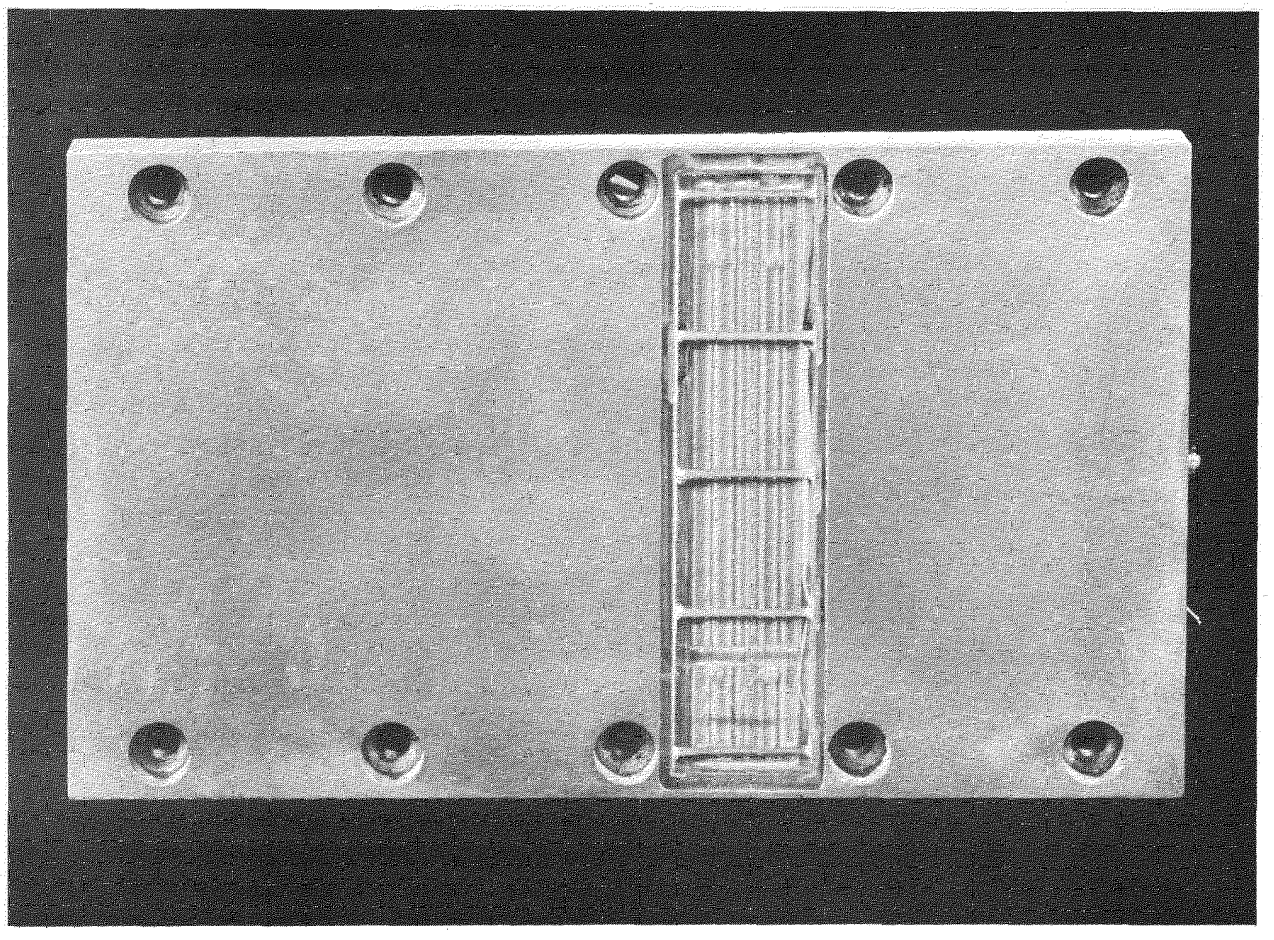

End plate 6 x 3 1/2 in. shock-tube showing heat transfer plate with thin film gauges. See Fig. 16 for description of essential features

FIG.16

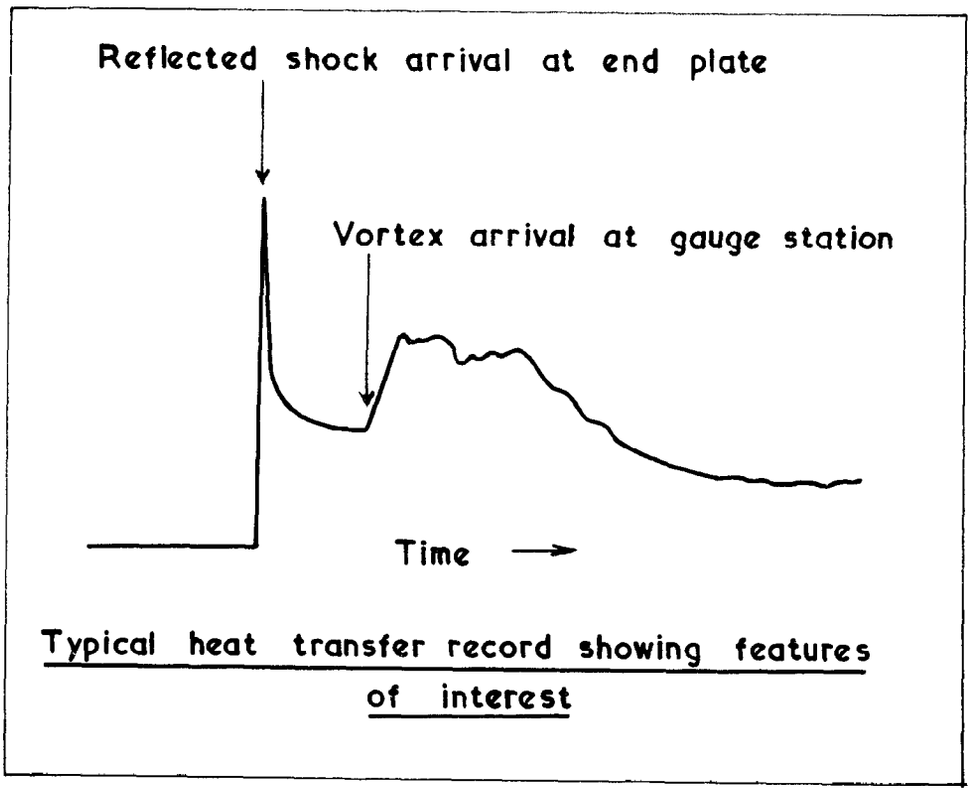

Typical heat transfer record showing features of interest

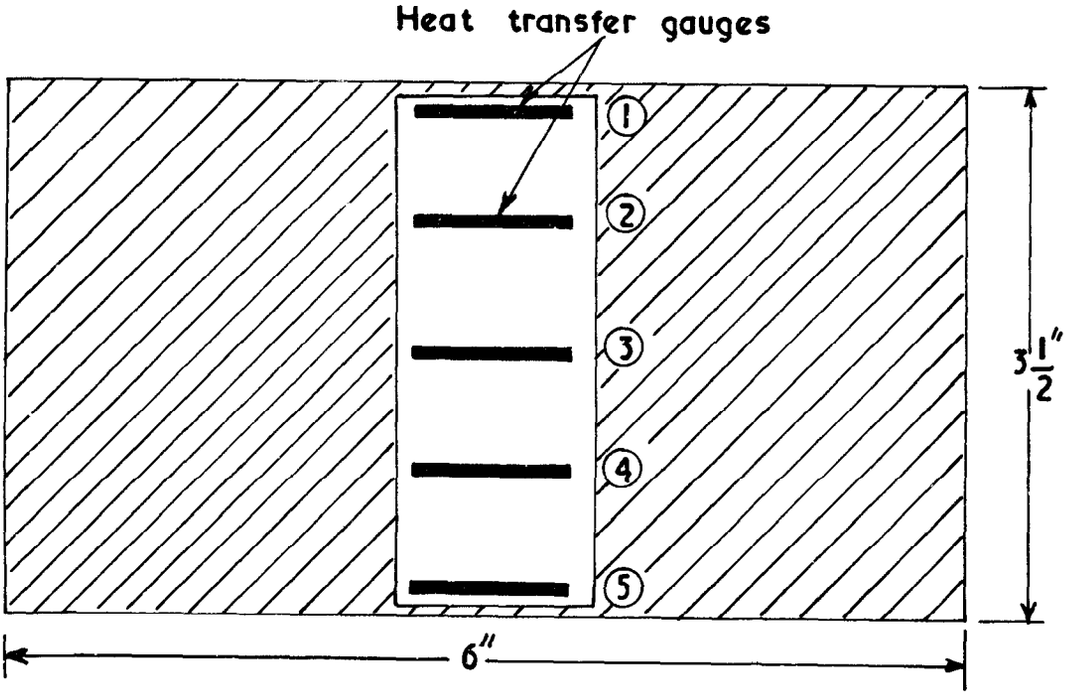

End plate layout showing gauge positions

FIG. 17 (a)

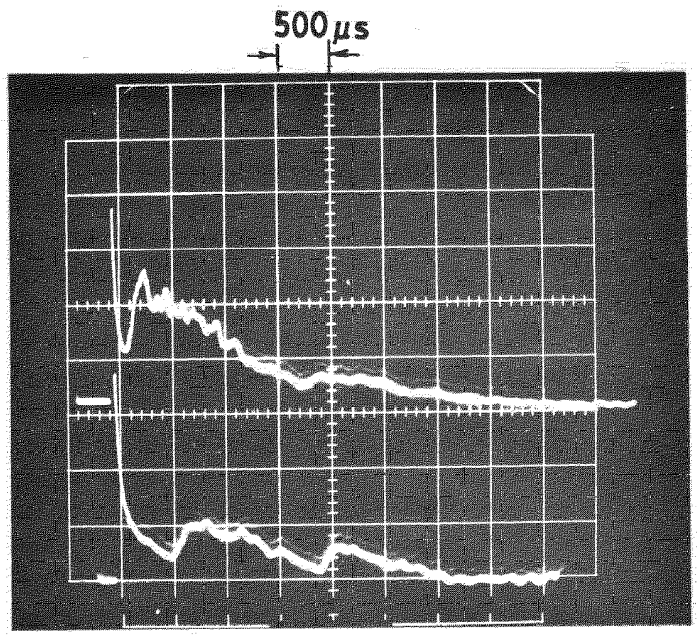

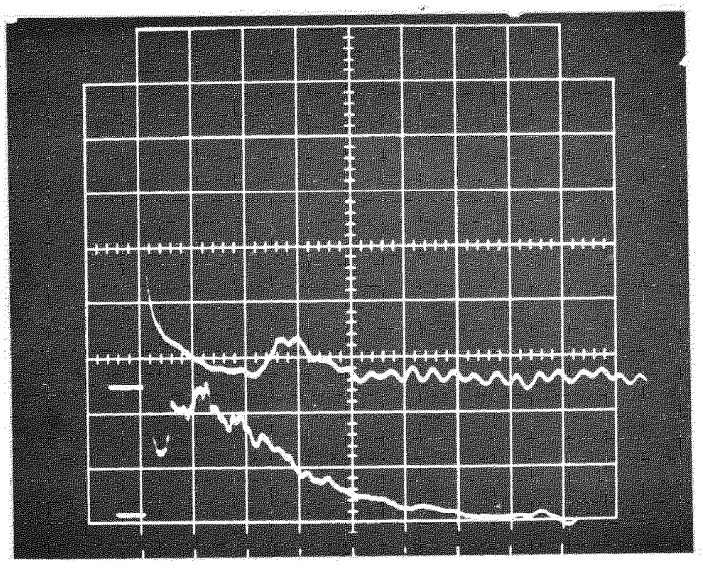

Heat transfer records

End plate
$6 \times 3\frac{1}{2}$ inch
shock tube

$M_1 = 3.56$ $p_1 = 22.5$ mm .

Numbers (1) (2) (3) (5) refer to gauge positions shown in Fig. 16

FIG. 17 (b)

500 μs

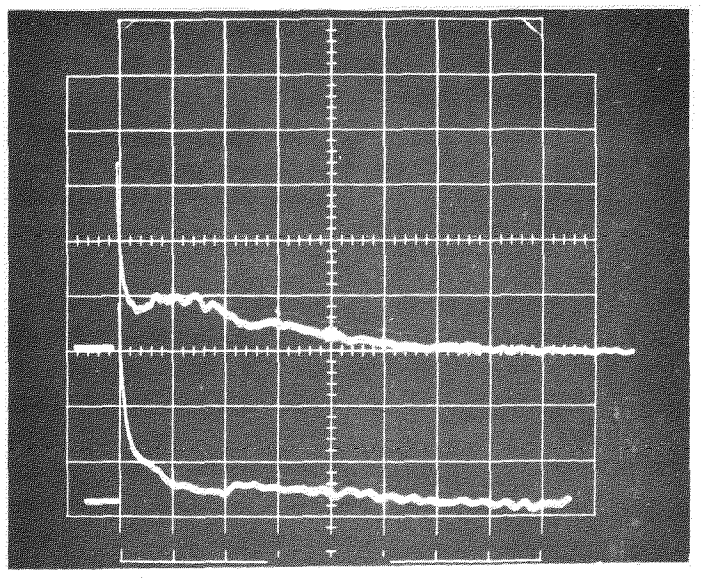

①

②

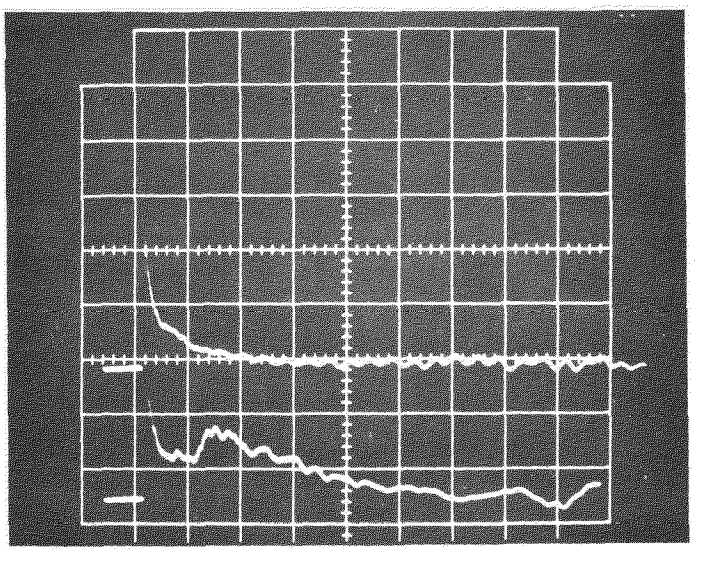

③

⑤

Heat transfer records

End plate
6 x 3 1/2 inch
shock tube

$M_1 = 3.14$ $p_1 = 64$ mm.

Numbers ① ② ③ ⑤ refer to gauge positions shown in Fig. 16

FIG. 17 (c)

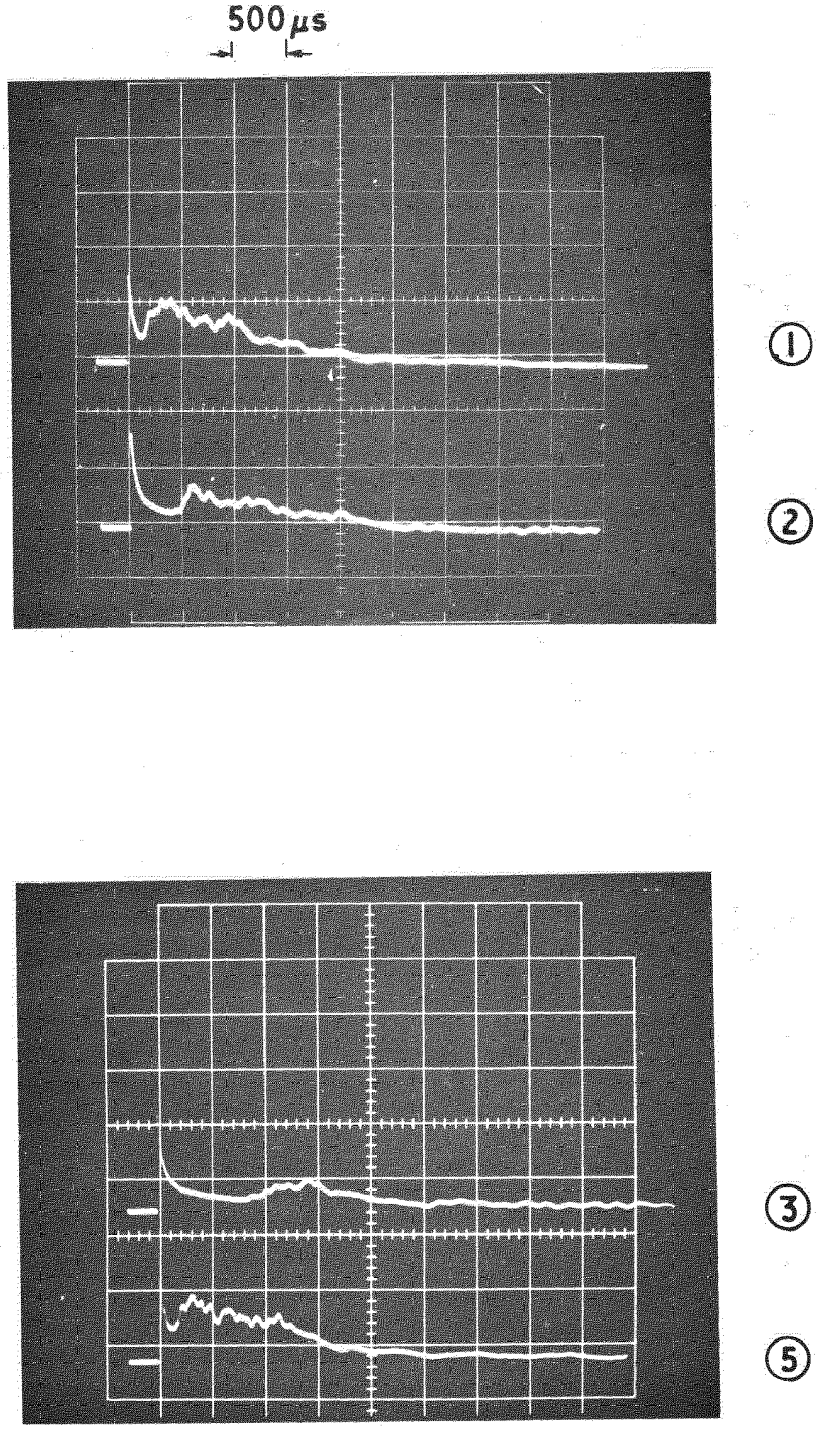

Heat transfer records

End plate
6 x 3 1/2 inch
shock tube

Numbers ① ② ③ ⑤ refer to gauge positions shown in Fig. 16

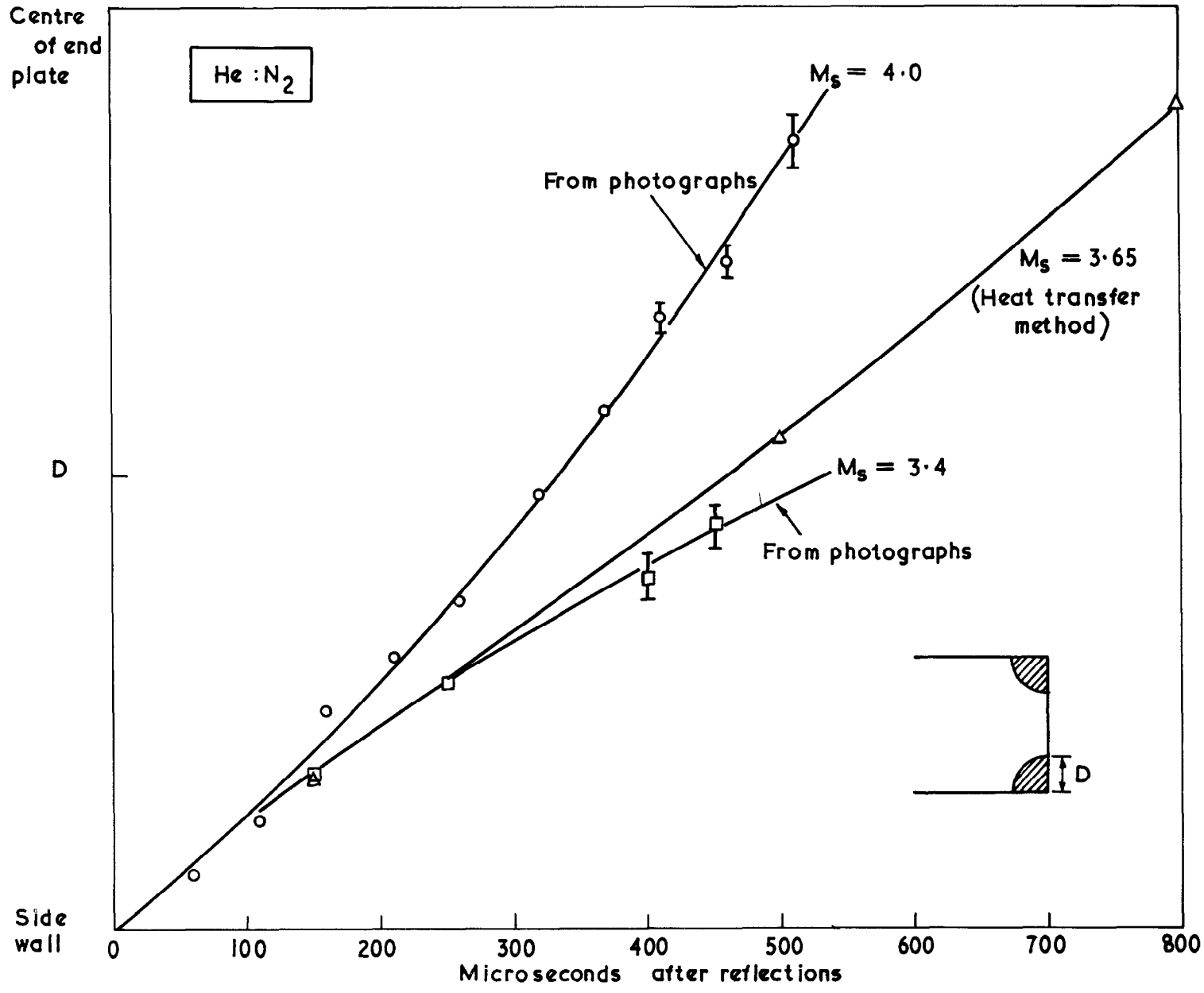

FIG. 18

Gas movement across the end plate in the 6 in. x 3 1/2 in. shock tube

FIG. 19

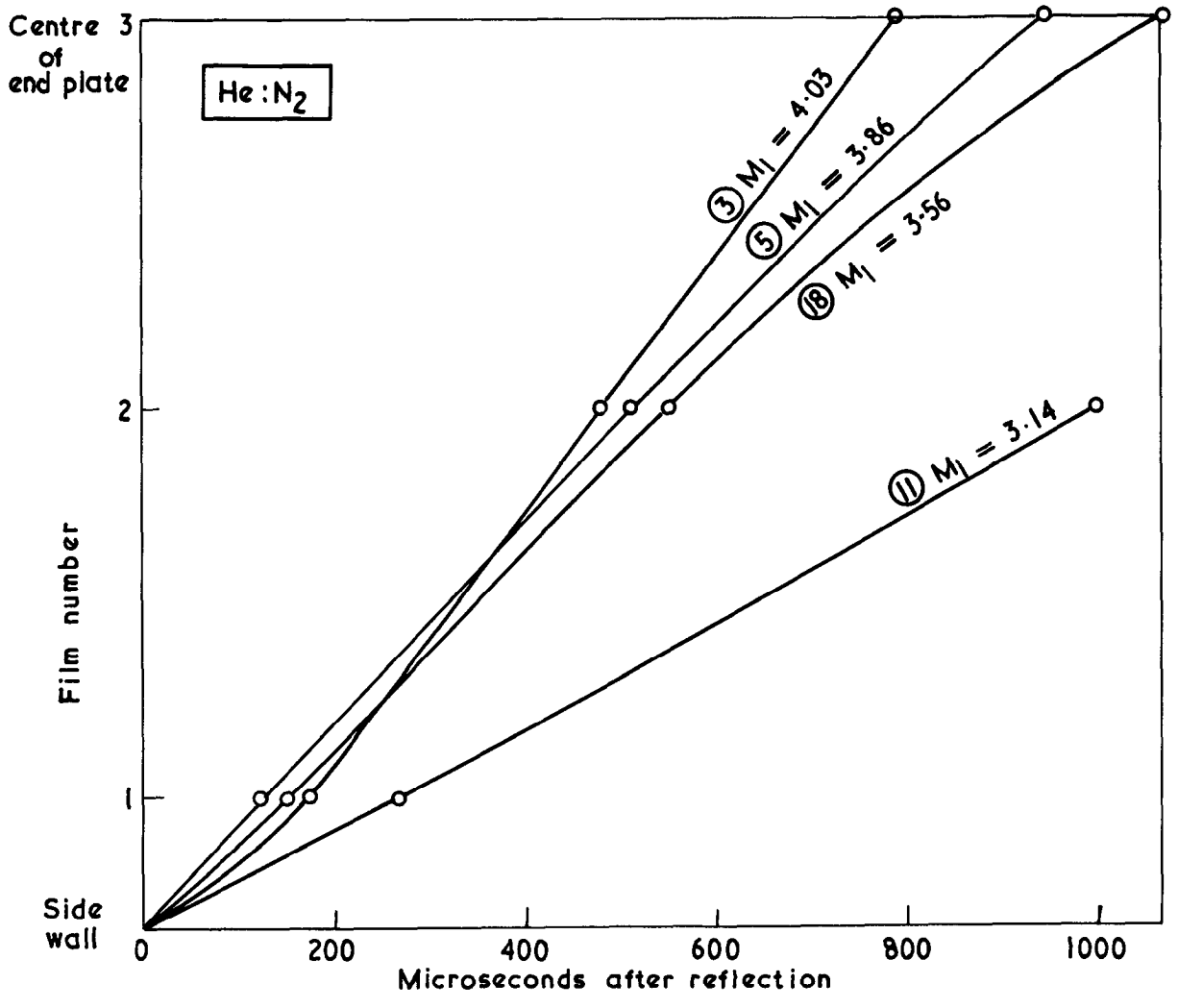

Gas movement across the end plate in the 6 in. x 3½ in. shock tube

FIG. 20

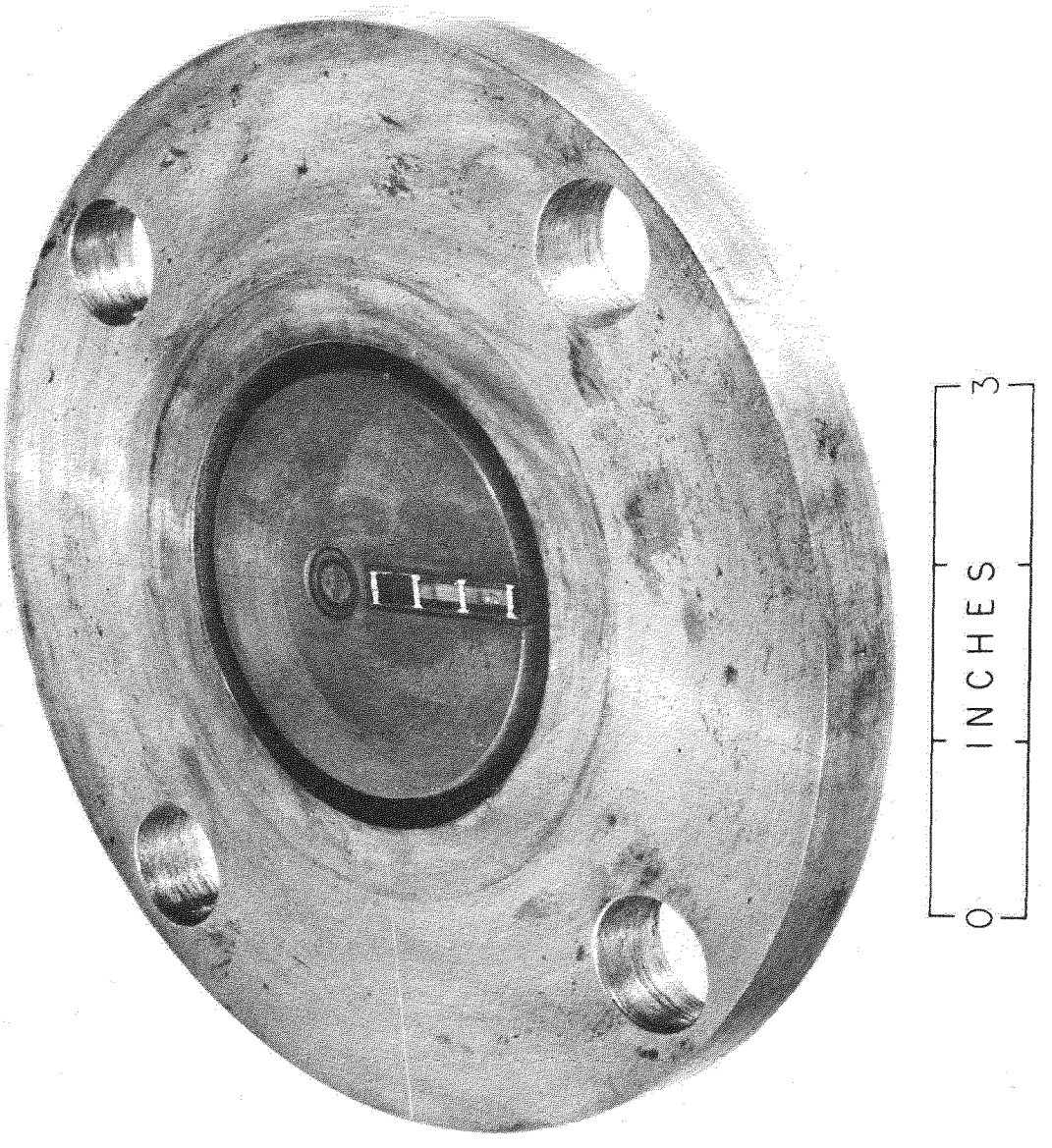

End plate 3 inch shock tube

FIG. 21

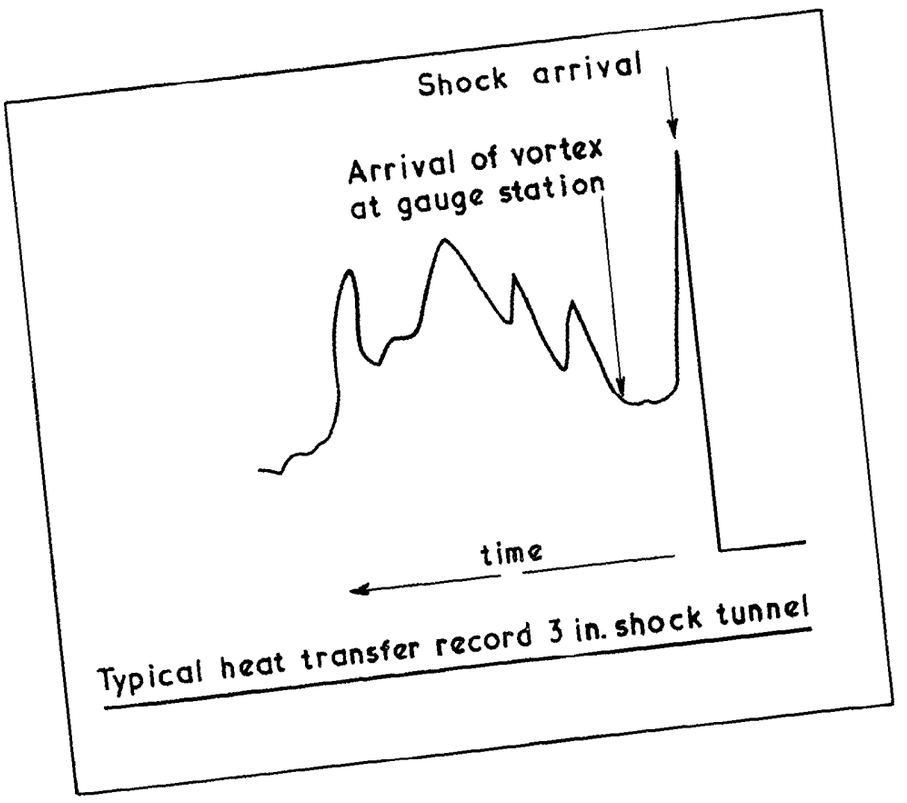

Typical heat transfer record 3 in. shock tunnel

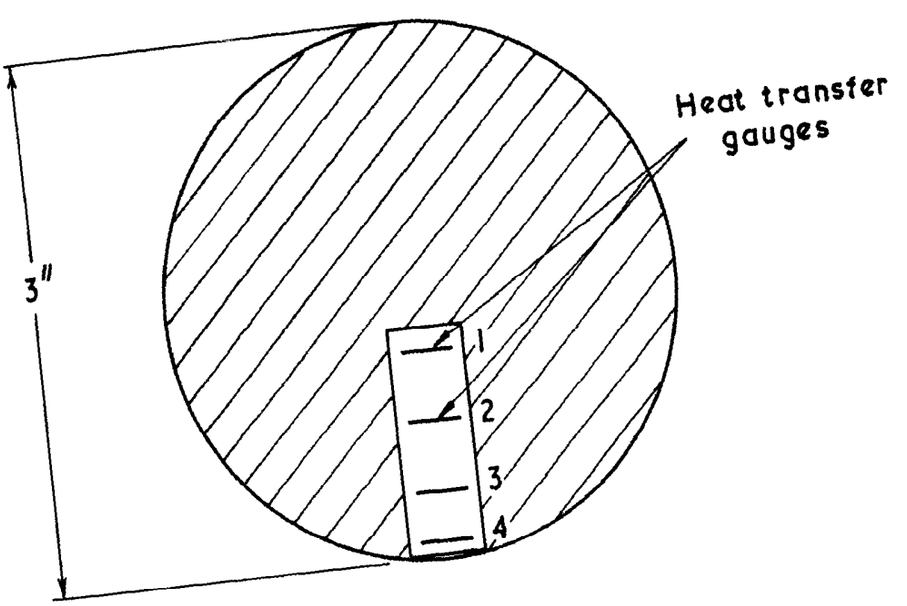

End plate layout 3in. shock tube

FIG. 22

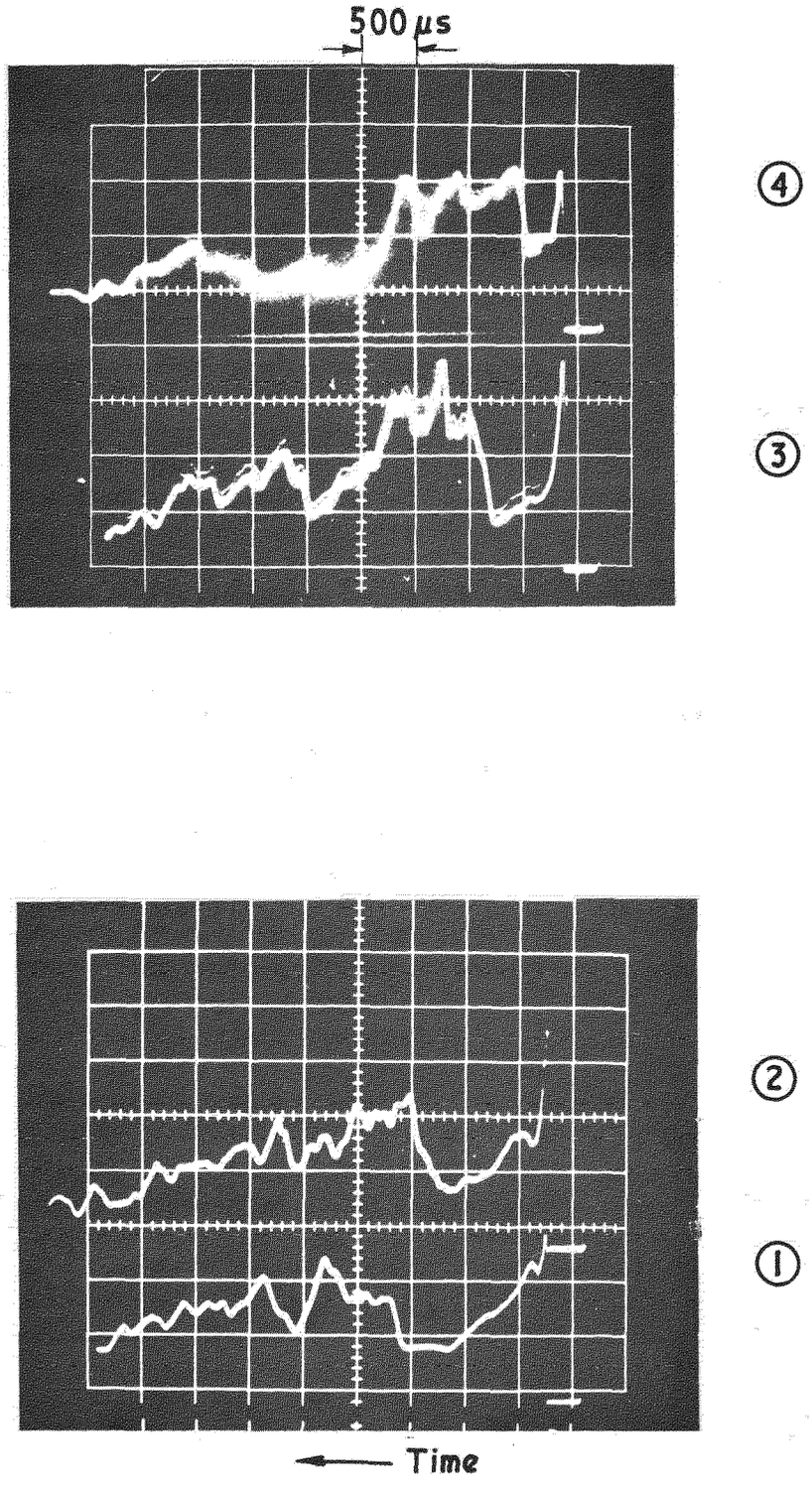

$M_1 = 3{\cdot}7$ $p_4 = 400$p.s.i.

Numbers ①②③④ refer to gauge position as shown in Fig. 21

FIG. 23

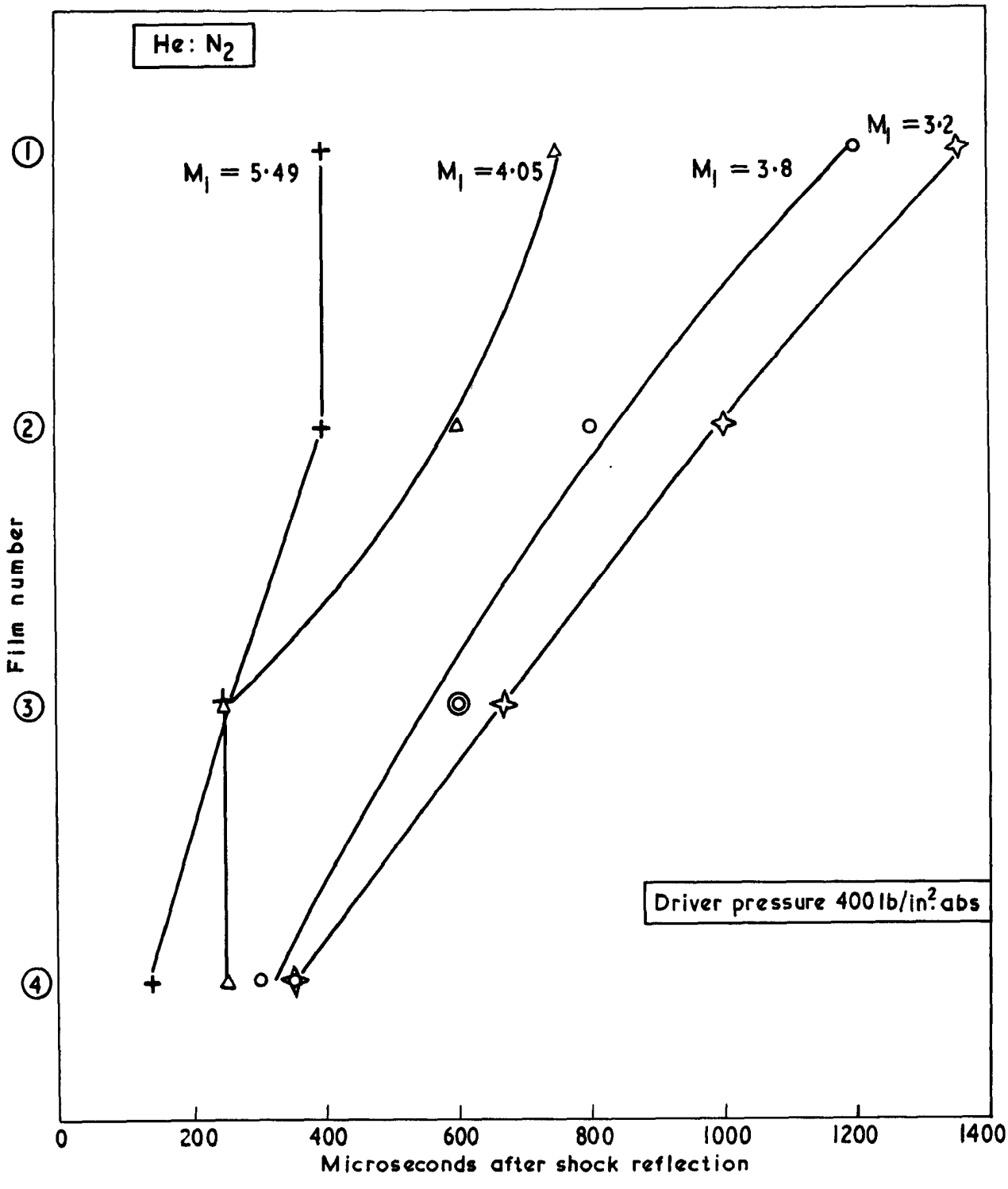

Vortex growth at the end plate of a 3 inch shock tube

FIG. 24(a)

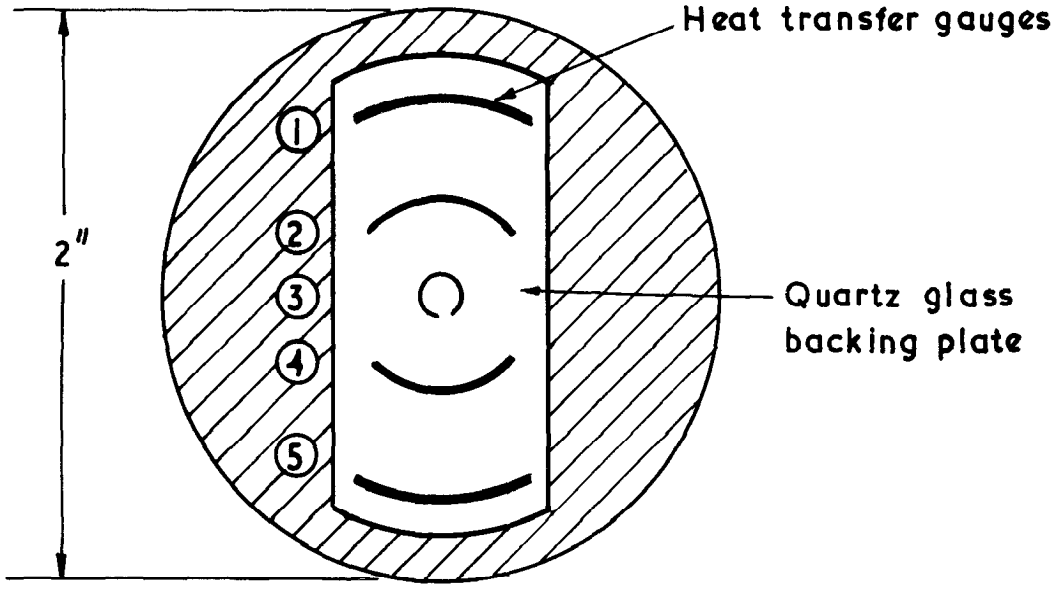

End plate 2 inch shock tunnel showing heat transfer gauge layout

FIG. 24 (b)

P_4 = 140 He P_1 = 1·2 N_2 M_1 = 3·56

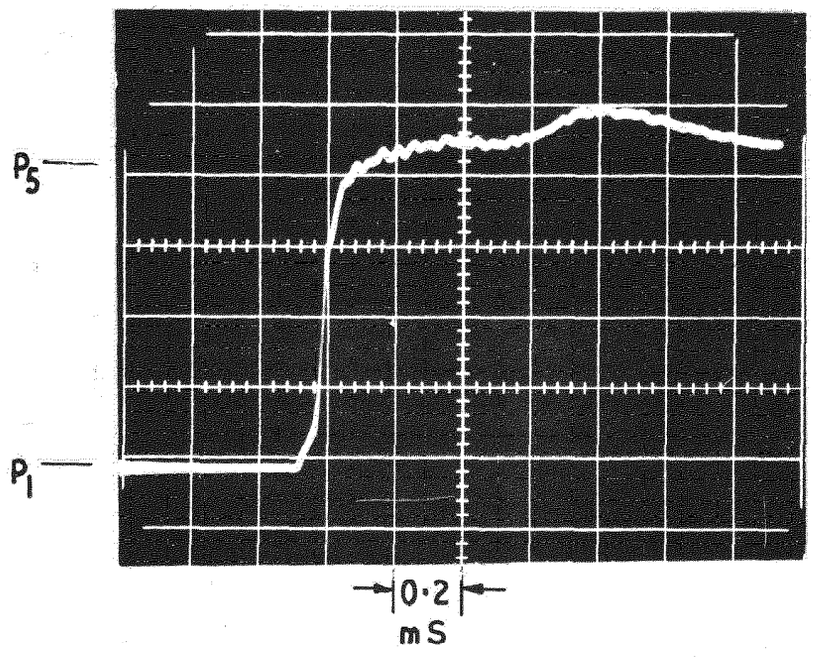

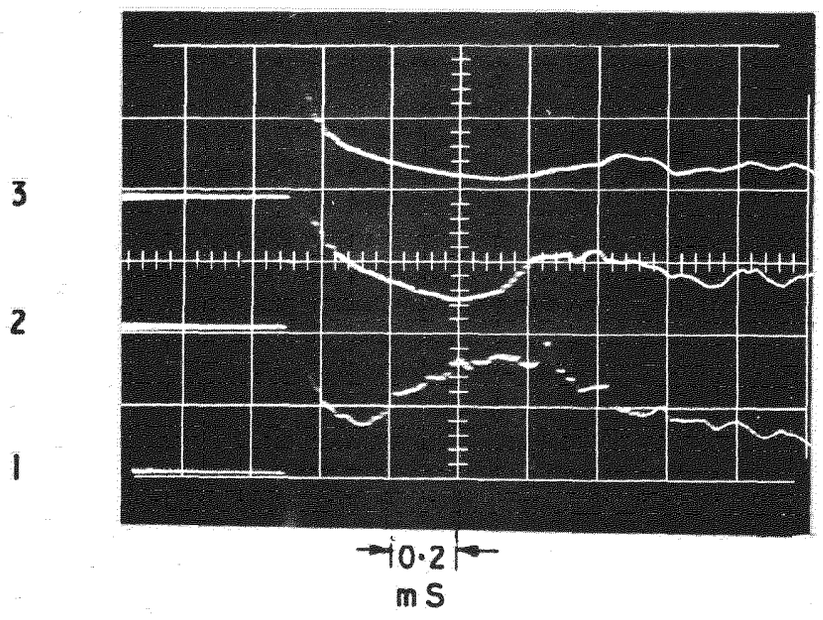

FIG. 24 (c)

P_4 = 189 He P_1 = 3·2 N_2 M_1 = 3·51

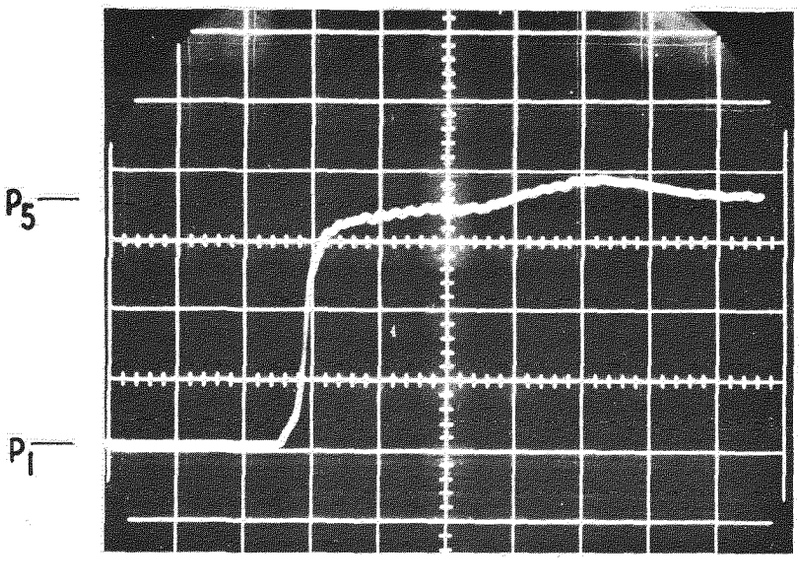

Pressure Record

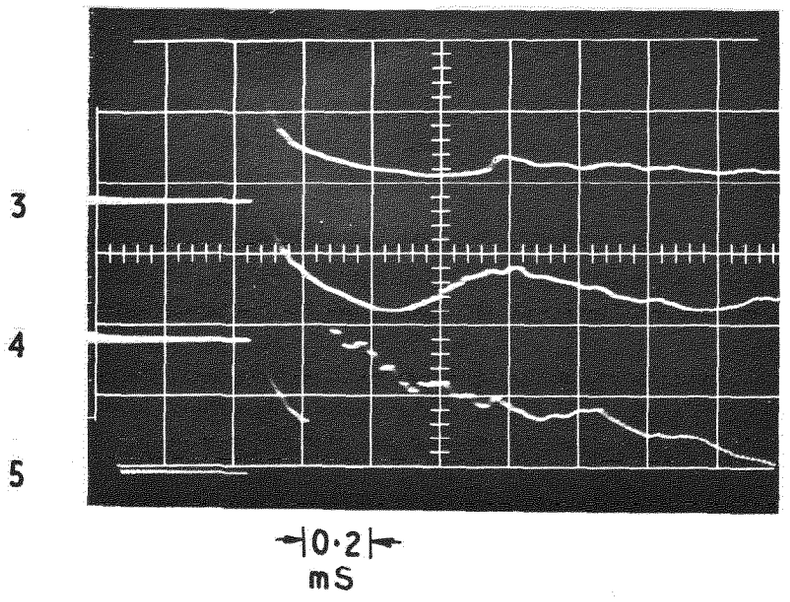

Heat Transfer Record

FIG. 24 (d)

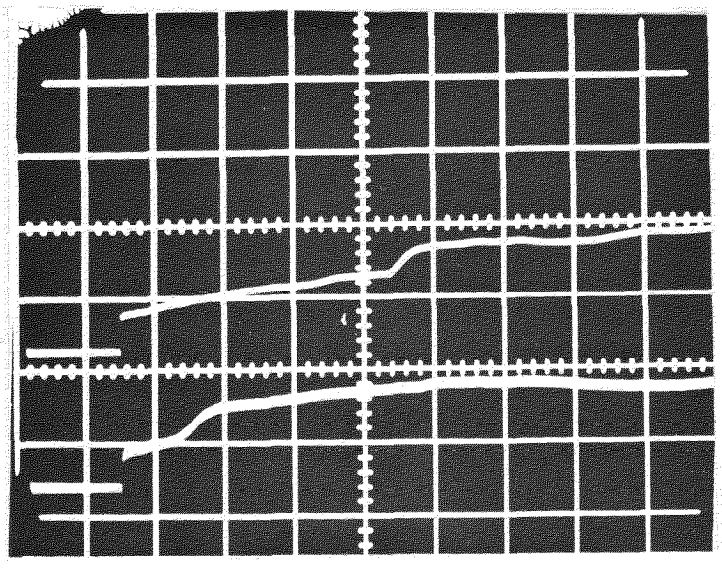

Temperature Record
0·2mS/cm

P_4 = 1000 He P_1 = 16 N_2 M_1 = 3·11

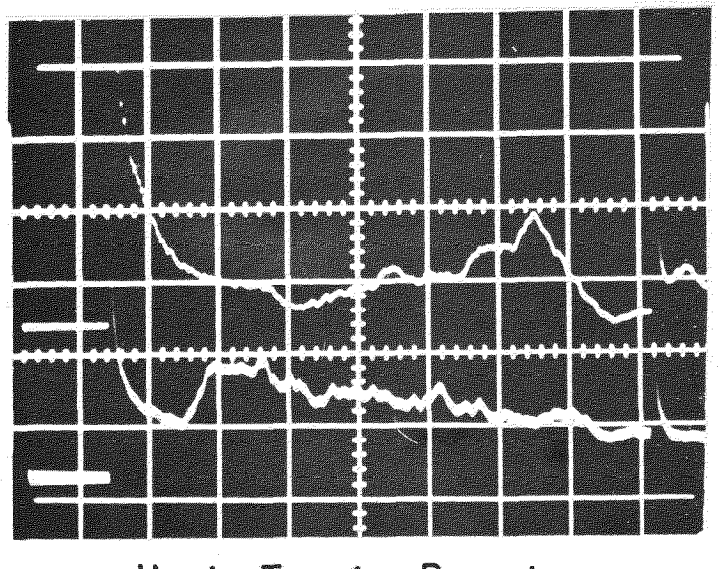

Heat Transfer Record
0·2 mS/cm

P_4 = 1000 He P_1 = 10 N_2 M_1 = 3·45

FIG. 25

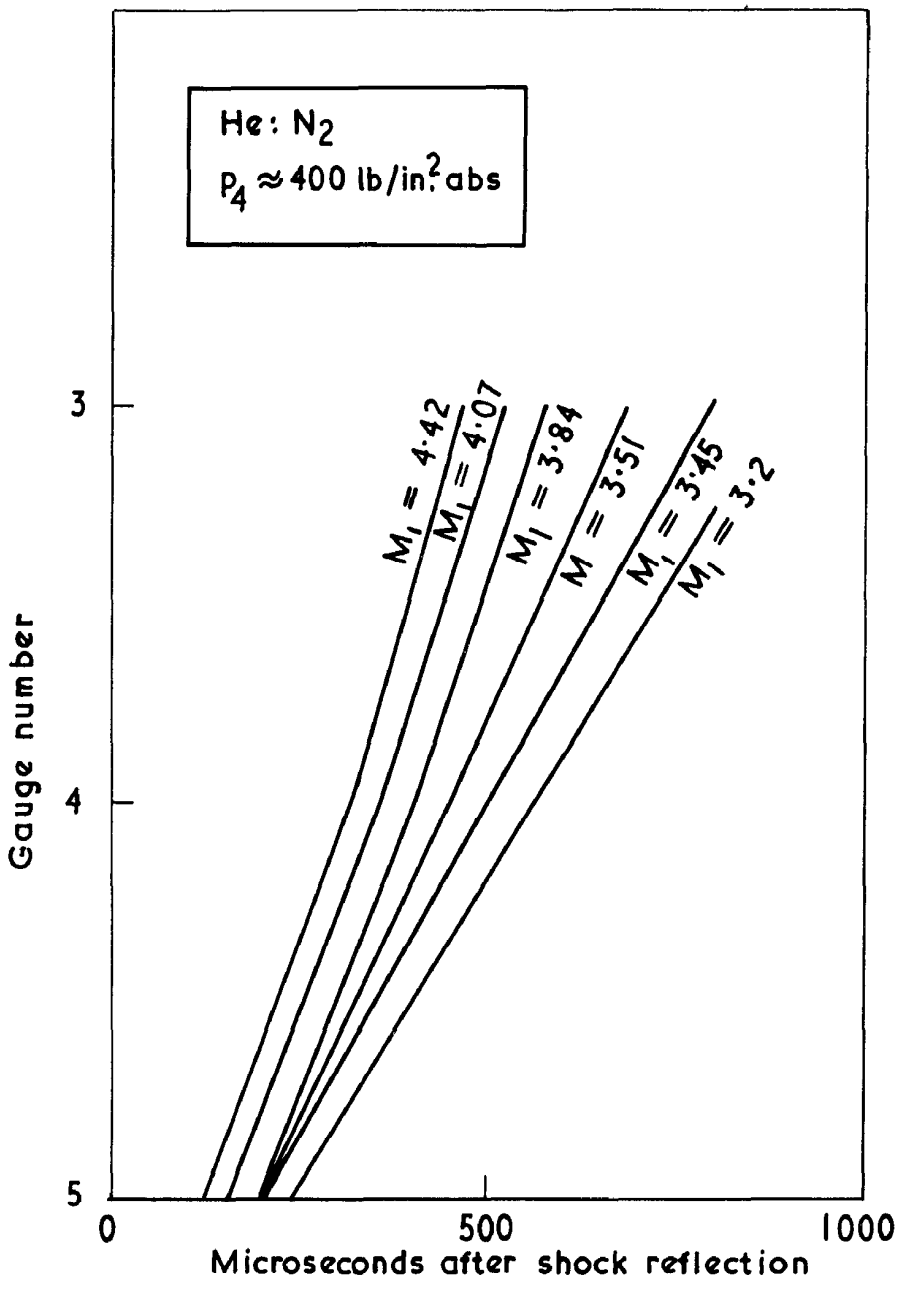

Rate of movement of gas across the end plate

2 in. shock tunnel

FIG. 26 (a)

P_4 = 305 lb/in.^{2} H P_1 = 4·0 lb/in.^{2} Argan M_1 = 3·18

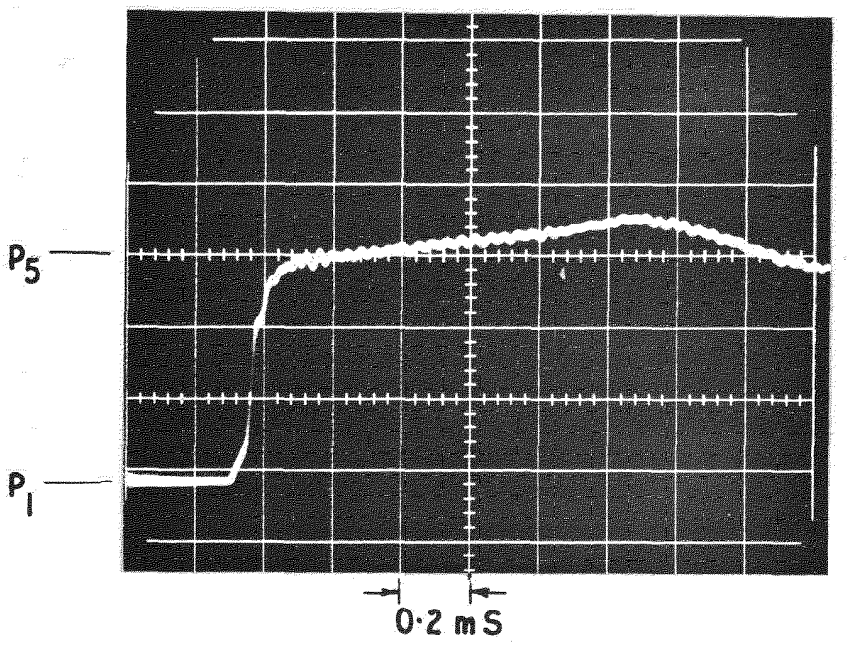

Reflected shock pressure profile

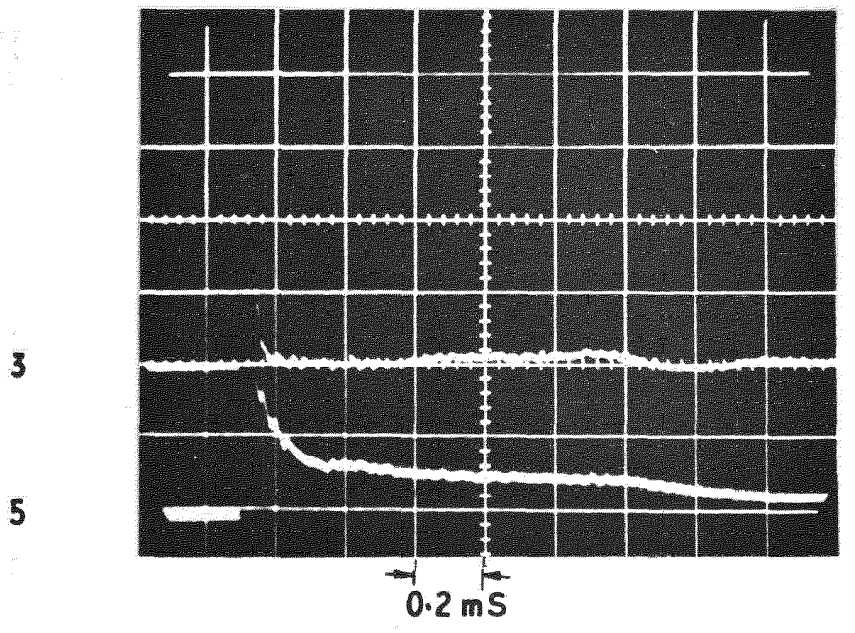

Heat transfer records

Pressure and heat transfer records He:A. 2 inch shock tunnel

FIG. 26 (b)

P_4 = 379 lb/in.^{2} He P_1 = 5 lb/in.^{2} N_2 M_1 = 3·2

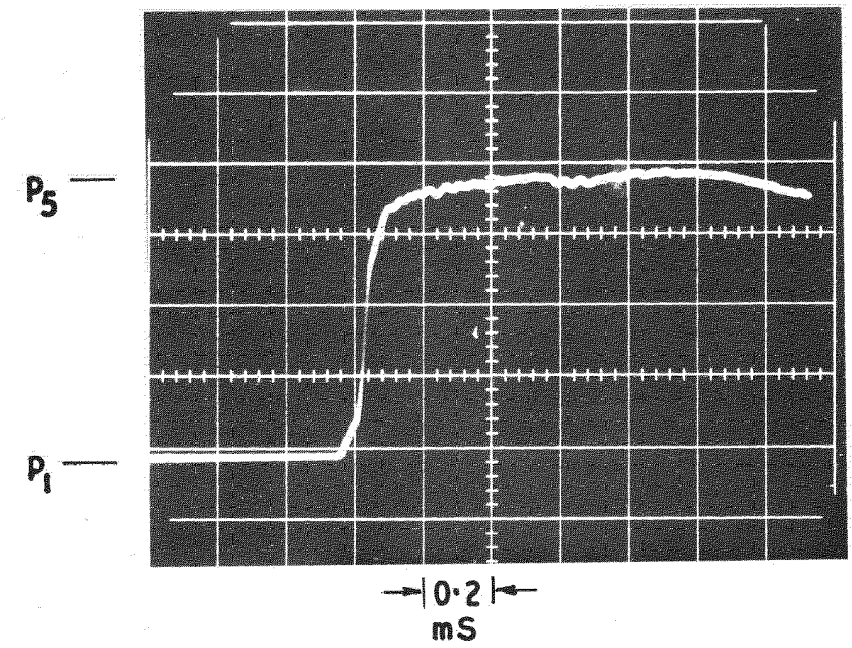

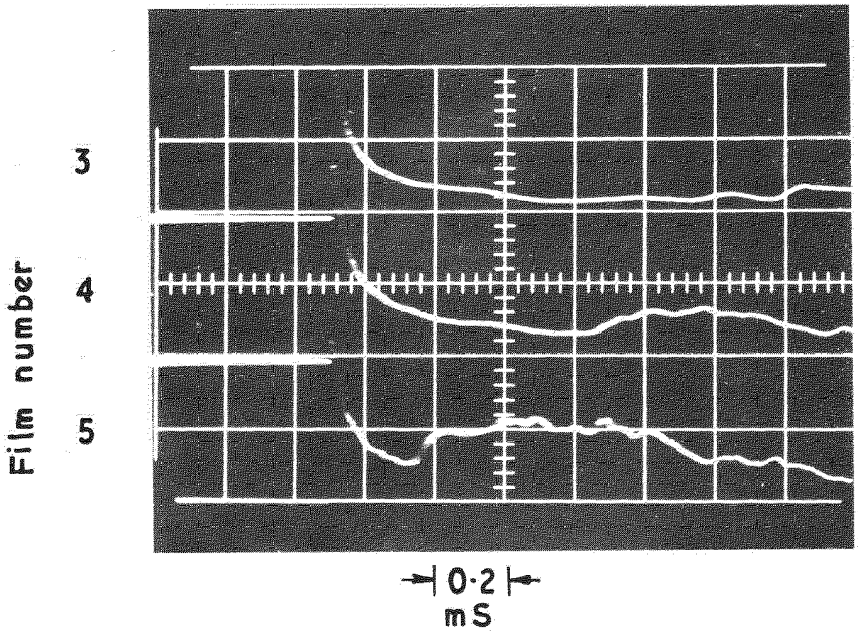

Pressure and heat transfer records 2 inch shock tunnel He:N_2

FIG. 27

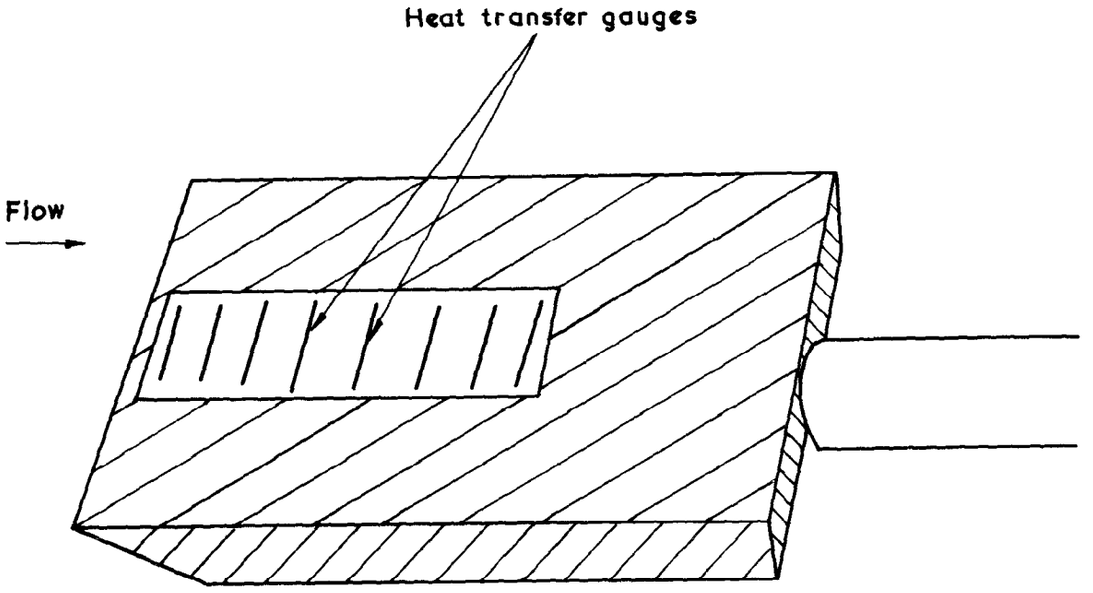

Working section flat plate with heat transfer gauges

FIG. 28

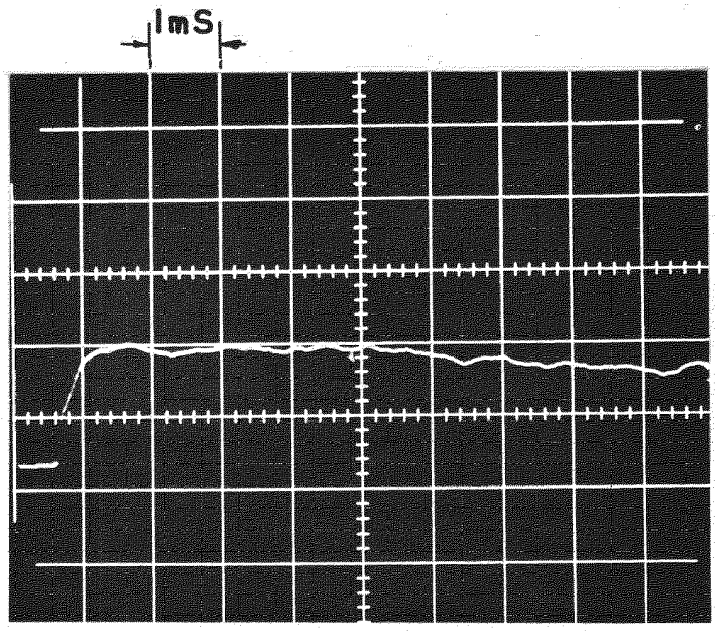

$M_1 = 3{\cdot}35$

$M_\infty = 11{\cdot}6$

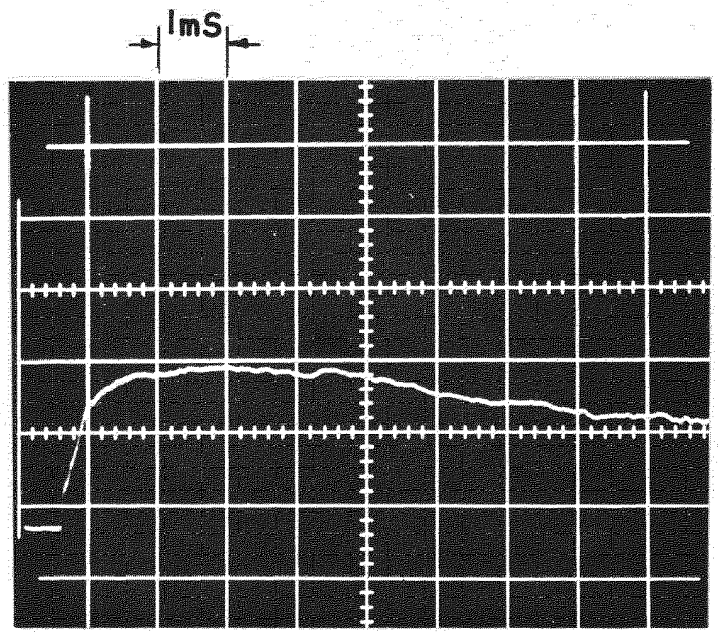

$M_1 = 3{\cdot}82$

$M_\infty = 11{\cdot}6$

Working section. 2 inch shock tunnel

Flat plate heat transfer data

$He : N_2$, $p_4 = 1000$ lb / in.^{2} abs

FIG. 29(a)

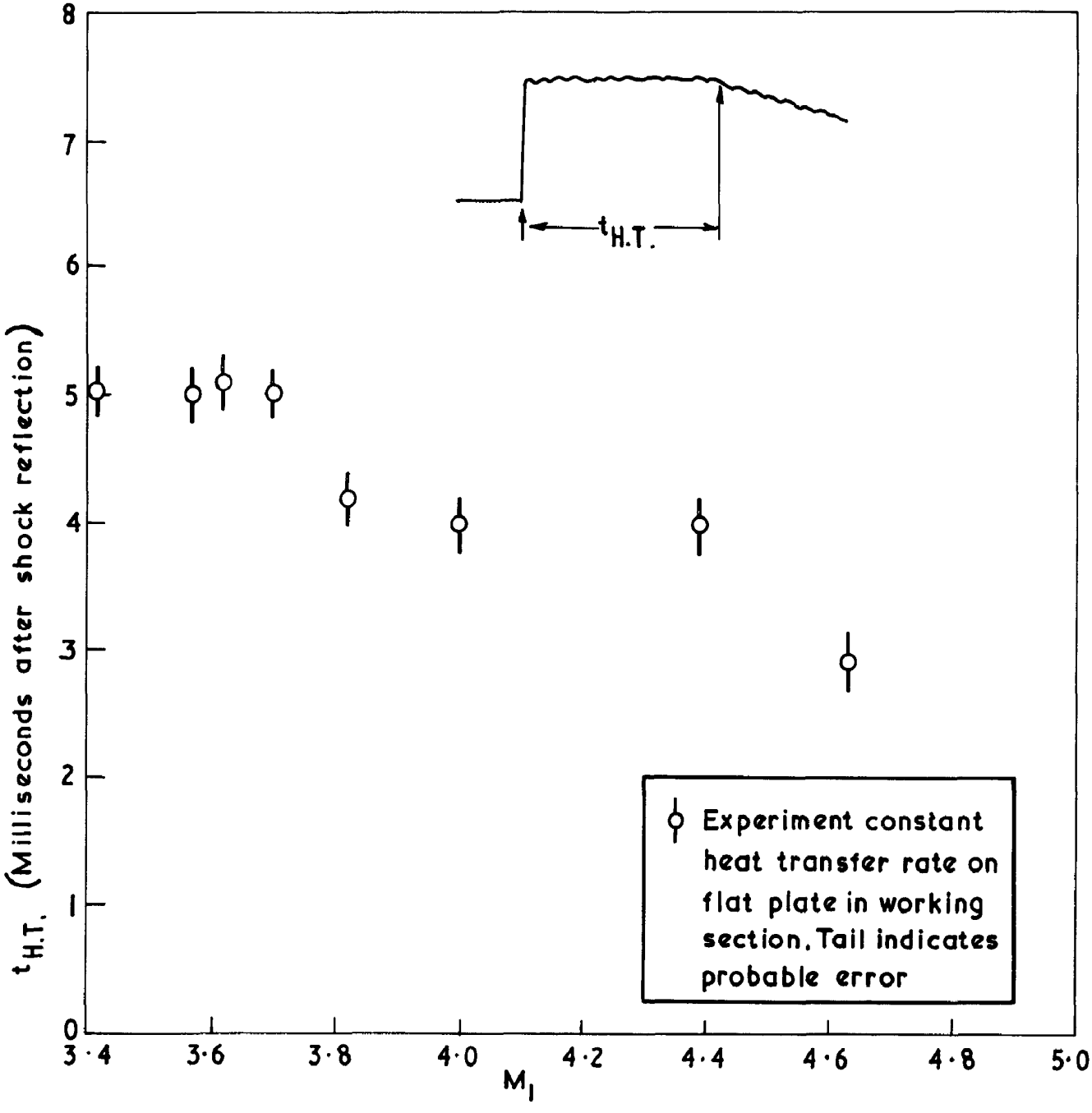
8
7
6
5
4
3
2
1
0
$t_{H.T.}$ (Milliseconds after shock reflection)
$t_{H.T.}$
3·4
3·6
3·8
4·0
4·2
4·4
4·6
4·8
5·0
M_1
Experiment constant heat transfer rate on flat plate in working section. Tail indicates probable error

FIG. 29 (b)

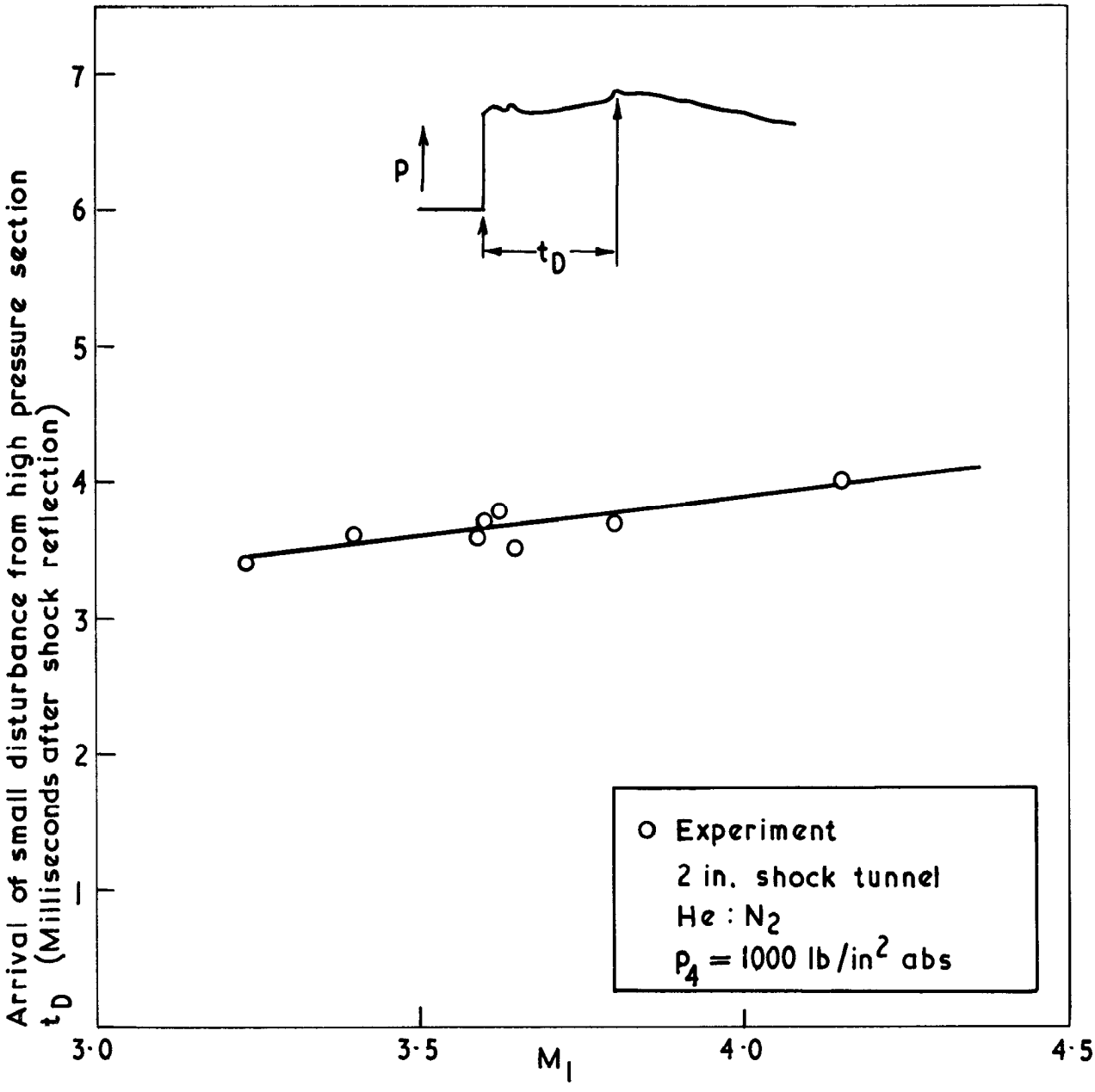

Graph showing the arrival time – after shock reflection – of the first disturbance from the high pressure section at the end plate

FIG. 29 (c)

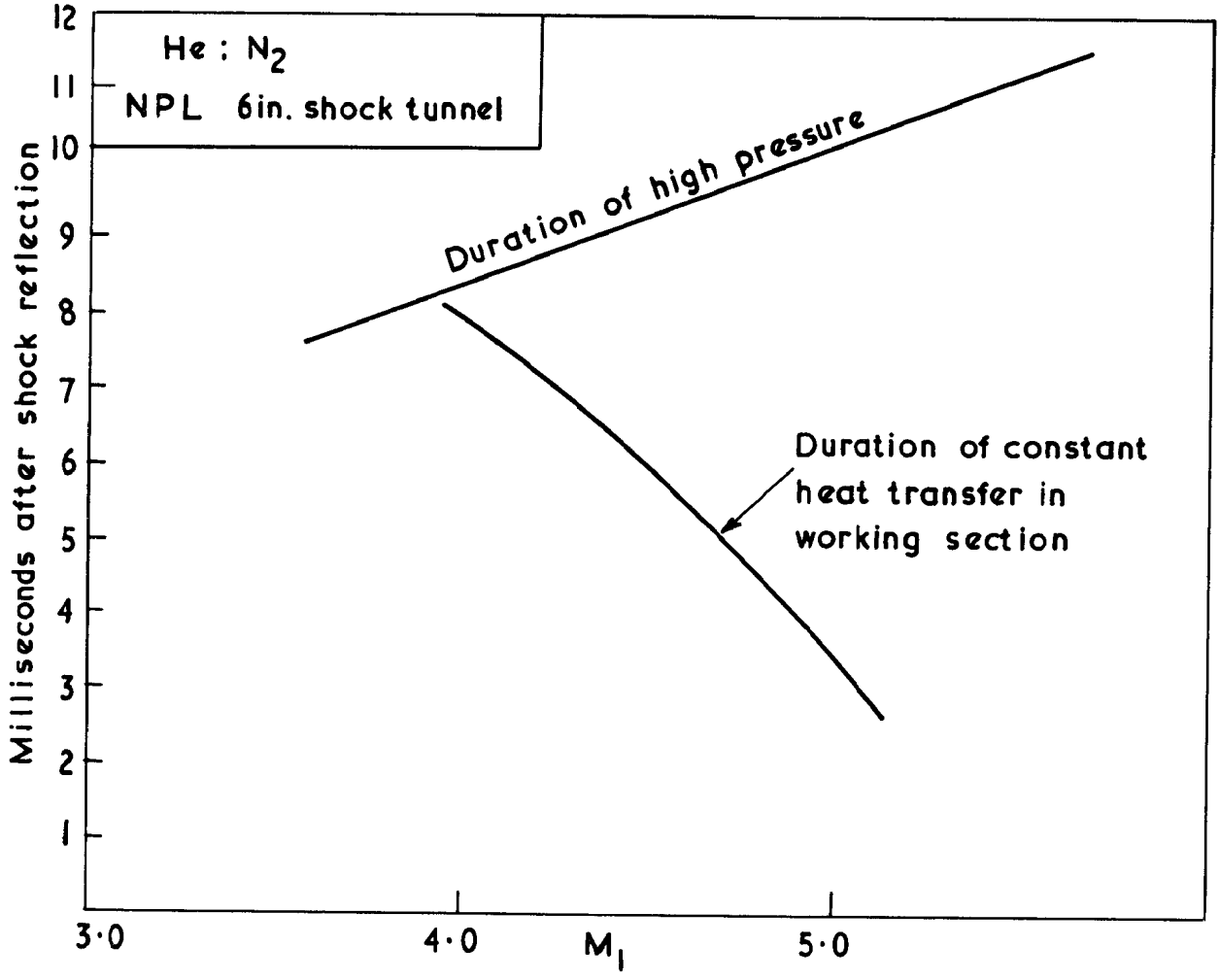

Diagram showing the decrease in constant heat transfer with increasing M_1 as compared with the duration of constant high pressure in the reservoir

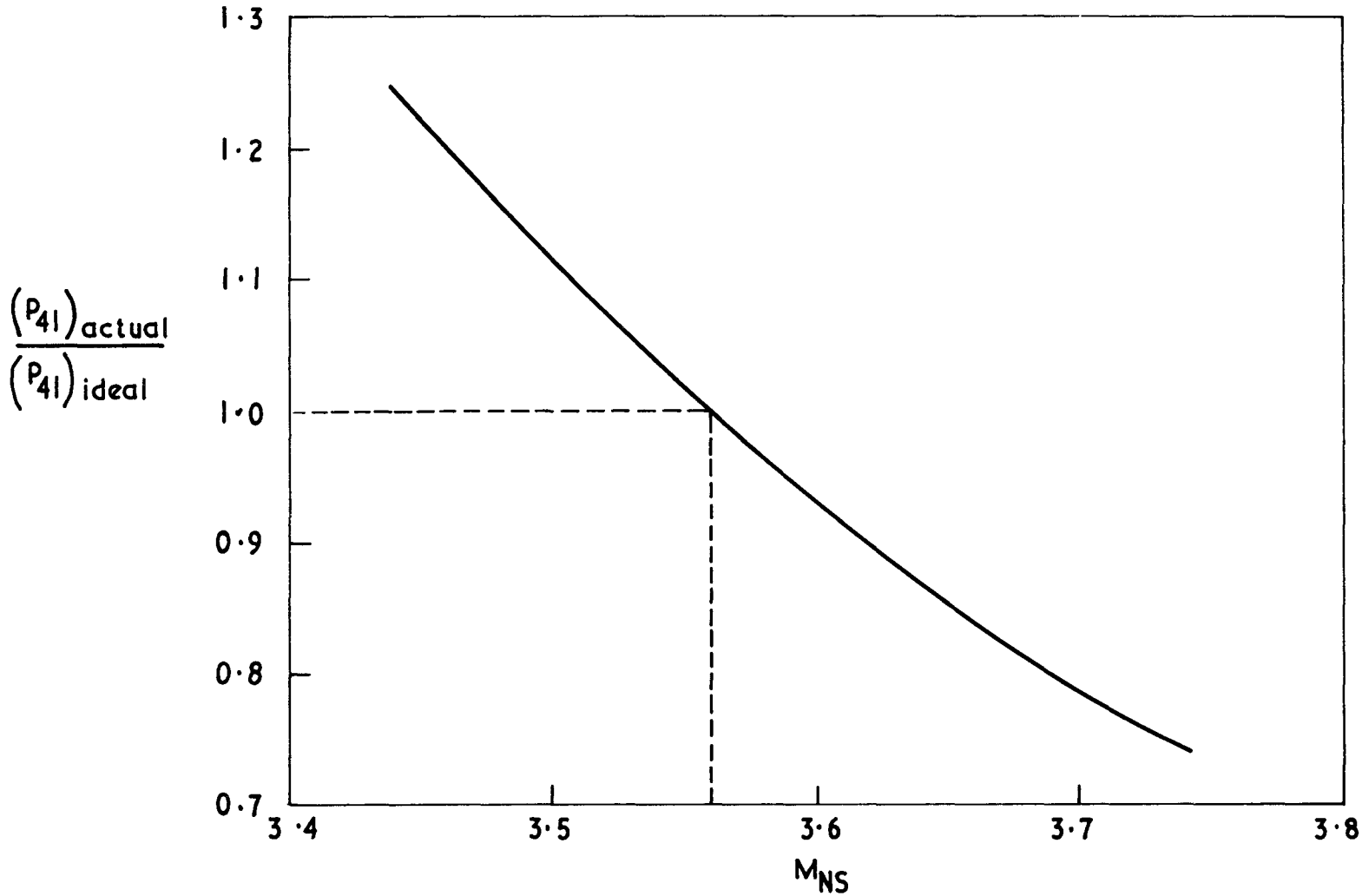

FIG. 30

Variation of neutral stability Mach number, for $He:N_2$ with $(P_{41})_{actual}/(P_{41})_{ideal}$

FIG. 31

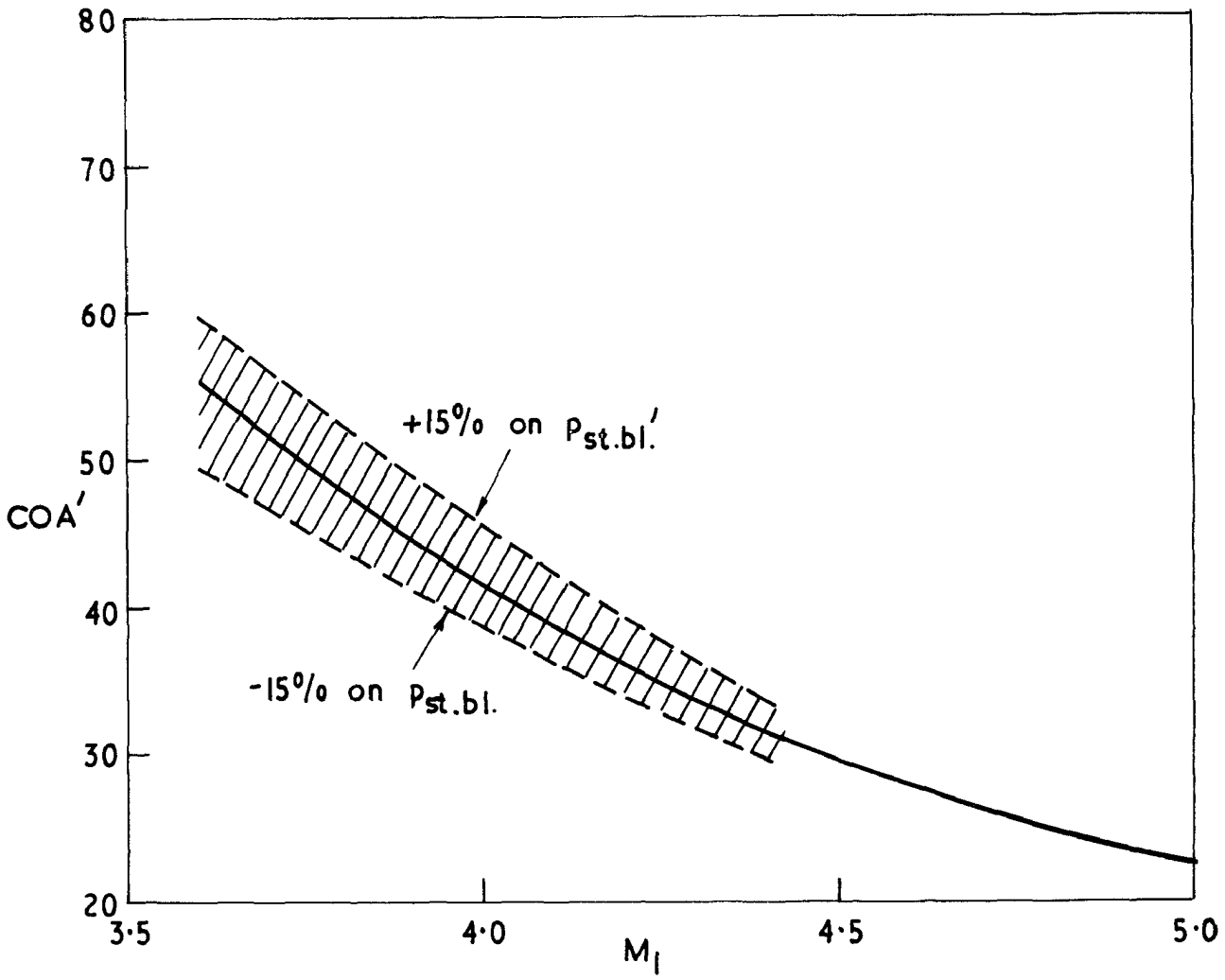

COA' vs M_1 showing sensitivity of calculated value of COA' to ±15% variation in estimating $P_{st.bl}'$ for the transmitted wave

FIG. 32 (a)

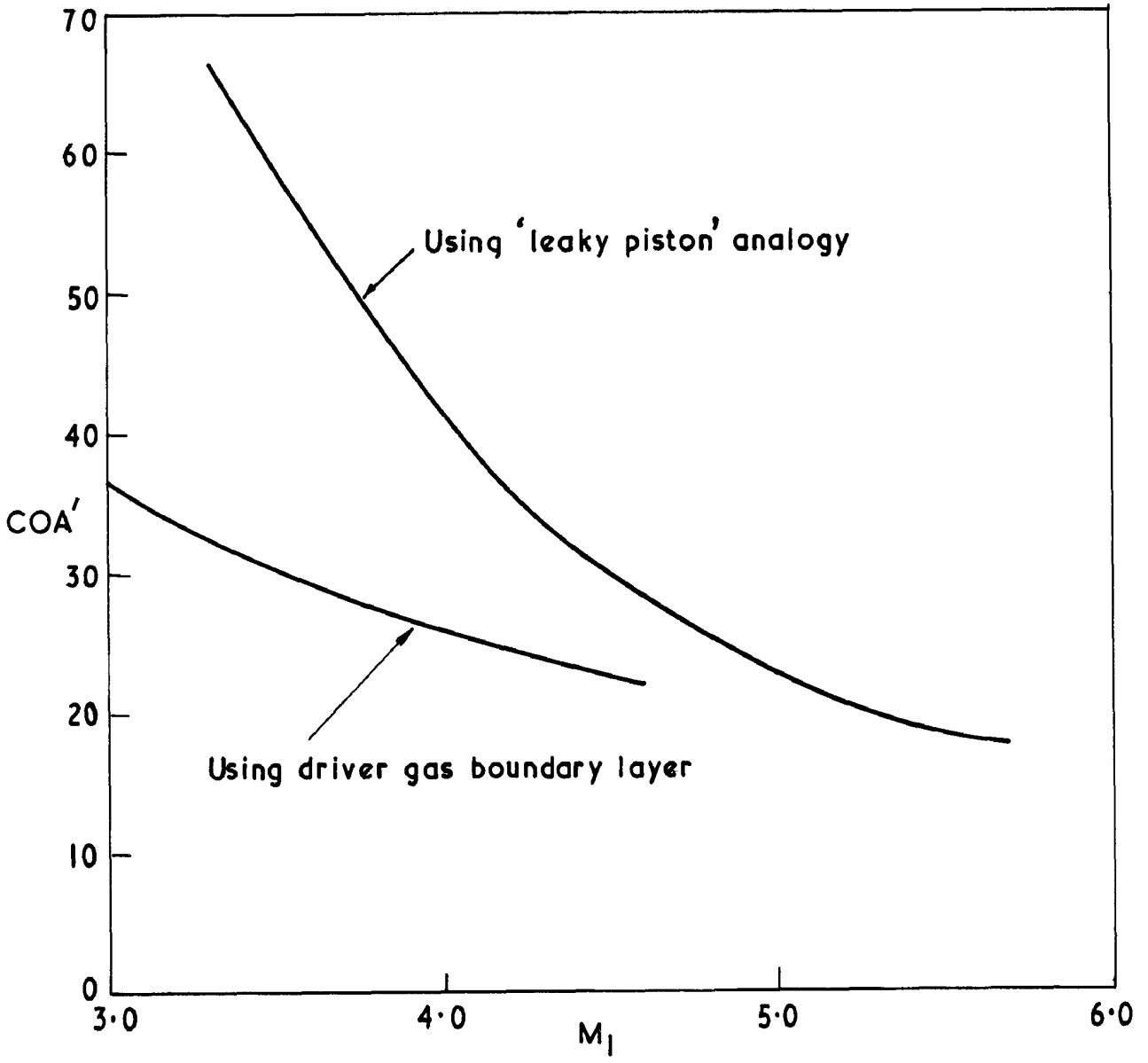

COA' vs M_1 for transmitted shock showing effect of real shock tube behaviour

FIG. 32 (b)

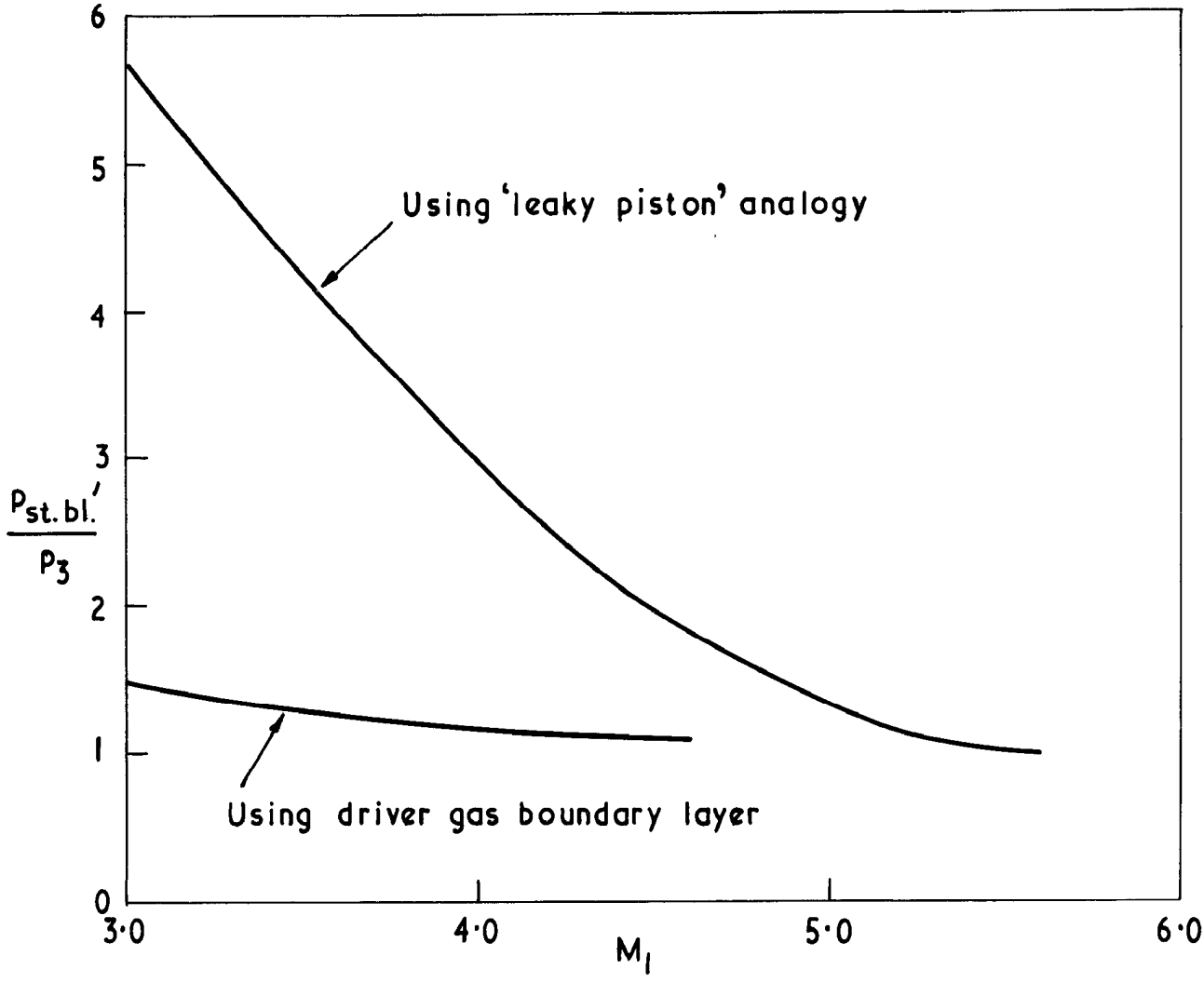

$P_{st.bl.}/P_3$ vs M_1 for transmitted shock showing effect of real shock tube behaviour

A.R.C. C.P. No.880
July, 1965
Davies, L.

THE INTERACTION OF THE REFLECTED SHOCK WITH THE BOUNDARY LAYER IN A SHOCK TUBE AND ITS INFLUENCE ON THE DURATION OF HOT FLOW IN THE REFLECTED-SHOCK TUNNEL. PART 1

A simple flow model is proposed to account for the early cooling of the reservoir gas in the reflected-shock tunnel. Supporting experimental evidence is presented.

A.R.C. C.P. No.880
July, 1965
Davies, L.

THE INTERACTION OF THE REFLECTED SHOCK WITH THE BOUNDARY LAYER IN A SHOCK TUBE AND ITS INFLUENCE ON THE DURATION OF HOT FLOW IN THE REFLECTED-SHOCK TUNNEL. PART 1

A simple flow model is proposed to account for the early cooling of the reservoir gas in the reflected-shock tunnel. Supporting experimental evidence is presented.

A.R.C. C.P. No.880
July, 1965
Davies, L.

THE INTERACTION OF THE REFLECTED SHOCK WITH THE BOUNDARY LAYER IN A SHOCK TUBE AND ITS INFLUENCE ON THE DURATION OF HOT FLOW IN THE REFLECTED-SHOCK TUNNEL. PART 1

A simple flow model is proposed to account for the early cooling of the reservoir gas in the reflected-shock tunnel. Supporting experimental evidence is presented.

DETACHABLE ABSTRACT CARDS

Printed and published by

HER MAJESTY'S STATIONERY OFFICE

To be purchased from
49 High Holborn, London W.C.1
423 Oxford Street, London W.1
13A Castle Street, Edinburgh 2
109 St. Mary Street, Cardiff
Brazennose Street, Manchester 2
50 Fairfax Street, Bristol 1
35 Smallbrook, Ringway, Birmingham 5
80 Chichester Street, Belfast 1
or through any bookseller

Printed in England

C.P. No. 880

S.O. Code No. 23 - 9016 - 80